Dynamic Modeling of ERK Signaling Pathway: Sensitivity, Bistability and Oscillations

by

Mohammadreza Yasemi

A Thesis Submitted to the
Graduate School of Sciences and Engineering
In Partial Fulfillment of the Requirements for
the Degree of

Master of Science
in
Chemical and Biological Engineering

Koc University

September 2017

MSc Thesis

Koç University

Graduate School of Sciences and Engineering

This is to certify that I have examined this copy of a master's thesis by

Mohammadreza Yasemi

and have found that it is complete and satisfactory in all respects,
and that any and all revisions required by the final
examining committee have been made.

Committee Members:

Prof. Dr. Yaman Arkun (Advisor)

Prof. Dr. Ozlem Keskin

Doç. Dr. Burak Alakent

Date: _____

Abstract

Cell signaling is the process by which extracellular information is transmitted into the cell to perform biological functions. ERK signaling pathway controls several cellular processes such as cell growth, proliferation, and gene expression. Deregulation caused by Ras mutations leads to various types of cancers. ERK signaling is triggered by binding of ligands to epidermal growth factor receptors (EGFRs). Upon binding, EGFR becomes phosphorylated on its tyrosine residues. Adaptor protein Grb2 binds to the phosphorylated EGFR and afterwards forms the Grb2-SOS complex. Ras, which is a small GTP binding protein, interacts with this complex and transforms to its active conformation by exchanging GDP for GTP. Active Ras acts as a decisive switch which starts phosphorylation of MAPK cascade that consists of Raf/MEK/ERK signaling molecules. In the literature, there exist mathematical models built for the distinct parts of this pathway. However, this thesis combines several existing models and develops a thorough model of the system starting from the ligand binding step to the nuclear processes mediated by ERK. The model is derived from mass-action kinetics and conservation laws. Several feedback loops which are embedded in ERK signaling pathway were closely studied and the range of the parameters leading to specific responses were identified. In particular, feedback loops were added based on an intensive literature review for the purpose of justifying experimental observations or in some cases for the providing new hypotheses subject to further validation. The complete model comprises 46 ordinary differential equations, 17 algebraic equations and 143 parameters. The mathematical analysis techniques, i.e. bifurcation analysis, parameter sensitivity and dynamics simulation were applied to determine the dynamic characteristics and steady-state responses of the system. We showed that any mutations or alterations in the feedback loops strength can lead to the irreversible adverse effects ultimately resulting in disease states. We establish conditions under which bistability and oscillations emerge for this important pathway. Using our model, we generated new hypotheses that hopefully can pave the way for future experimental design and verification.

Acknowledgment

I am grateful for all the opportunities that I have been provided in the last two years. First of all, I would like to express my gratitude to Prof. Dr. Yaman Arkun, for his support and motivation. This work would not have been possible without his persistence and help. Special thanks to Prof. Dr. Ozelm Keskin and Assoc. Prof. Dr. Burak Alakent for their advice and review of my thesis and for being on my thesis committee.

I have been so fortunate for having great friends and a supporting family around me. I would like to thank them all, specially my beloved sister Shohreh, for her unconditional support and encouragement and my love Ghazaleh, for being beside me in every challenging moment of my life, and for offering me her unlimited love through ups and downs.

Finally, I like to dedicate this thesis to the inspiring memory of my late father, who was a decent broad-minded teacher and taught me to be faithful and fearless in pursuing my dreams.

Table of Contents

List of Tables

List of Figures

Chapter 1: Introduction

Cell signaling is the process by which extracellular information is transmitted into the cell. Signal transduction pathways are interconnected networks of signaling proteins that communicate through complex molecular mechanisms. A complex network of cellular interactions and feedback loops are usually arranged in a hierarchical fashion in space and time to transform the information content of extracellular signals to the DNA in the nucleus which in turn converts this information into several useful cellular functions[1]. Signaling faults due to mutations and failures in the regulatory mechanisms of signal transduction pathways are known to result in several types of cancer[2], [3].

The signal transduction pathway under study in this thesis is ERK signaling. In mammalian cells all receptor tyrosine kinases (RTKs) are known to exploit a highly conserved signal-transduction pathway, carrying the signal triggered by binding of ligand to activate MAPK (mitogen-activated protein kinase), a serine/threonine kinase also recognized as ERK (extracellular signal-regulated kinase). As a case in point, ERK signaling plays a key role in numerous cellular processes such as proliferation, apoptosis, DNA synthesis and differentiation[4], [5]. The pathway of interest is illustrated in Fig 1.

Activation of EGFR (epidermal growth factor receptor) by binding of its specific ligands, namely epidermal growth factor (EGF) and transforming growth factor α (TGF α), starts the ERK signaling pathway. Upon ligand binding, two subunits of EGFR are dimerized, leading to increase

in the enzymatic activity of its cytoplasmic tyrosine kinase domain [6]. Adapter protein ShC-Grb2 binds to the phosphorylated RTK followed by the recruitment of SOS forming the ShC-Grb2-SOS complex [7], [8]. Membrane-bound protein Ras, which is a small GTP binding protein, interacts with Grb2-SOS complex, and it is transformed to its active conformation by exchanging GDP for GTP. Active Ras acts as an important molecular switch which starts the sequential phosphorylation of MAPK pathway that consists of the Raf/MEK/ERK signaling cascade [9], [10].

Activated ERK, when translocated to the nucleus, phosphorylates nuclear transcription factors (e.g. Myc), that govern cellular responses [11], [12]. Phosphorylated transcription factors stimulate transcription of genes which are responsible for encoding different proteins, including ones required for cell cycle progression (e.g. Cyclin D) [13].

Use of systems biology tools and computational approaches in molecular biology have made the analytical investigation of intracellular dynamics possible. Investigations being carried out based on mathematical models which mimic the intracellular networks, have achieved much attention in recent years [14]–[16].

Mathematical modeling as part of a holistic approach in addressing biological complex systems, has been applied to understand the ERK signaling pathway and to generate hypotheses to be experimentally tested. Informative models explaining this pathway were constructed by several scholars [7], [8], [17], [18]. Usually each model is tailored in a way that fulfills the demands upon which it is built.

In this present work, a quantitative mechanistic model including mass conservation and mass action kinetics has been developed for the complete system presented in Figure 1. This model is reconstructed by integrating some of the current models available for separate sections of MAPK signaling pathway. Several feedback loops were modeled and embedded in this intracellular network of reactions.

The developed model was analyzed with sophisticated mathematical techniques, to understand the steady-state and dynamic properties of ERK signaling under feedback control. In particular, bifurcation analysis proved to be a very useful technique in obtaining enlightening results that explain the behavior of this complex dynamical system.

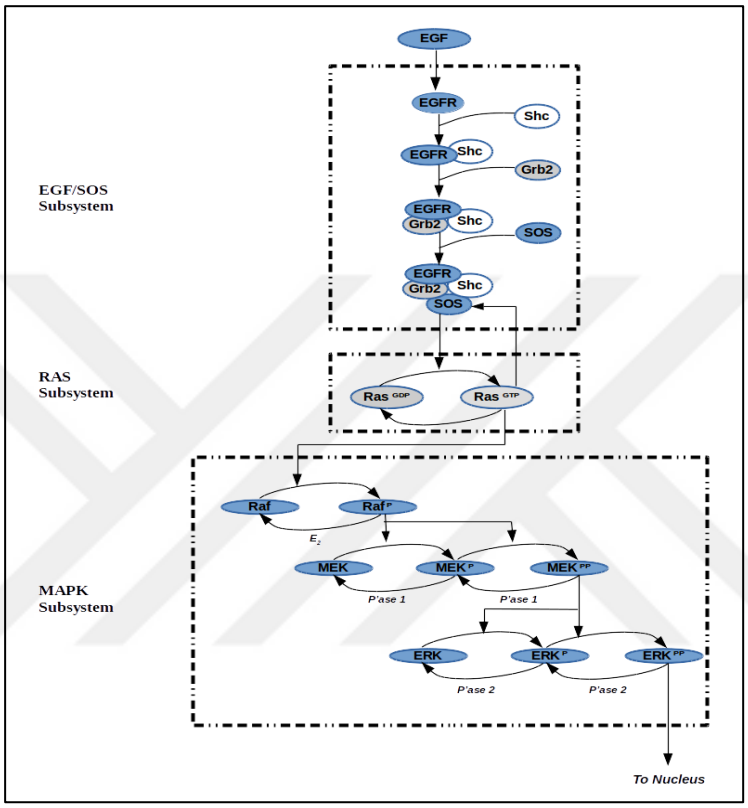

Figure 1 – ERK signaling pathway divided to three subsystems: EGF/SOS subsystem, RAS subsystem, MAPK subsystem. Activated ERK is then translocated to the nucleus.

The rest of the thesis is organized as follows:

Chapter 2 provides a review of the literature which covers the research results related to the modeling and analysis of the ERK signaling pathway. Definitions of the most common theories and technical phrases are given in this chapter.

In Chapter 3, the models which were reconstructed and developed are presented and the

methods to analyze and develop the desired mathematical model are outlined.

Chapter 4 shows the results that were obtained. This includes steady-state and dynamical responses of the constructed system to several scenarios which were designed to clarify the system's behavior.

In Chapter 5 which is the last chapter of the thesis, the prominent conclusions derived from our results are pointed out.

Chapter 2: Literature Review

2.1 Overview

Mathematical models are useful in many ways. First, they can be used to discriminate among the alternative causal mechanisms. Based on the model predictions, new hypotheses can be postulated and experiments can be designed to validate these hypotheses. Knowing all the proteins involved in a complex pathway is not enough to describe how a particular signal transduction pathway functions. Moreover, computer simulation of the developed models is a necessity in order to realize how the system responds to its inputs and changes in its parameters [19]. Increasing importance of mathematical models over the years resulted in building a wide variety of mathematical or computational representations of MAPK pathway. Every valuable model of this system unravels how it functions and sheds light on formerly unclear biological processes taken place in the heart of this important molecular-signaling network [19].

Systems biology adopts a holistic approach in general and turns the abstract biological descriptions into mathematical and computational formalisms. However, models are useful and applicable only when they are faithful to the topological representation of the real system. Possibly the most encouraging outcome of modeling, is its power to explain unpredicted behavior that emerges out of the biological design of the network. Well-documented recurring motifs like ultra-sensitivity, bistability and oscillations are a few valuable gains of mathematical investigation of biological systems [20], [21].

As stated in [19] and depicted in Figure 2, the actual process of modeling involves five steps:

Step 1: system delimitation – Choosing the biological system and determining the

biological question that the model claims to answer.

Step 2: definition – This step is the key step in the modeling process. In this step, one gathers all the essential data required to define the model. This includes depicting topological representation of the system that shows all the species involved, finding parameter values and reaction kinetics, conducting laboratory experiments, and using computational techniques in order to estimate the missing parameters.

It should be noted that since most of the biological systems are not fully understood, making simplifying assumptions to reduce complex interactions into simple ones that can still explain observed data is crucial.

Step 3: simulation – A set of ODEs defining kinetic reactions and showing how the concentration of species changes over time is built in this step. Then it can be simulated by means of available software tools.

Step 4: validation – This step can be considered as a 'debugging' step, during which the model is tested against experimental data to see whether or not it matches previously known data. It may be needed to go back and redefine the model several times before it captures the observed biological data. The model can be trusted for generating hypotheses only after being validated.

Step 5: analysis – Overall aim of this step is to increase our understanding of the system by performing distinct analysis techniques on the system. System robustness or sensitivity to different parameters is tested in this step.

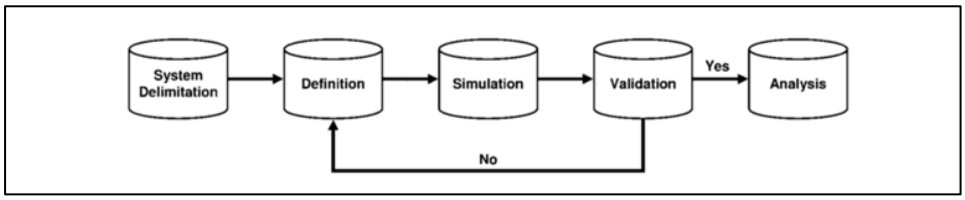

Figure 2 – Mathematical modeling steps [19].

2.2 ERK signaling pathway

The ERK signaling pathway is one of the most important and intensively studied signaling pathways [19], [20]. ERK signaling is comprised of three subsystems as shown in Figure 1. Figure 3 shows a timeline of models built for explaining ERK signaling mechanisms up to year 2005.

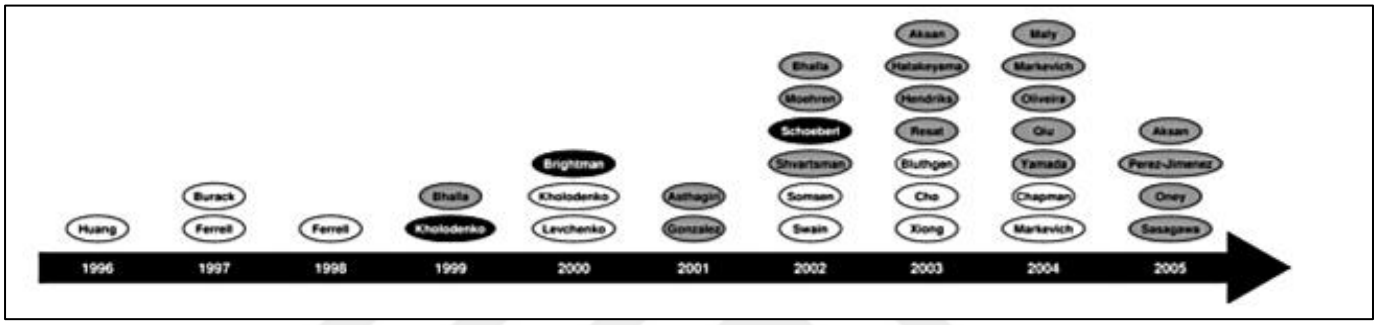

Figure 3 – Evolution of ERK models [19] .

Kholodenko et al. [7] developed an ODE-oriented model in 1999. This model includes reactions and species starting with the stimulus EGF and ending with the formation of SOS (Son of Sevenless homolog protein) complex (see Figure 4). This model has received much attention because it has successfully incorporated EGFR and the adapter proteins associated with this receptor. The second subsystem of ERK signaling consists of activation of Ras which is catalyzed by the SOS complex as shown in Figure 5.

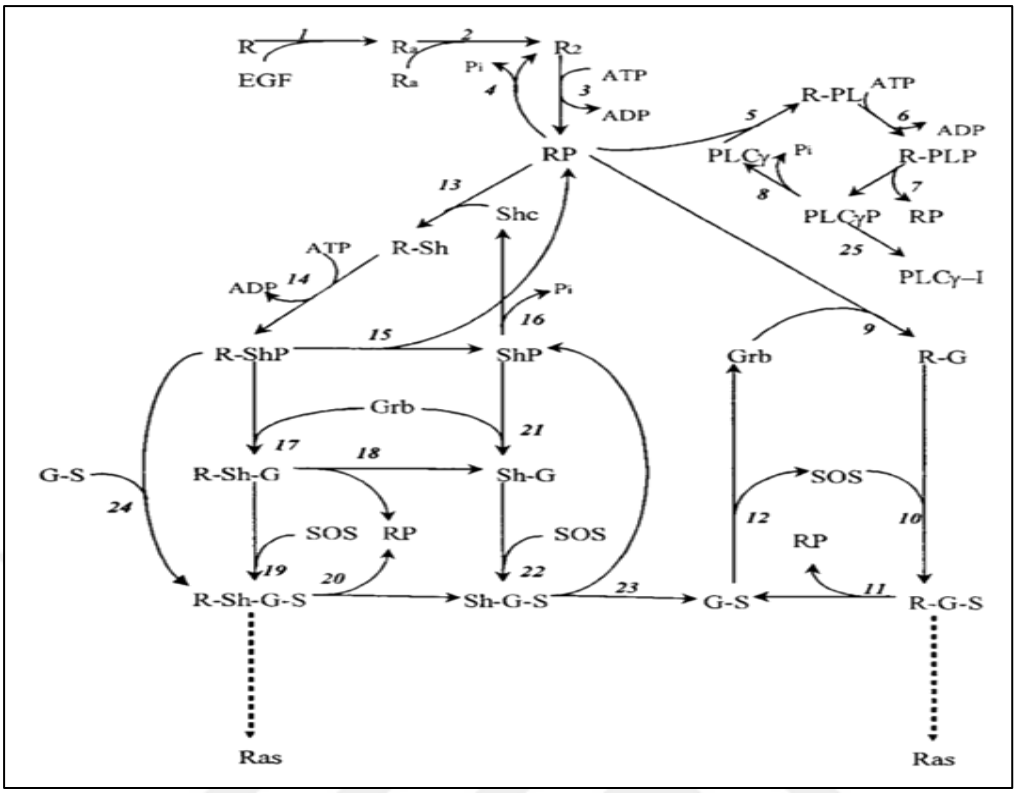

Figure 4 – Model offered by Kholodenko et al. [7]

Das et al. [10] proposed a mechanism for SOS-mediated activation of Ras that stresses the existence of a positive feedback loop resulting in digital signaling in lymphoid cells. This feedback loop causes hysteresis in the dose-response curve for activation of Ras. However, this study suggests that there are two conditions required for bistable Ras activity: (1) SOS should catalytically activate Ras while RasGTP (already activated form of Ras) is bound to its allosteric site, (2) RasGAP (Ras GTPase activating protein) catalytically deactivates RasGTP. Figure 5 shows the suggested mechanism.

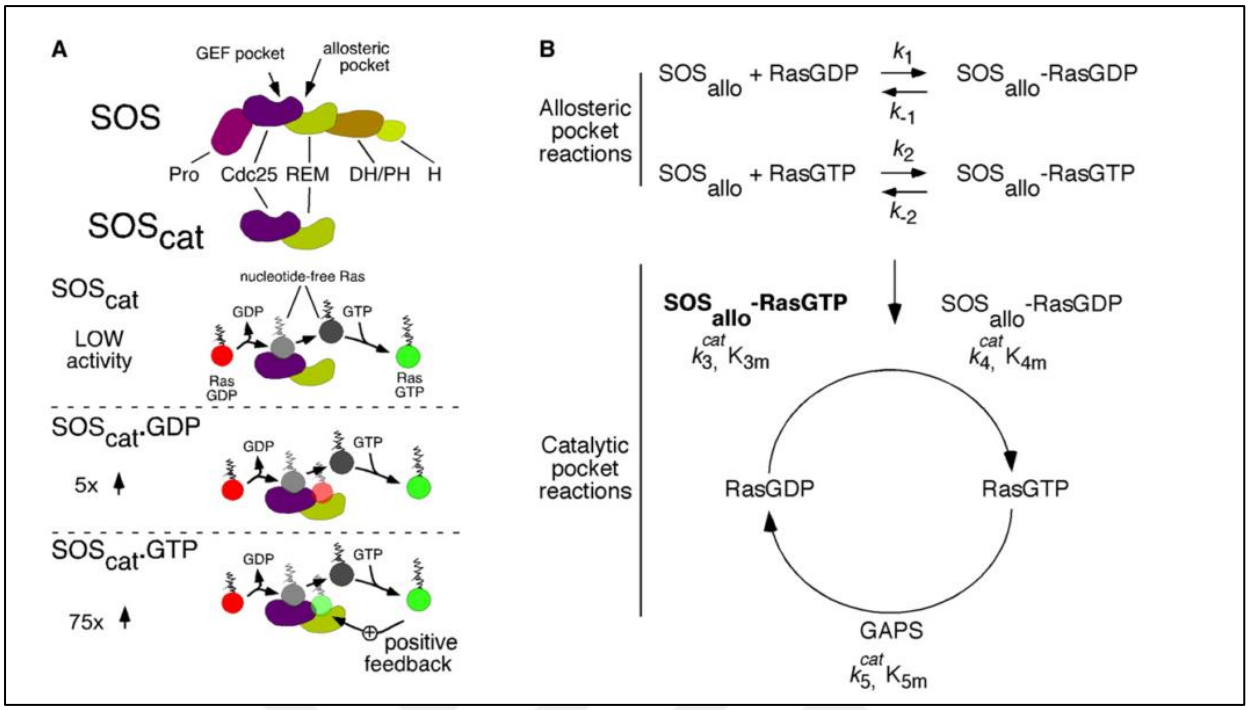

Figure 5- Ras activation mechanism based on [10].

Active Ras starts the sequential phosphorylation of MAPK pathway that consists of the Raf/MEK/ERK signaling cascade [9], [10] as seen in Figure 6. The very first mathematical model describing this cascade was built in 1996 by Huang and Ferrell [17]. This model studied ultra-sensitivity as one of the emergent properties of this cascade, and predictions were proved to be correct by experiments on Xenopus oocytes. Huang and Ferrell's model was followed by a growing number of mathematical models, each of which focusing on various facets of biological behavior of ERK signaling.

In 2000, Brightman and Fell [21] proposed that negative feedback regulation from activated ERK to SOS complex accounts for difference in ERK response to EGF and NGF (nerve growth factor). In their model, they showed that negative feedback is the most significant factor determining signal duration. ERK-PP (active form of ERK) catalyzes inhibition of SOS by phosphorylation at serine/threonine residues, producing ShcP and GSP (Grb2-phosphorylated SOS complex) out of dissociation of ShcGS complex [22].

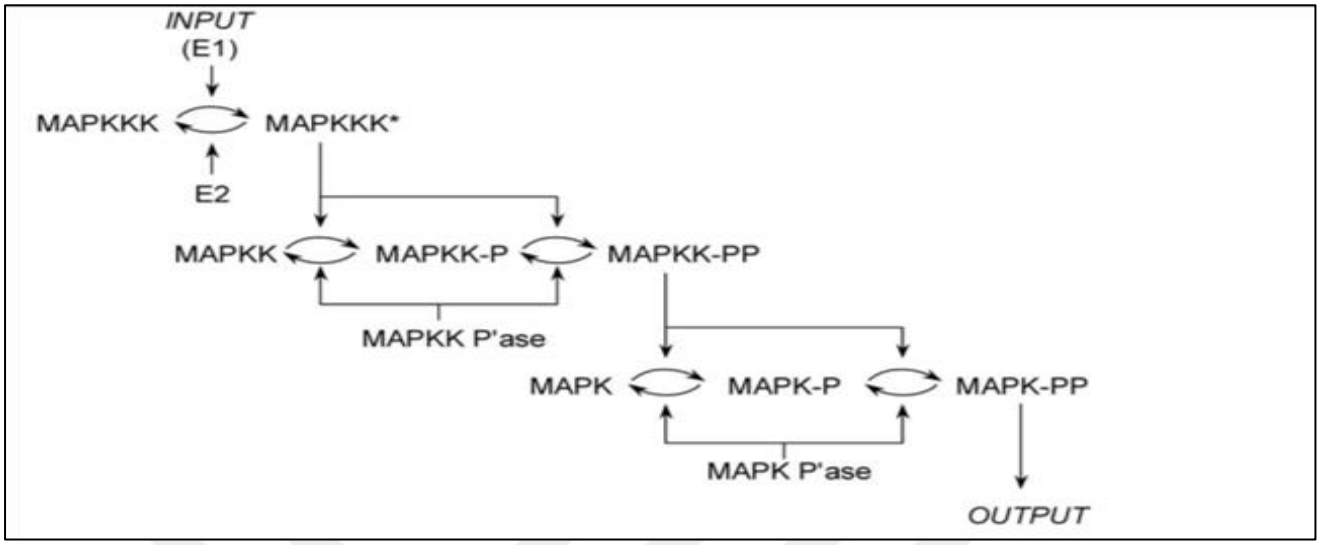

Figure 6 - Three-tiered kinase cascade of MAPK pathway [17].

However, one should consider the fact that most of mathematical models show notable level of uncertainty due to unknown parameters and the inherent differences between processes in the different cell lines. [23,24].

2.3 Different Response Types and Ultra-sensitivity

2.3.1 Ultra-sensitivity

Biochemical systems exhibit different types of steady-state and dynamic responses that affect the way they function. In particular, ultra-sensitivity is an inherent property of a great number of signal transduction pathways [24]–[26]. In order to understand ultra-sensitivity, it helps to introduce Michaelian response first.

Consider the phosphorylation and dephosphorylation reactions shown in Figure 7.

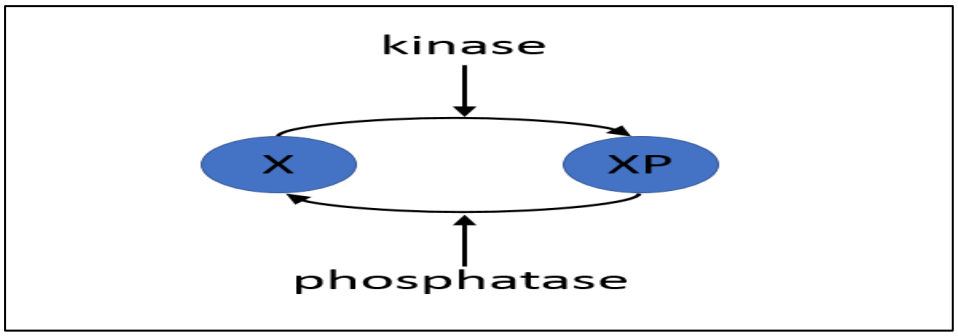

Figure 7- Reversible phosphorylation reaction. Kinase and phosphatase are the enzymes, X is the substrate for phosphorylation reaction, XP is the substrate for dephosphorylation reaction.

Assuming mass action kinetics, the resulting steady-state input-output response is called Michaelian and given by:

$$Output = \frac{Input}{K + Input} \tag{1}$$

Input is the concentration of the kinase, *Output* is the fraction of *X* in the phosphorylated form i.e. *Xp/Xtotal*, and *K* is the level of *Input* where half of *X* is phosphorylated. This is also referred to as EC50.

It is worth mentioning that Michaelian response describes the steady-state output response to the enzyme concentration in systems where the law of mass action applies for modeling enzymatic reactions. However, when enzymatic reactions are saturable, they are described by the Michaelis-Menten kinetics. The following mathematical representation highlights the difference [27]:

$$Michelian\ response: Output = \frac{Input}{K + Input} \tag{2}$$

$$Michaelis - Menten\ mechanism: Reaction\ velocity\ (v) = \frac{V_{max}S}{K_M + S} \tag{3}$$

$$\text{and the rate of product formation is given by: } \frac{dP}{dt} = \frac{V_{max}S}{K_M + S} \tag{4}$$

In Michaelian response, the input is usually the kinase (enzyme) concentration, and the output is the steady-state amount of activated protein over total protein concentration, while in Michaelis-Menten kinetics the input is the substrate concentration (S) and the output is the reaction velocity (v). Derivation of $Michaelis-Menten\ mechanism$ is summarized in Appendix I.

The formula for the calculation of local sensitivity in a signaling cascade is given by [28]:

$$\mathrm{S_{local}} = \lim_{\Delta Input} \frac{\Delta Output}{Output} / \frac{\Delta Input}{input} = \frac{d\ lnOutput}{d\ lnInput} \tag{5}$$

Note that S_{local} is the slope of a log-log plot of *Input* vs. *Output*. A global sensitivity is usually defined as the *EC*90:*EC*10 ratio. For a Michaelian response, this ratio is equal to 81 .

Goldbeter and Koshland were the pioneers who have established the characteristics of ultra-sensitivity. They called an ultrasensitive response to be any response with an *EC*90:*EC*10 ratio less than 81 [29].

Hill function, first introduced by Archibald Hill in 1910 [30], has been used to model the ultrasensitive sigmoidal response curve of biological systems. Hill Equation is given by:

$$Output = \frac{Input^n}{(K^n + Input^n)} \tag{6}$$

Where n is called the Hill coefficient or Hill exponent. Eq. (6) can be derived assuming the enzyme has *n* cooperative active binding sites [31], [32]. If an enzyme has *n* binding sites that are cooperative i.e. the more substrates are bound, the easier the binding of additional substrate is.

If the response is approximated by a Hill function, the Hill exponent is given by [33][27]:

$$n = ln[81]/ln[EC90/EC10] \quad (7)$$

Hill functions and sensitivity curves for different Hill exponents are illustrated in Figure8.

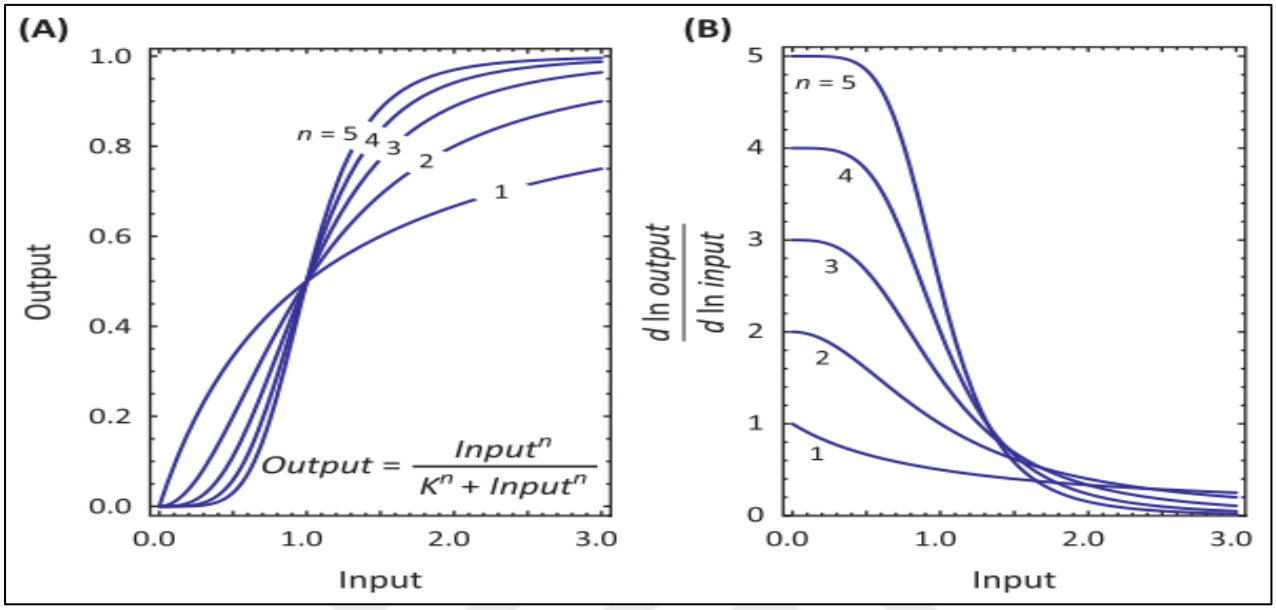

Figure 8 – Hill function and ultra-sensitivity. ***(A)*** *n=1 is a hyperbola, resembling Michaelian response. As n increases, the response gets steeper.* ***(B)*** *local sensitivity. When input is low, the sensitivity approaches corresponding coefficient (n) [27].*

There are at least four well-studied mechanisms generating ultrasensitive responses in natural biochemical systems. These are: zero-order ultra-sensitivity, multistep mechanisms, stoichiometric inhibitors and positive feedback loops, reviewed by Ferrell Jr & Hoon Ha [27], [31], [34]. The first two are discussed in this section, and impact of positive feedback loop on ultra-sensitivity will be discussed in next section.

For reactions in Figure 7 one can observe four regimes, dependent on the saturation level of kinase and phosphatase. Assuming k_1 and k_{-1} for the phosphorylation and dephosphorylation rate constants, respectively, the rate of phosphorylation of protein *X* is given by:

$$\frac{dXP}{dt} = k_1 * kinase * f(XP) - k_1 * p'ase * g(XP) \quad (8)$$

The mechanisms for different regimes are given in Table 1; phoshorylation and dephosphorylation rate curves and steady-states plots are shown in Figure 8.

Table 1- Mechanisms for modeling phosphorylation and dephosphorylation reactions. (Mechanisms from [27], names and description from [33][27])

	$\boldsymbol{Phosphorylation\ f(XP)}$	$\boldsymbol{Dephoshorylation\ g(XP)}$	Saturation level
Hyperbolic (Fig. 8A)	$(X_{tot} - XP)$	(XP)	Kinase:unsaturated P'ase: unsaturated
Threshold-hyperbolic (Fig. 8B)	$(X_{tot} - XP)$	$\frac{XP}{K_{m2} + XP}$	Kinase: unsaturated P'ase: saturated
Signal-transducing (Fig. 8C)	$\frac{X_{tot} - XP}{K_{m1} + X_{tot} - XP}$	(XP)	Kinase: saturated P'ase: unsaturated
Ultrasensitive (Fig. 8D)	$\frac{X_{tot} - XP}{K_{m1} + X_{tot} - XP}$	$\frac{XP}{K_{m2} + XP}$	Kinase: saturated P'ase: saturated

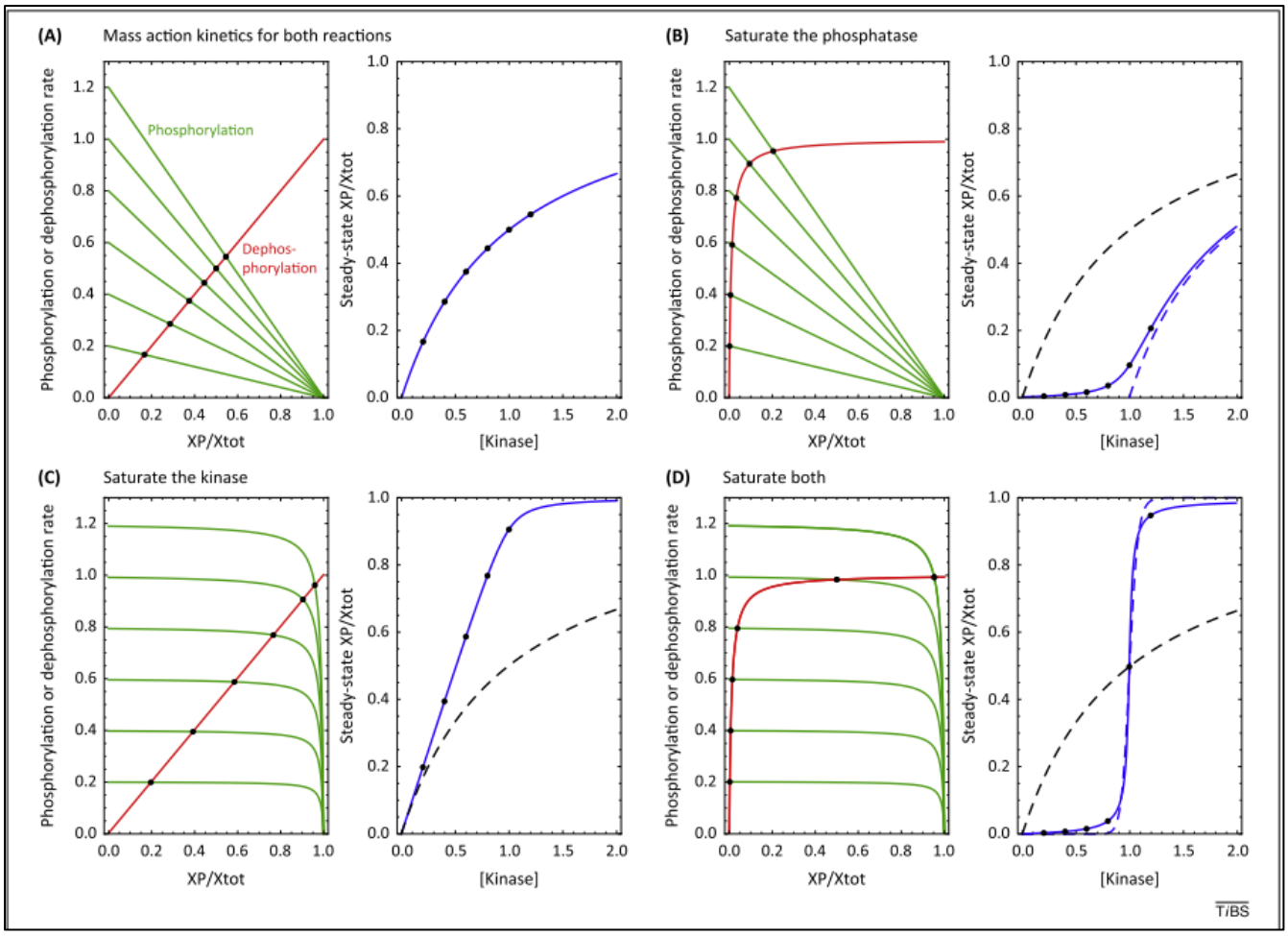

*Figure 9- Rate curves and steady-state input-output relationship [27]. **(A)** Mass action kinetics assumed for both reactions. **(B-D)** One or both of the reactions are taking place close to saturation. Dashed black curves are Michaelian approximation of the responses. Dashed blue curve in B, is Michaelian response shifted to the right for one concentration unit. Dashed blue curve in D shows a Hill function with Hill exponent of 26.1 to compare with actual response. kinase=0.2, 0.4, 0.6, 0.8, 1 or 1.2 (see [27] for constant values).*

In Figure 9, rate curves are on the left-hand of each sub-figure. Intersections of the two curves give the steady-state values of *XP* (on the x-axis). In Figure 8A, both enzymes, i.e. kinase and phosphatase, are unsaturated, meaning that the reactions are described by mass action kinetics, in which case, substrate and enzyme concentrations are comparable. In this case, a Michaelian (hyperbolic) curve represents the relationship between kinase as input, and steady-state value of XP/X_{tot} as output. In Figure 9D, both enzymes are saturated; it means that both

enzymatic reactions are modeled by Michaelis-Menten kinetics. Thus, the rate-balance plots are Michaelian, and the substrate is in excess compared with the sum of enzyme concentration and its Michaelian constant. However, since in this regime, the phosphorylation (dephosphorylation) reaction rate is zero-order with respect to *X (XP)*, it is called 'zero-order ultra-sensitivity' [33].

The mechanism by which p21 inhibits cyclin E-Cdk_2 complex exemplifies *stoichiometric inhibition* as one of the possible ways to bring about ultra-sensitivity. Cdk_2 activity is ultrasensitive with a sharp jump after cyclin E exceeds concentration of the inhibitor, p21 [35]. Figure 10 gives the reaction mechanism and the generic steady-state response of inhibitor ultra-sensitivity. This mechanism is the simplest one for creating ultrasensitive response and is capable of being used in the synthetic biological systems to generate ultra-sensitivity.

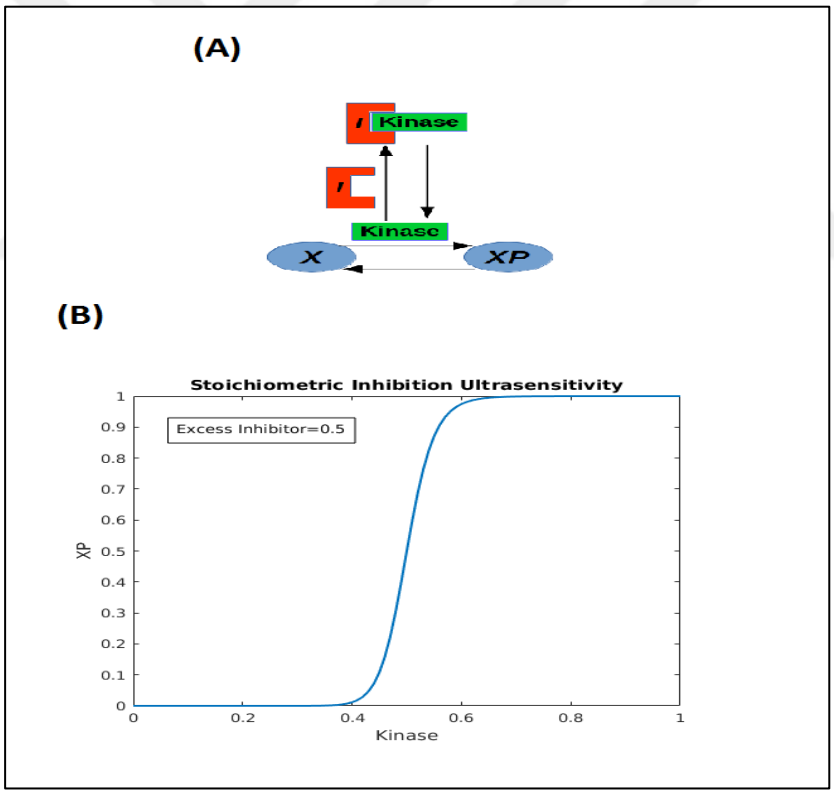

Figure 10 - The stoichiometric inhibition. ***(A)*** *The reaction mechanism of stoichiometric inhibition.* ***(B)*** *The ultrasensitive XP to kinase steady-state relationship. Adapted from [35].*

The multisite phosphorylation is another way of generating ultra-sensitivity. In the dual phosphorylation of ERK, a distributive mechanism is assumed to happen rather than a processive one [36][28]. The phosphorylated MEK, kinase for the ERK phosphorylation, dissociates after the first collision producing monophosphorylated ERK, and the second phosphorylation reaction happens in the second collision of active MEK and monophosphorylated ERK, producing double-phosphorylated ERK. What make the distributive dual phosphorylation create ultra-sensitivity are enzymes (kinase and phosphatase) saturation, and competition between substrates (*X, XP, XPP*) for binding to the kinase or phosphatase. Figure 11, shows a simplified model of the dual phosphorylation (dephosphorylation) of ERK [31]. As the total concentration of X (ERK) increases, due to the saturation of enzymatic reactions we observe ultra-sensitivity.

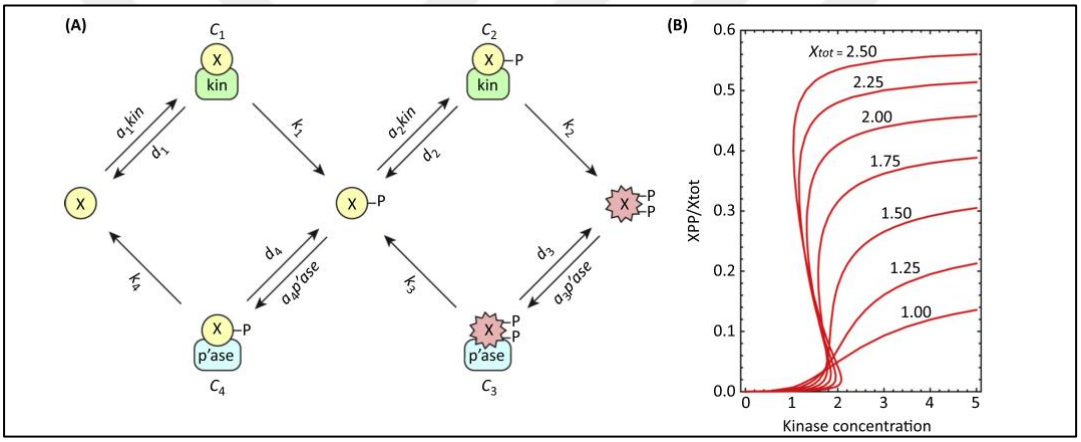

Figure 11 – Dual phosphorylation. ***(A)*** *A simplified representation of the dual phosphorylation in MAPK pathway. [37]* ***(B)*** *Input-output diagram for several* X_{tot} *values . [31]*

Ultra-sensitivity is an important property, because this property enables complex signaling systems to function fully [34]. In other words, ultra-sensitivity, regardless of its origin, can contribute to formation of on-off switches, sensitivity amplifiers, and oscillatory dynamics. If each level of a cascade is slightly ultrasensitive, the output-input response of the whole cascade shows amplified sensitivity. 'Sensitivity amplification' [38] has proved to be implemented both by nature [17] and in the synthetic biological systems [39].

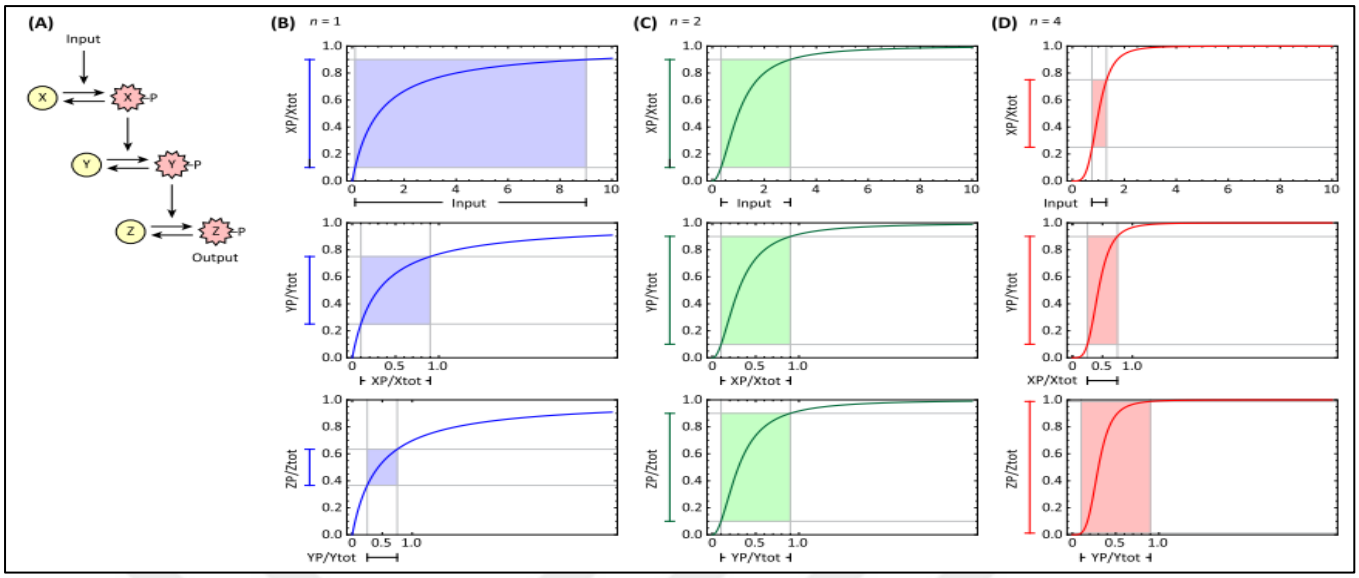

Figure 12 - Sensitivity amplification in a three-tiered cascade. ***(A)*** *Cascade representation. Activated protein (output) in each level is the kinase (input) for the next level.* ***(B)*** *Enzymatic activation reactions modeled with MM equation.* ***(C)*** *Enzymatic activation reactions modeled with Hill function, n=2.* ***(D)*** *Enzymatic activation reactions modeled with Hill function, n=4. [34]*

Figure 12 shows that as a signal descends the cascade, it can be diminished (Figure 12B), or amplified (Figure 12C, D), based on Hill coefficient of the Hill function chosen for description of the reactions. In Figure 12B, an 81-fold change in the input ends up in 70% change in the ultimate output, ZP. Conversely, a $\sqrt{3}$-fold (70%) increase in the input of the cascade when Hill coefficient is n=4, yields an 81-fold increase in the ZP.

Impact of ultrasensitive responses on bistability and oscillations will be discussed in the following section of this thesis.

2.3.2 Bistability and Oscillations

Complex circuitry of inhibitory and activating feedbacks are responsible for coordinating dynamics of the components of ERK signaling pathway [40]. Before being able to predict behavior of the cell and intervene with it, systems biologists need to discover and understand the

mechanism of regulatory feedback motifs. When functionality and significance of the regulatory control modules are determined, it is feasible to regulate signal processing and output generation [41].

Feedback loops are ubiquitous in signal transduction pathways. Theoreticians investigated these control loops, because they can be well-explained in mathematical terms, and are versatile regulators identifying biochemical response of the signaling networks. Regulatory circuits are observed in multiple compartments of the cell such as regulatory loops inside the cytoplasm and nucleus, autocrine loops, and transcriptional feedback loops [14], [40], [42].

In a bistable regime, the dynamical system can settle on either of the two-discrete stable steady-states depending on its initial conditions. Biological systems usually exhibit the bistability property for a subset of their inputs. A bistable response is considered as 'digital' compared with graded or 'analog' response [43]–[45]. Positive feedback or double negative feedback loops can generate bistable responses. They can convert linear dose responses to steep sigmoidal ones. Hysteresis, as an inseparable feature of the bistable curves, explains steady-state behavior of the system in the case where reverse changing of an input to its initial value does not necessarily result in the initial value of the output. In other words, the value of the input leading to the on (off) state, depends on previous state of the system; therefore, hysteresis accounts for 'biochemical memory' of the system [46].

Negative feedback loops are crucial to maintain homeostasis for several important variables in the cell, i.e. concentration of proteins involved in cellular reactions. As a rule, negative feedbacks tend to counteract any adverse changes and bring back the system to its desired target state, which confirms their stabilizing feature [28].

Positive feedback action when it is too strong, may result in destabilization of the system, or in oscillatory behavior. Generally, oscillations are outcome of the combination of positive and negative feedback loops for a specific range of their strengths. In principle, negative and positive

regulators can yield a wide range of dynamic and static responses when they are interconnected [47].

Tian et al. [48] proposed a minimal model for a gene regulatory system, in which positive and negative FBLs (feedback loops) are coupled (Figure 13). They explain how this system can function as a bistable switch and oscillator by adjusting the feedback strengths. Mathematical investigation shows that the system moves from monostability to the bistable regime by increasing the positive feedback strength. Next, when strength of the negative feedback increases, the oscillatory behavior emerges. This trend is reversed in response to the further rise of positive feedback strength. Moreover, they prove that coupled feedback loops are more flexible compared with the single ones. For example, oscillations out of a single time-delayed negative feedback loop have smaller amplitude and are responsive to a narrower range of stimulus rather than the oscillatory behavior reported in this system.

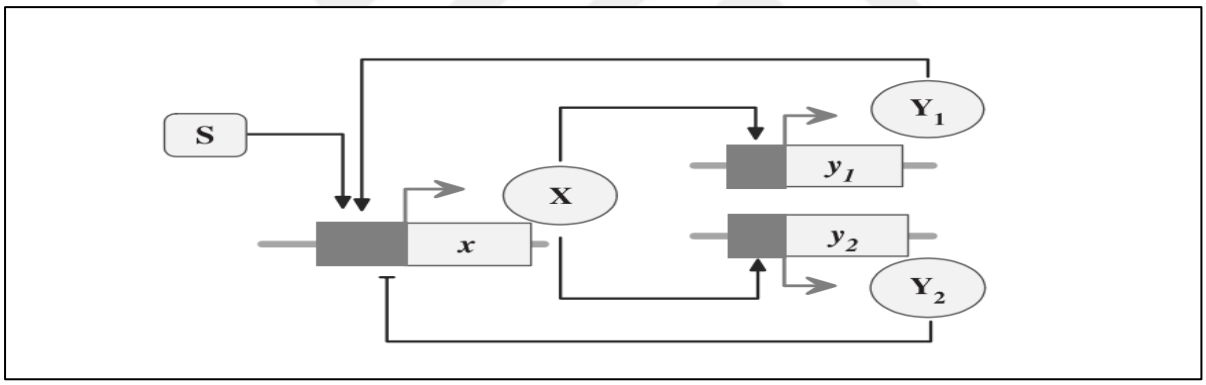

Figure 13 - Tian et al. [48] minimal model of the gene regulatory network.

The transcription factor X, triggers expression of the genes, y1 and y2. Y1 upregulates X, forming a positive feedback loop. Y2 suppresses X, forming a negative feedback loop. S is an external stimulus.

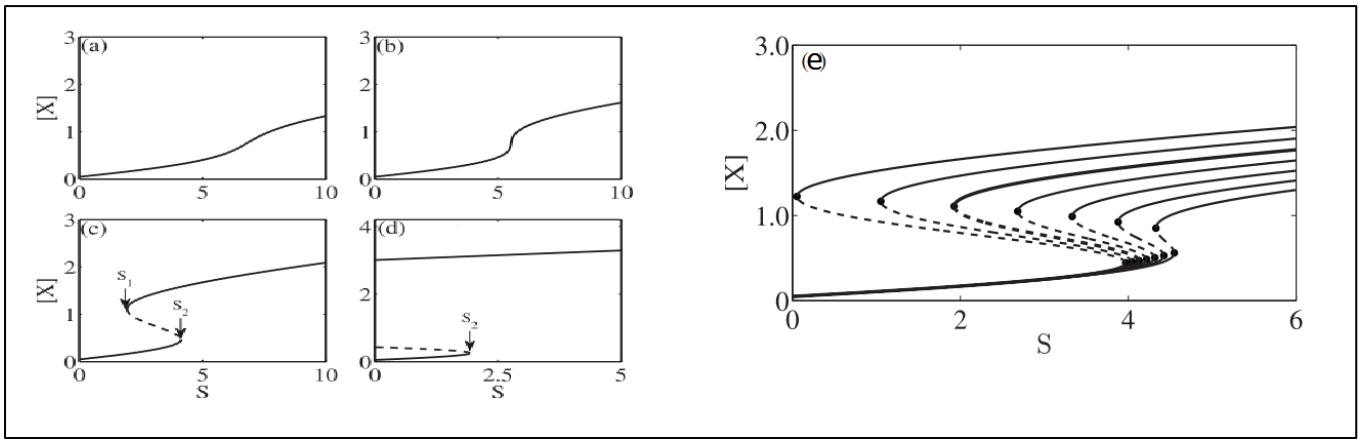

*Figure 14- **(a-d)** The effect of positive feedback**:** While the strength of negative feedback is kept constant, the strength of positive feedback increases gradually. **(e)** The strength of negative feedback is increased from the left to the right. The thick black line is the curve in figure (c). [Figure modified from [48]]*

Figure 14(a-d) represents how increasing the strength of positive FBL creates a bistable regime. In Figure 14(c), continuous input is changed to a discontinuous reversible switch. Owing to hysteresis, if the input, S, changes to a value in the range between S_1 and S_2, [X] can settle on either of higher or lower stable steady-state branch depending on the *previous* state of [X]. Figure 14(d) shows that by further enhancement of the strength, this switch becomes irreversible, meaning that if the system is switched on it will stay on, even after the stimulus is totally removed. As effect of the negative FBL increases, bistable region of the system shrinks accordingly (Figure 14(e)).

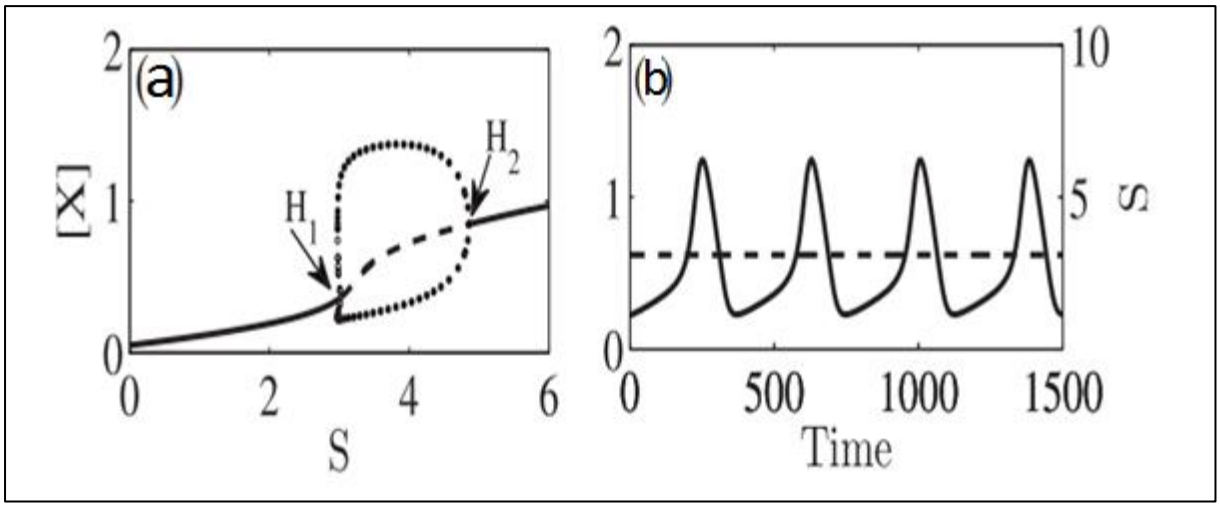

Figure 15 - The dynamics and the bifurcation diagram of Tian et al. [48] system under the strong negative feedback. ***(a)*** *The presence of two Hopf bifurcation points.* ***(b)*** *The dynamics of [X] for S=3.1. [Modified form [48]].*

When the strength of negative feedback is large enough, for the range of input between H_1 and H_2, the system demonstrates sustained oscillations. It is worth mentioning, that this type of oscillations occurs in the absence of a time delay and based on hysteretic bistability of the system (due to the presence of the positive feedback loop) [49], [50]. In this regime, the negative feedback is strong enough to make the system switch back and forth between discrete stable states generated by the positive FBL. This kind of hysteresis-driven oscillatory behavior is also known as a subset of the relaxation oscillations. In this type of non-sinusoidal oscillations, in each cycle the output undergoes a gradual, slow rise (fall) and then falls (rises) to the minima (maxima) abruptly [48], [51].

ERK shapes the cell's outcome by implementing its impact via distinct regulatory loops. For example, the activated ERK negatively affects SOS-complex formation. SOS-Grb2 is dissociated because of SOS phosphorylation by ERK, which in turn suppresses Ras activation [40], [52]. The reduced Ras activity is transmitted to the ERK itself, through Ras-Raf-MEK-ERK pathway. Therefore, a negative FBL started by phosphorylation of SOS is generated [40]. In principle, topology of the FBLs and the value of parameters included in the reaction kinetics are two major factors in determination of the signaling pattern [48], [53], [54]. Figure 15, borrowed

from Kholodenko et al. [53], illustrates six different dynamics of the activated ERK classified according to the inclusion of feedback loops and the parameter values.

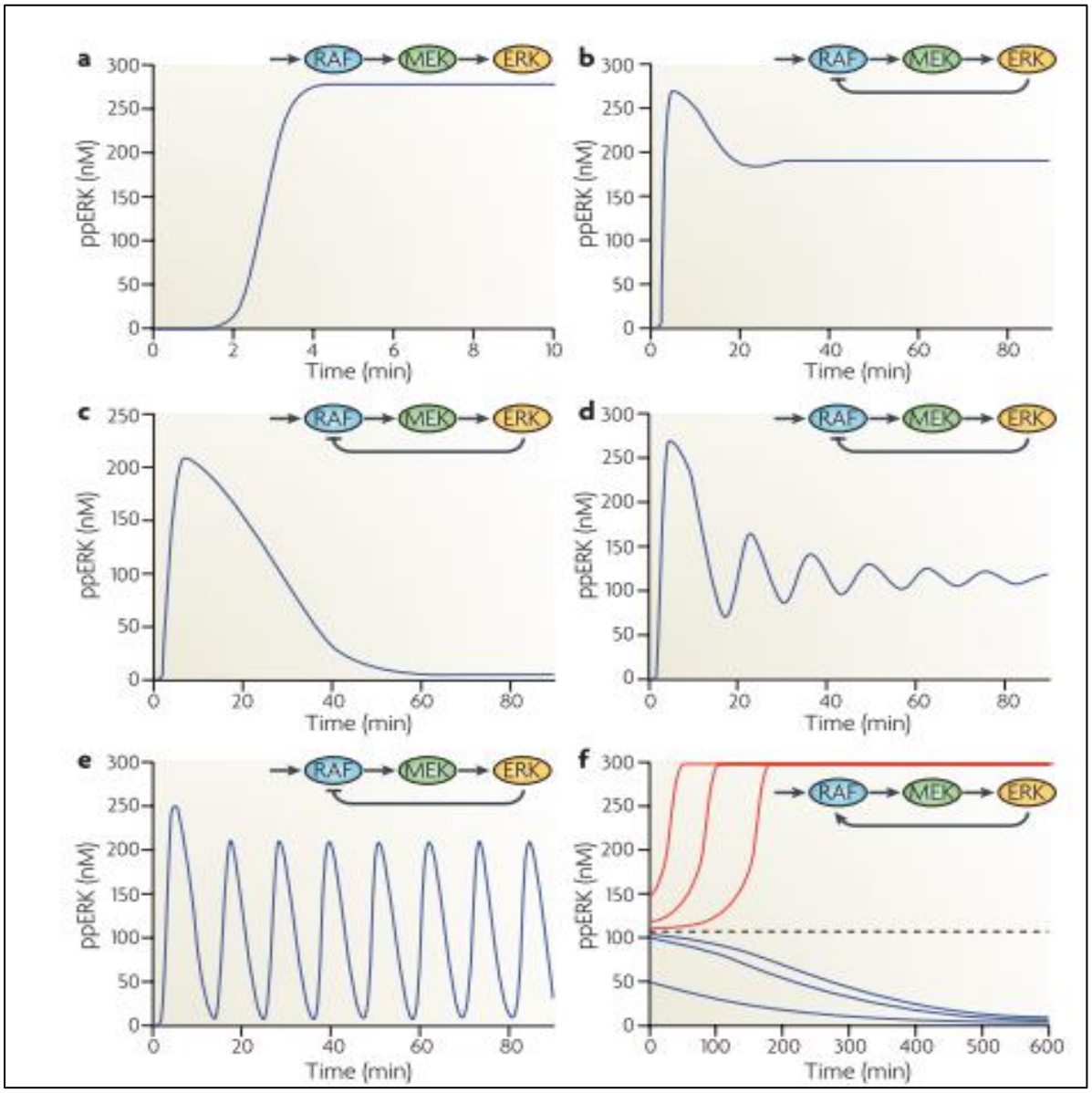

Figure 16 – The classification of ERK dynamics. The input to the system is constant Ras-GTP concentration. ***(a)*** *$RasGTP \rightarrow Raf \rightarrow MEK \rightarrow ERK$ cascade without any feedback* ***(b-e)*** *The same cascade with the included negative feedback. The strength of negative feedback is different in each plot.* ***(f)*** *Including a positive feedback from ERK to RAF. For the initial conditions above the dashed line activated ERK approaches high activity steady state (switch on), while for the initial conditions below the threshold it settles on the lower steady state (switch off) [53].*

The noteworthy message of the Figure 16 is that the same feedback loop can bring about completely distinct dynamics, owing to the changing of strength and parameter values. The importance of this message becomes clearer, when it is reminded that these distinct dynamics are related to the specific cell decisions.

As proposed by Brightman et al. [21] different dynamics of ERK in response to EGF compared with NGF (nerve growth factor), is predominantly based on the differences in integration of the negative regulators, not the intensity of receptor signaling [55]. It was observed that EGF-induced pathway demonstrates transient ERK dynamics, while being induced by NGF leads to the sustained ERK activation, each ending up in a different cell fate [4][1][21]. Both ligands activate ERK and in both cases, activated ERK downregulates Shc-Grb2-SOS complex, however, in case of NGF after a transient downregulation of SOS complex, Grb2-SOS complex is rapidly reformed and causes a second sustained phase of ERK and MEK activation [21].

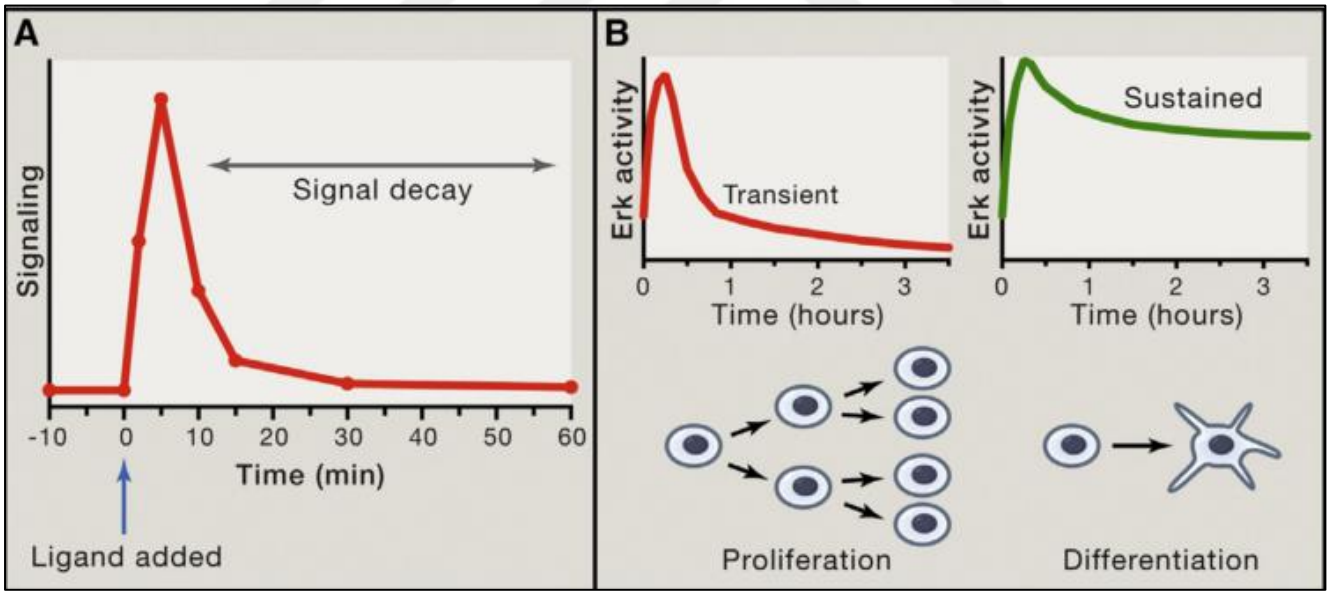

Figure 17 - PC12 cell fate in response to EGF vs. NGF [55]

Qiao et al. [44] took a statistical approach in studying the MAPK pathway model offered by Huang and Ferrell , Figure 18. They generated 20000 parameter sets and developed a procedure to classify the input-output relationships out of these generated models. It was shown that almost 80% of the models exhibited single-valued input-output relationship, while each of bistable and oscillatory responses comprise for 10% of the provided results, Figure 19.

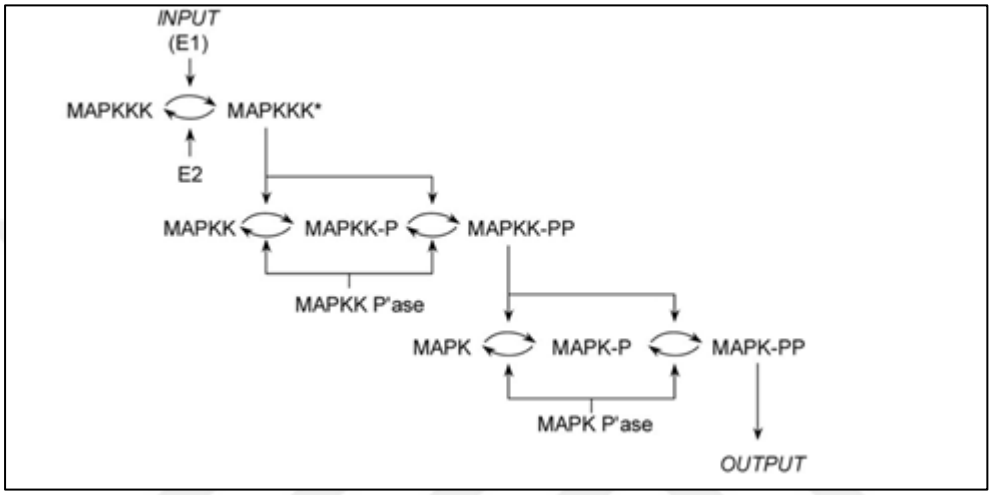

Figure 18 - Huang and Ferrell model of MAPK pathway [44]

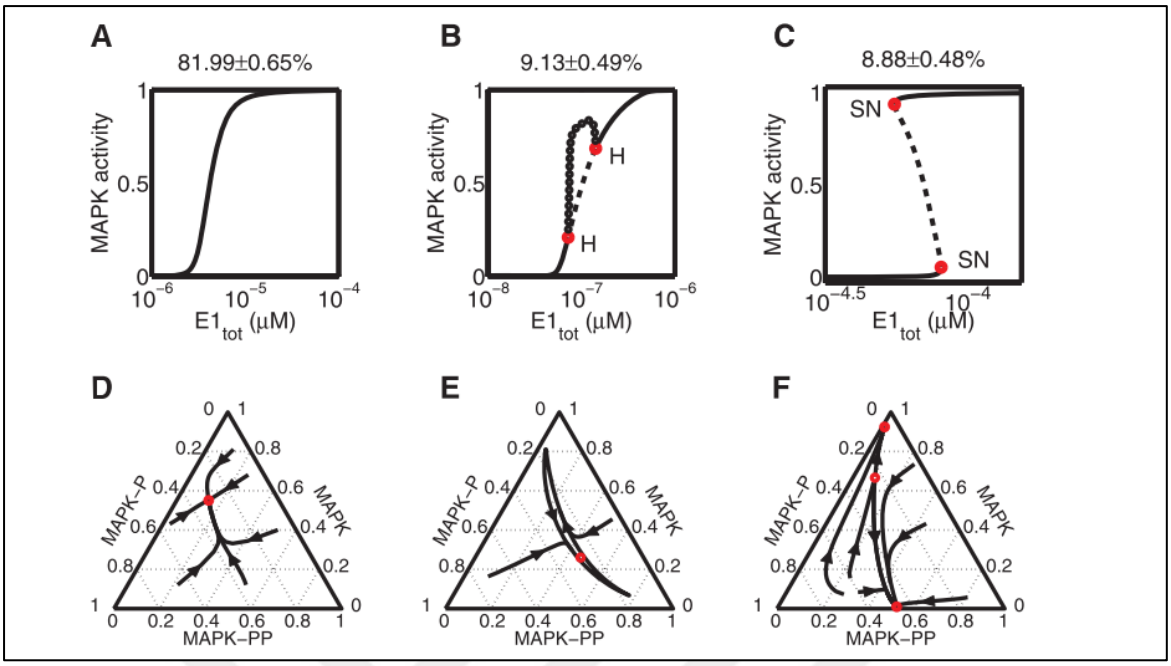

Figure 19 - Three distinct classes of input-output relationship of MAPK signaling pathway proposed by [44] ***(A)*** *"Single-valued" class. It is the most frequent type of responses.* ***(B)*** *"Oscillatory" class. The red points labeled with H denote Hopf bifurcation points.* ***(C)*** *"Hysteretic class". This category of the responses is also known as bistable regime. The red point labeled with SN denote Saddle-node points. They appear where stable branch merges into unstable one.* ***(D-F)*** *The phase diagrams. E1tot is set to* $10^{-5.5}$, 10^{-7} *and* $10^{-4.1}$ *from left to the right. The red points denote steady-state values.*

It was stressed that although the first stage of MAPK pathway is monostable, the other two which consist dual phosphorylation of the kinases, support bistability. Qiao et al. further proved that, theoretically, the necessary condition for generating multistage oscillations, is the existence of a bistable stage.

2.4 ERK-mediated processes in the nucleus

2.4.1 Feedback Loops

Autocrine loops are a certain type of positive feedback loops managing pattern of the cellular responses, exploiting extracellular components [56]. Autocrine signaling, a positive feedback loop is constructed as follows: pathways induced by the specific ligands participate in

releasing the same ligands which further stimulate them [57]. Ligand-releasing proteases, known as *sheddases*, can be activated by the same pathways which are induced by released ligands. In particular, EGFR/ERK/Rhomboid/Spitz positive feedback loop was studied in epithelial layers by Přibyl et al. [58].

The autocrine mechanism includes several steps (Figure 20), namely, ligand-receptor binding, transport of the ligand and intracellular processes involving transcription and new proteins synthesis [58]. Intracellular processes take place on a relatively slower dynamics compared with other steps; therefore, ligand-releasing proteases can be modeled to be produced as a function of ERK concentration.

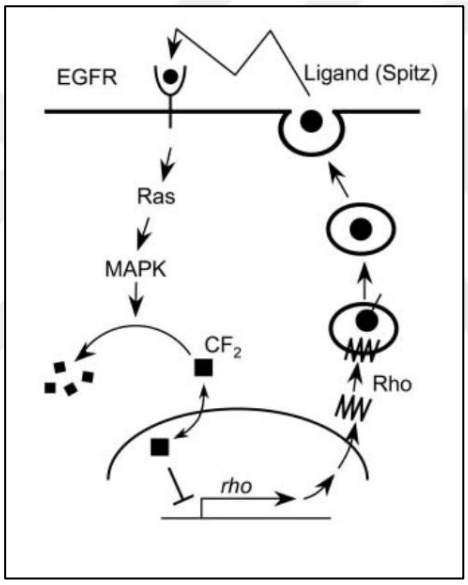

Figure 20 - Autocrine positive feedback loop [58].

Shvartsman et al. [57], studied the dynamics of autocrine feedback loop including Argos as the inhibitor of EGFR (Figure 21). In their model, protein Gurken acts as the localized input for the EGFR on the surface of *follicle cells;* induced ERK pathway activates several genes in response to this stimulus. ERK signaling induced by Gurken is then spatially expanded and amplified by the positive feedback from Rhomboid and another secreted EGFR ligand called Vein. However, among the large number of negative regulators of EGFR, an endogeouns inhibitor, Argos, downregulates EGFR signaling. Argos which is a secreted protein interacts directly with

the EGFR leading to inhibition of ERK signaling which was induced by Gurken, Vein and Spitz [59].

Klein et al. [60], observed biochemically that Argos downregulates EGFR activation by isolating Spitz, corresponding ligand for the EGFR. Long-range effect of Argos can be explained in two ways. First, it isolates EGFR ligands right after their releasing, thus preventing them to reach distant cells. Second, by diffusing in the distant cells and sequestration of the ligands away from their secretion point. It is worth mentioning, that Argos association with Spitz is stronger than Spitz binding to EGFR, and fundamentally irreversible [60], [61].

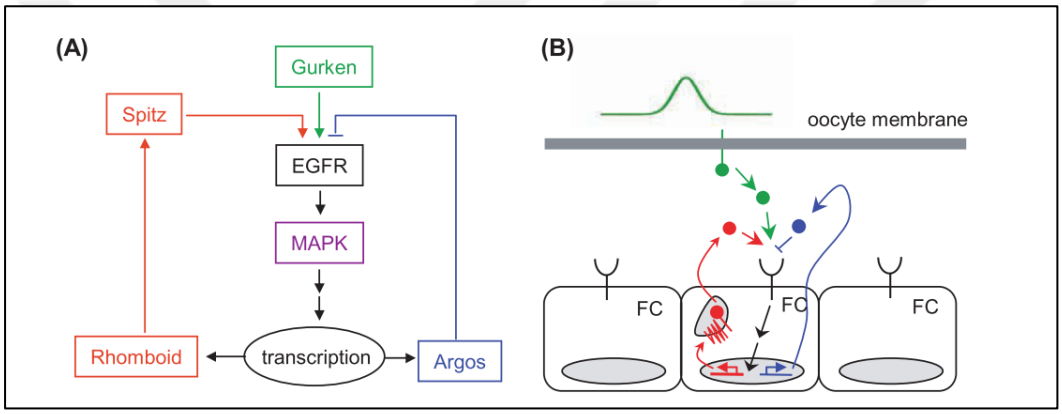

Figure 21 -The ligands inducing EGFR in follicle cells [57] ***(A)*** *EGFR is induced by two ligands, Spitz from autocrine loop and Gurken released form oocyte. Argos inhibits EGFR.* ***(B)*** *The Gurken released from oocyte (green). Spitz ligands (red) and Argos (blue).*

It was shown in another study [62] that autocrine loops give rise to context-dependent cell signaling. Specifically, in ERK signaling pathway, the autocrine positive feedback loop can modulate amplitude and duration of the ERK activation. The dynamic interactions between different parts of an autocrine loop shape signals characteristics. Consequently, the same external stimulus to two cells benefiting from similar intracellular signaling capabilities but different mechanisms in the secreting and employing autocrine ligands, may result in distinguished responses from the cells [62].

2.4.2 Cell cycle

Cell proliferation is defined as production of two cells from one, where cell growth is followed by cell division. Since uncontrolled cell proliferation results in cancer, cell cycle must be tightly regulated.

The cell cycle comprises four sequential stages: G_1, S, G_2 and M. Mitosis (M) and synthesis (S) phases are separated by two gap phases (G_1, G_2). Cyclin-dependent kinases (Cdks) drive the cell through these stages by turning specific proteins, corresponding to each stage, on and off. However, Cdks become activated when associated with the cyclin proteins. Since cyclins are produced and degraded during the cell cycle, they can provide a temporal regulation over the cyclin-Cdk complexes. Figure 22 represents the cell cycle along with Cdk cycle.

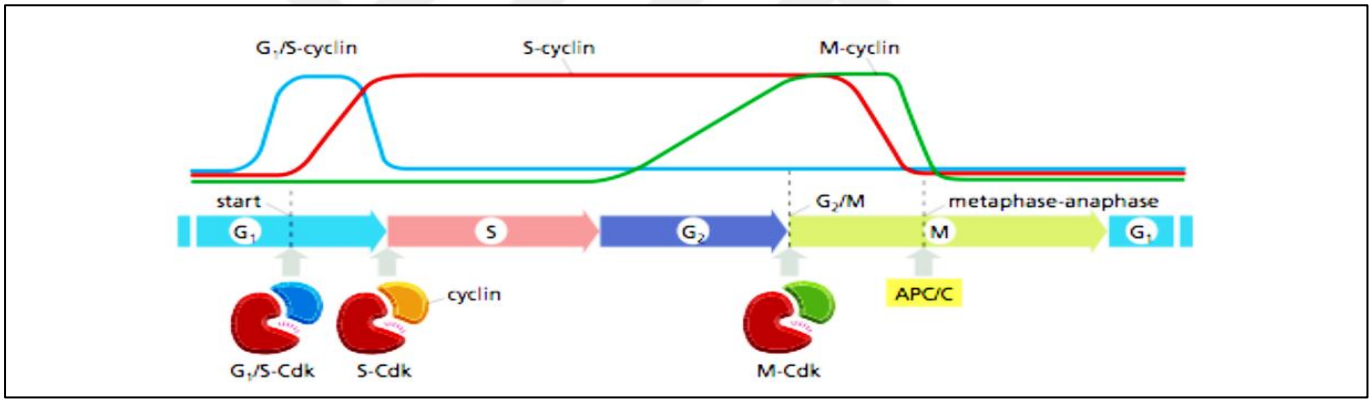

Figure 22 - The cell cycle along with Cdk cycle [63].

Extracellular signals can affect the cell cycle only during the G_1 phase. *Restriction point* is a crucial point in late G_1 after which the cell is committed to undergo S phase even though the growth factor-dependent signal is removed. This point, also referred to as Start, is usually dysregulated in the cancerous cells [63]. Transcription and synthesis of the cyclin E is one of the crucial steps in order to enter late G_1 phase. For this end, the transcription factor E2F should be activated, but E2F is bound to another protein called Rb (rebinoblastoma). Rb which has a key role in regulating cell proliferation becomes activated in an underphosphorylated state [64][63].

Therefore, Rb functions as a ‘brake’ for the cell cycle and the cyclin D-dependent kinases are responsible to release this brake by deactivation (phosphorylation) of the Rb protein (Figure 23) [64][12].

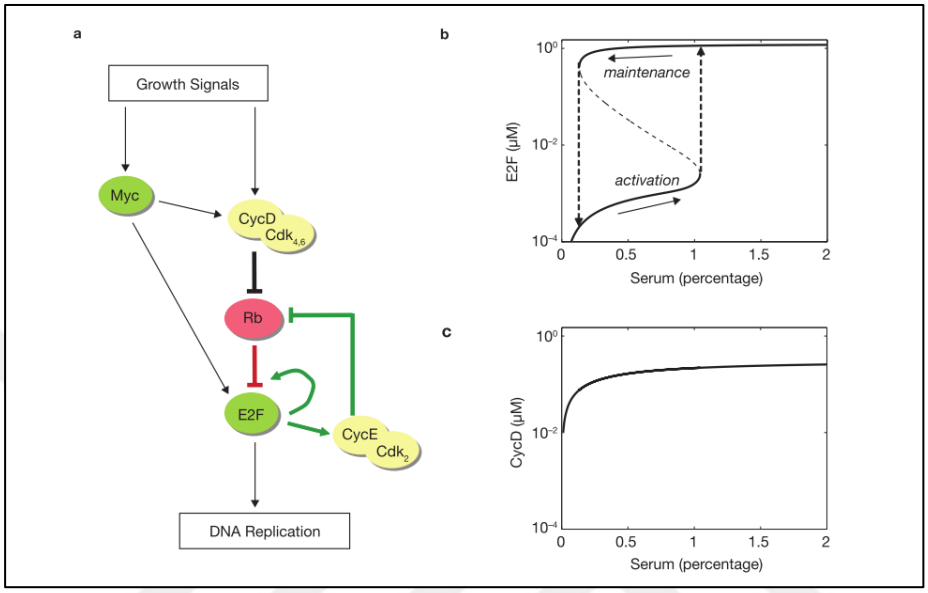

Figure 23 - The positive feedback loop leading to Rb-E2F switch [12].

Figure 23 represents positive feedback loop between the proteins regulating cell cycle entry, E2F expression increases cyclin E, which in turn phosphorylates and inhibits Rb, which means more E2F production. This positive feedback loop creates a bistable switch that determines whether the cell should enter DNA replication phase or not (Figure 23b) [12]. After a certain threshold for the input, this switch is ON, which means Rb is inhibited and E2F is in its active form. However, when the cell is in the quiescent state, the switch is OFF and E2F settles on the inactivated stable steady-state [12][64]. This simplified model was built by Guang Yao et al. [12] to account for the qualitative behavior of this control system, thus it does not include upstream signals triggering this Rb-E2F pathway.

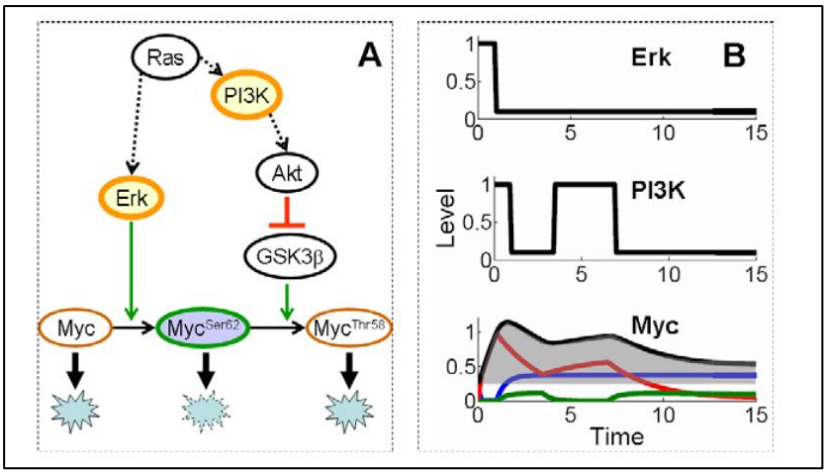

*Figure 24- Myc protein as the signal integrator for ERK and PI3K signals [65]. **(A)** The active Ras activated its downstream pathways, ERK and PI3K. The active ERK catalyzes Myc phosphorylation at Ser62 residue, to its stable form Myc^{Ser62}. The active PI3K inhibits GSK3β from phosphorylating Myc^{Ser62} to the unstable Myc^{Thr58}. **(B)** The effect of ERK and PI3K dynamics on Myc dynamics. [Myc^{Ser62} (red line), Myc^{Thr58} (green line), unmodified Myc (blue line) and total Myc level (black line)].*

Active ERK when translocated to the nucleus, phosphorylates transcription factors to promote cell proliferation. *Myc* protein, the product of *c-Myc* gene, is one of these essential transcription factors which is upregulated by the ERK [66], [67]. Tae Lee et al. [65] exploited a well-defined signaling module, named dual-kinase motif, to address *Myc* regulation. In particular, *Myc* plays the pivotal role of a signal integrator of its upstream signals (Figure 24). This model shows that *Myc* is sensitive to the temporal features of ERK and PI3K, but not to the maximum amplitude of them. The strong enough ERK pulse leads to the conversion of unmodified *Myc* to the stable Myc^{Ser62}, PI3K pulses inhibit further phosphorylation of Myc^{Ser62} to the Myc^{Thr58}.

Chapter 3: Models and Methods

3.1 Systems Biology Approach

When facing a natural phenomenon, a scientist can choose either of two approaches: reductionist or systems approach. In a reductionist approach, the object is decomposed to several parts and each part is disconnected from other parts and evaluated separately. In this fashion, it is hard to see the big picture. On the other hand, in systems approach, the system is analyzed as a whole by paying attention to the interactions among its detached components [68].

Recent breakthroughs in molecular and computational biology have set the ground for application of a systems approach to the biological systems. While study of the genes and proteins is still important, systems biology approach tries to understand the structure and dynamics of the system. In systems biology, the emphasis is on the most outstanding pattern that data suggests. If we consider biological cartoons as roadmaps, Hiroaki Kitano [69] believes systems biology helps us to reveal traffic patterns, reasons for their emergence and ways to control them.

In this thesis, we seek to get insight about the structure, dynamics and control of the ERK signaling pathway. Success in any of these properties is a significant step toward construction of more useful models that pave the way for spotting malfunctions and comprehending causality relationships between the signaling molecules.

3.2 Mathematical Modeling

In this thesis, we model and analyze the ERK signaling pathway. In the literature, there

exist mathematical models built for the distinct parts of this pathway. However, in the present work, we developed and reconstructed a thorough model of the system starting from the ligand binding step to the nuclear processes mediated by the ERK.

Several feedback loops which are embedded in the ERK signaling pathway were closely studied and the range of the parameters leading to specific responses were identified. In particular, feedback loops were added based on an intensive literature review for the purpose of justifying experimental observations or in some cases for providing new hypotheses subject to further validation.

Figure 25 represents the whole system including the feedback loops. For the sake of simplicity, the cell cycle reactions are not shown in this figure. They will be shown and explained in the last section of this chapter.

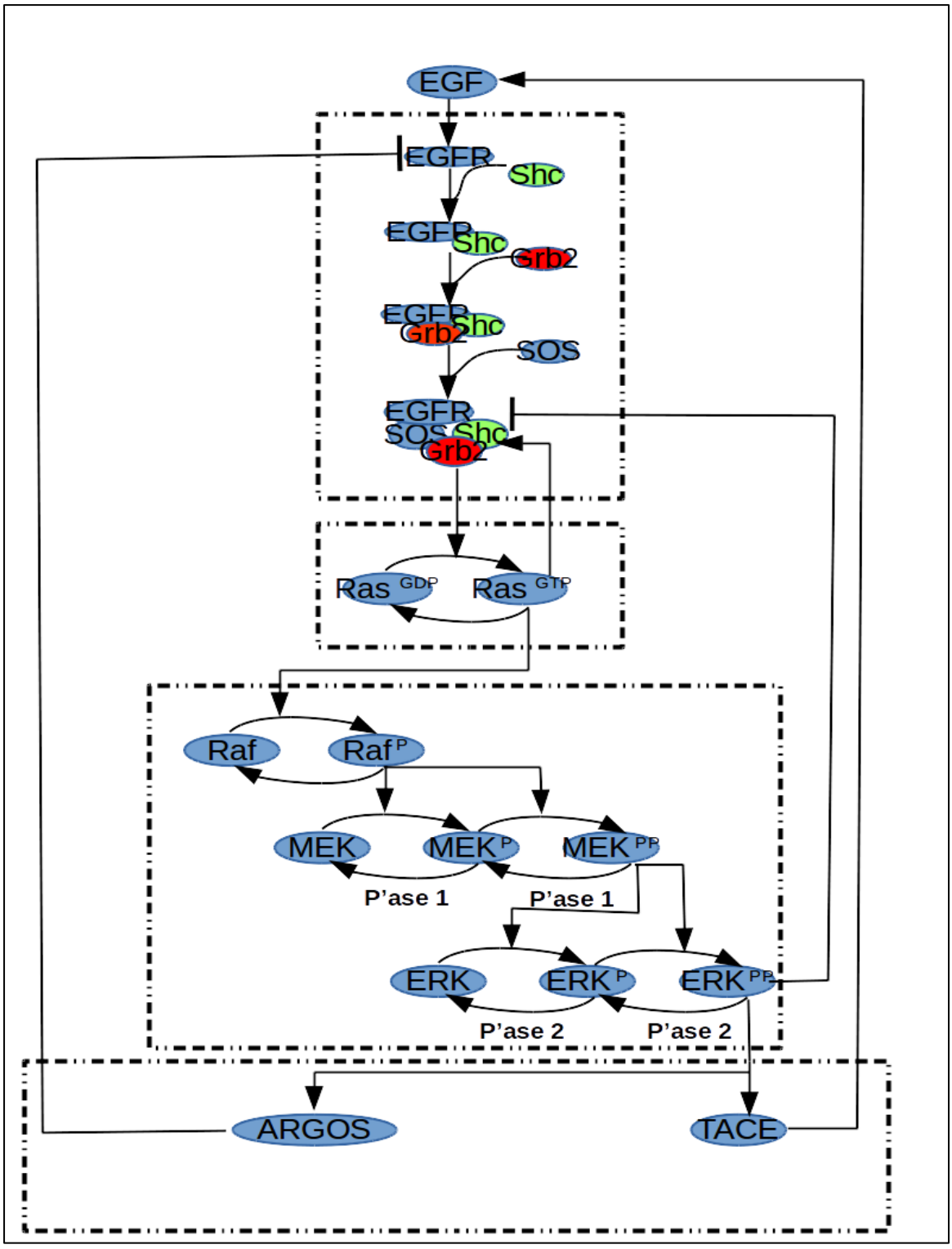

Figure 25 - The topological structure of the complete system (the cell cycle excluded).

Although the basis for a mathematical model is the topological representation of the system, it is the detailed description of reactions which empowers the model to explain complex biological behaviors. Kinetic reactions explain the interactions between signaling molecules. These reactions are formulated in terms of mass action law expressed as ODEs which in turn account for mass balance of the molecules. Steady-state values of the species are obtained from the same ODEs by setting the time derivatives equal to zero.

Algebraic equations are also included in the mathematical model to account for the conservation of the total amounts of the species which are distributed among different forms (i.e. active, inactive, bound to enzyme).

We tried to keep the models as simple as possible while capturing the dominant qualitative response of the system to the inputs. For this end, signaling molecules or intermediate species were lumped as needed. Kinetic and conservation laws were applied and quasi-steady state (QSS) assumption was employed where it is applicable for the enzymatic reactions (see Appendix I).

The complete model comprises 46 ordinary differential equations, 17 algebraic equations and 143 parameters. The mathematical analysis techniques, i.e. bifurcation analysis, parameter sensitivity and dynamics simulation were done in *XPPAUT* software (http://www.math.pitt.edu/~bard/xpp/xpp.html) and in Matlab (https://www.mathworks.com/). The plots were reproduced in Matlab as well. Input files for *XPPAUT* are text files which contain the mathematical models, and they can be found in Appendix II.

3.2.1 EGFR signaling model – Model 1

Kinetic structure of Model 1 which was borrowed from [7], starts from binding of EGF to its receptor, EGFR. Upon ligand binding, activated EGFR recruits adapter proteins Grb2 and Shc. SOS protein further binds to this complex in order to form EGFR-SOS-Grb2-Shc complex. However, when SOS-Grb2-Shc dissociates from EGFR, it can activate Ras in its downstream.

Figure 26 shows the lumped structure of this model, and Table 2 represent the kinetic reactions and nominal parameter values.

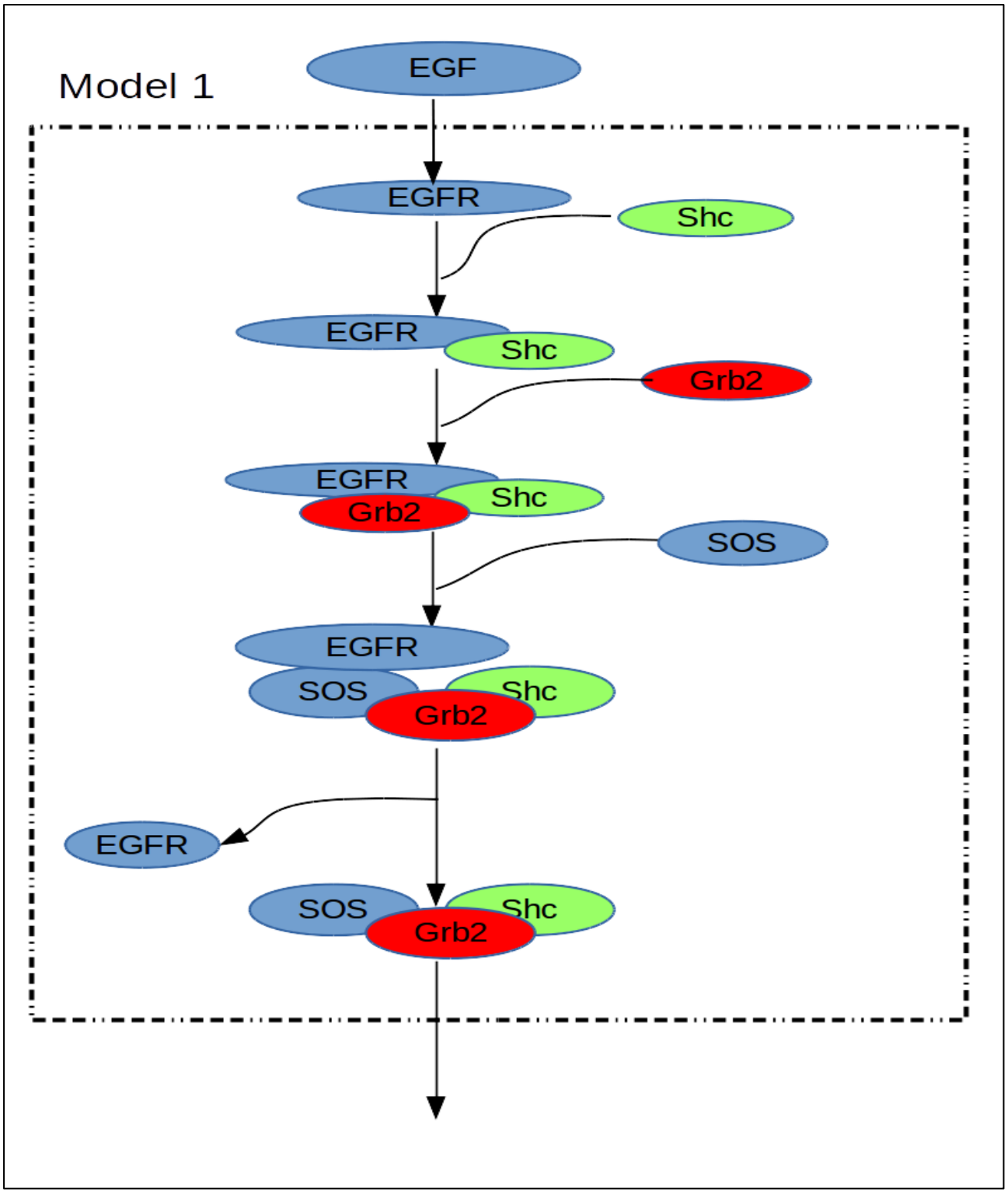

Figure 26 - The topological representation of Model 1. Adapted and modified from [7].

Table 2 - The parameter values and the reactions for Model 1. Concentration and MM constants in (nM). Vu's in $(nM * s^{-1})$ *. First-order rate constants in* (s^{-1})*, second-order rate constants in* $(nM^{-1} * s^{-1})$ [7].

Reaction No.	Parameter value	Reaction
1	kf1=0.003, kb1=0.06	kf1*[EGFR*EGF]-kb1*[EGF_EGFR]
2	kf2=0.01, kb2=0.1	kf2*[EGF_EGFR]*[EGF_EGFR]-kb2*[(EGF_EGFR)2]
3	kf3=1, kb3=0.01	kf3*[(EGF_EGFR)2]-kb3*[(EGF_EGFR)2-P]
4	Vu4=450, Ku4=50	Vu4*[(EGF_EGFR)2-P]/(Ku4+[(EGF_EGFR)2-P])
5	kf5=0.06, kb5=0.2	kf5*[(EGF_EGFR)2-P]*[PLCg]-kb5*[(EGF_EGFR)2_PLCg]
6	kf6=1, kb6=0.05	kf6*[(EGF_EGFR)2_PLCg]-kb6*[(EGF_EGFR)2_PLCg-P]
7	kf7=0.3, kb7=0.006	kf7*[(EGF_EGFR)2_PLCg-P] -kb7*[(EGF_EGFR)2-P]*[PLCg-P]
8	Vu8=1, Ku8=100	Vu8*[PLCg-P]/(Ku8+[PLCg-P])
9	kf9=0.003, kb9=0.05	kf9*[(EGF_EGFR)2-P]*[Grb2]-kb9*[(EGF_EGFR)2_Grb2]
10	kf10=0.01, kb10=0.06	kf10*[(EGF_EGFR)2_Grb2]*[SOS] -kb10*[(EGF_EGFR)2_Grb2_SOS]
11	kf11=0.03, kb11=4.5e-3	kf11*[(EGF_EGFR)2_Grb2_SOS] -kb11*[(EGF_EGFR)2-P]*[Grb2_SOS]
12	kf12=1.5e-3, kb12=1e-4	kf12*[Grb2_SOS]-kb12*[Grb2]*[SOS]
13	kf13=0.09, kb13=0.6	kf13*[(EGF_EGFR)2-P]*[Shc]-kb13*[(EGF_EGFR)2_Shc]
14	kf14=6, kb14=0.06	kf14*[(EGF_EGFR)2_Shc]-kb14*[(EGF_EGFR)2_Shc-P]
15	kf15=0.3, kb15=9e-4	kf15*[(EGF_EGFR)2_Shc-P] -kb15*[Shc-P]*[(EGF_EGFR)2-P]
16	Vu16=1.7, Ku16=340	Vu16*[Shc-P]/(Ku16+[Shc-P])
17	kf17=0.003, kb17=0.1	kf17*[(EGF_EGFR)2_Shc-P]*[Grb2] -kb17*[(EGF_EGFR)2_Shc_Grb2]
18	kf18=0.3, kb18=9e-4	kf18*[(EGF_EGFR)2_Shc_Grb2] -kb18*[(EGF_EGFR)2-P]*[Shc_Grb2]

(continued on the next page)

19	kf19=0.01, kb19=2.14e-2	kf19*[(EGF_EGFR)2_Shc_Grb2]*[SOS] -kb19*[(EGF_EGFR)2_Shc_Grb2_Sos]
20	kf20=0.12, kb20=2.4e-4	kf20*[(EGF_EGFR)2_Shc_Grb2_Sos] -kb20*[Shc_Grb2_SOS]*[(EGF_EGFR)2-P]
21	kf21=0.003, kb21=0.1	kf21*[Shc-P*Grb2]-kb21*[Shc_Grb2]
22	kf22=0.03, kb22=0.064	kf22*[Shc_Grb2]*[SOS]-kb22*[Shc_Grb2_SOS]
23	kf23=0.1, kb23=0.021	kf23*[Shc_Grb2_SOS]-kb23*[Shc-P*Grb2_SOS]
24	kf24=0.009, kb24=4.29e-2	kf24*[(EGF_EGFR)2_Shc-P]*[Grb2_SOS] -kb24*[(EGF_EGFR)2_Shc_Grb2_Sos]
25	kf25=1, kb25=0.03	kf25*[PLCg-P]-kb25*[PLCg-P-I]
Conserved moieties (nM)		
$[EGFR_{tot}] = 10$, $[EGF_{tot}] = 5$, $[PLC\gamma_{tot}] = 105$, $[Grb2_{tot}] = 85$, $[Shc_{tot}] = 150$, $[SOS_{tot}] = 50$.		

3.2.2 Ras activation model – Model 2

Model 2 represents the activation of Ras as shown in Figure 27. The reactions and parameter values for Model 2 are given in Table 3.

Table 3 - The parameter values for Model 2. Concentrations and MM constants in (nM), kfi in $(nM^{-1} * s^{-1})$, kbi and kcati in (s^{-1}) [10].

Index	Parameter values	Reactions
1	kfi1=1.125e-4, kbi1=3	$SOS_{complex} + RasGDP \underset{kbi1}{\overset{kfi1}{\rightleftharpoons}} SOS_{complex}\text{–}RasGDP$
2	kfi2=1.0625e-4, kbi2=0.4	$SOS_{complex} + RasGTP \underset{kbi2}{\overset{kfi2}{\rightleftharpoons}} SOS_{complex}\text{–}RasGTP$
3	kcati3=1, ki3m=2.7388e3	$SOS_{complex}\text{–}RasGTP + RasGDP \xrightarrow[Ki3m]{kcati3} SOS_{complex}\text{–}RasGTP + RasGTP$
4	kcati4=0.003,ki4m=1.52304e4	$SOS_{complex}\text{–}RasGDP + RasGDP \xrightarrow[Ki4m]{kcati4} SOS_{complex}\text{–}RasGDP + RasGTP$
5	kcati5=0.1, ki5m=1.7869e1	$GAPS + RasGTP \xrightarrow[Ki5m]{kcati5} GAPS + RasGDP$
Conserved moieties (nM)		
$\alpha = [SOS_{complex}] + [SOS_{complex} - RasGDP] + [SOS_{complex} - RasGTP]$ $\beta = [RasGDP] + [RasGTP] + [SOS_{complex} - RasGDP] + [SOS_{complex} - RasGTP]$		

Das et al. [10] showed that the allosteric reactions produce $SOS_{complex} - RasGDP$ and $SOS_{complex} - RasGTP$, each of which catalyzes the activation of *RasGDP* to *RasGTP* by different extents. Since $SOS_{complex} - RasGTP$ is more than 75 times active than $SOS_{complex} - RasGDP$, it is the dominant catalyst of *Ras* activation (phosphorylation), (see Figure 27).

For modeling activation/deactivation reactions of the *RasGDP/RasGTP,* Michaelis-Menten kinetics was employed, while allosteric reactions were explained by mass action kinetics.

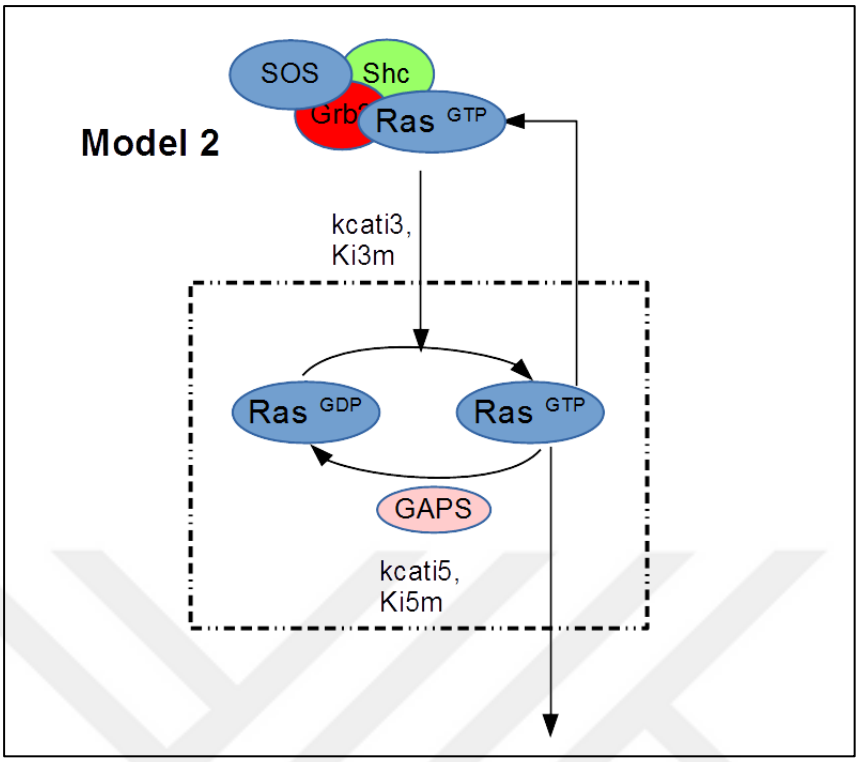

Figure 27 - Model 2 topological representation. Adapted from [10].

When this model is detached from the complete model and simulated separately, responses shown in Figure 28 are obtained. The reader is referred to Sec 3.2.6 for description of the positive FBL embedded in this mechanism (FBL 4).

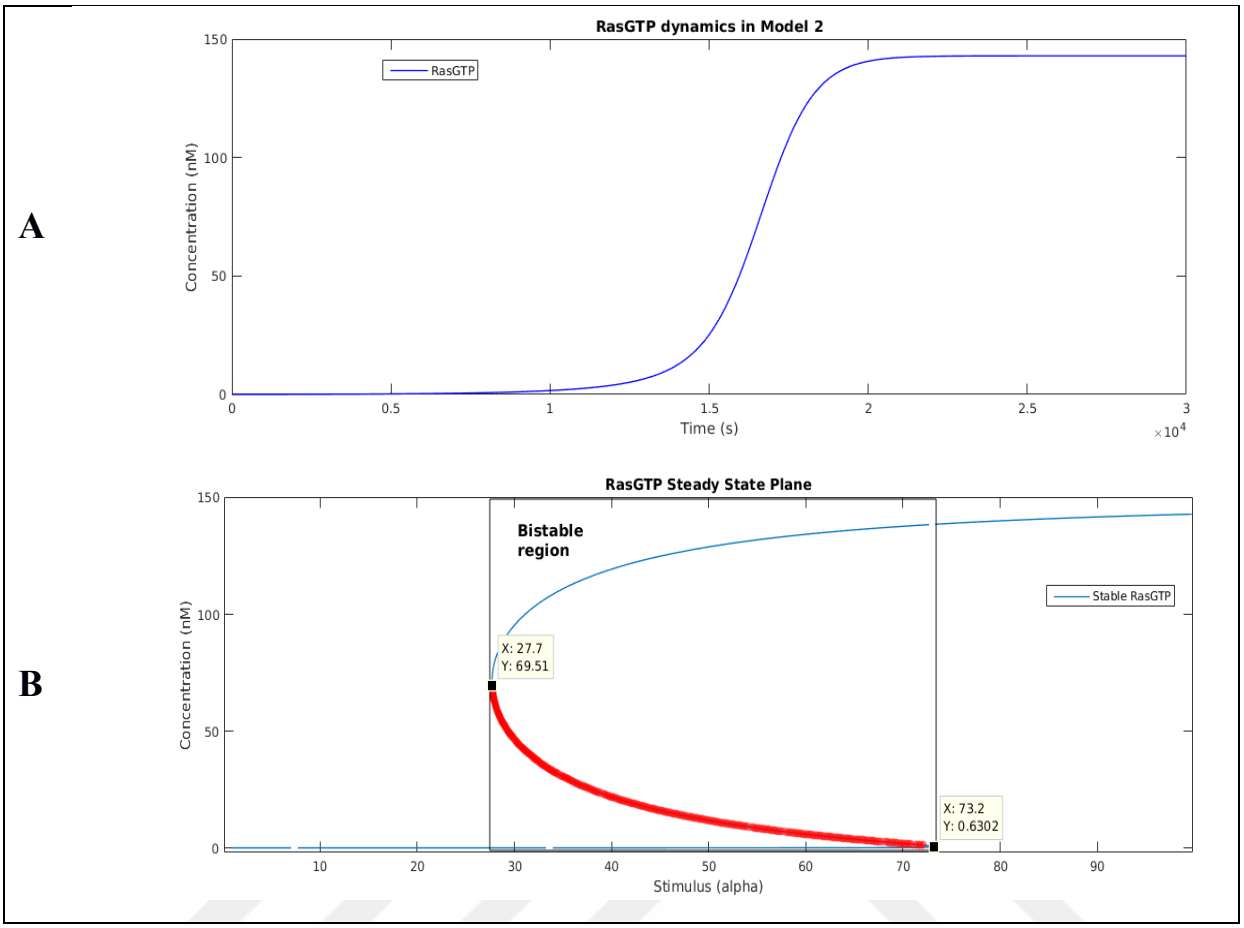

Figure 28 – The dynamics and steady-state plane of RasGTP in Model 2. ***(A)*** *RasGTP dynamics for β=160, GAPS=0.2. The stimulus is α and set to 100* ***(B)*** *The system bifurcation diagram with respect to the stimulus (α). A changed from 0 to 100. RasGTP is bistable for the 27.7 < α < 73.2.*

3.2.3 MAPK (ERK) cascade

The model for the three-tiered MAPK cascade is explained in this section. Activated Ras *(Ras-GTP)*, represented as E1 in Model 3, is the input for this part and consequently three kinases, namely, Raf, MEK and ERK become activated. Each activated kinase is the enzyme for the activation of the next step. MEK and ERK are fully activated when they are double phosphorylated. Specific phosphatase of each active kinase dephosphorylates it and makes it inactive.

Structure of this part is borrowed from [17]. Figure 29 provides the topological representation of the reactions and the signaling molecules. The reactions and the parameter values are given in Table 4.

Table 4 – The parameters and the reactions for Model 3. a in($nM^{-1} * s^{-1}$), d and k in(s^{-1}) [44].

Parameter values	**Reactions**
a1=0.00049; **d1**=0.049; **k1**=0.049;	$Raf + E_1 \underset{d1}{\overset{a1}{\rightleftharpoons}} Raf\text{–}E_1 \xrightarrow{k1} Raf^{P} + E_1$
a2=0.0307; **d2**=3.3078; **k2**=5.6407;	$Raf^{P} + E_2 \underset{d2}{\overset{a2}{\rightleftharpoons}} Raf^{P}\text{–}E_2 \xrightarrow{k2} Raf + E_2$
a3=0.0204; **d3**=10.3862; **k3**=7.0000;	$MEK + Raf^{P} \underset{d3}{\overset{a3}{\rightleftharpoons}} MEK\text{–}Raf^{P} \xrightarrow{k3} MEK^{P} + Raf^{P}$
a4=0.0493; **d4**=2.7167; **k4**=11.1367;	$MEK^{P} + P'ase_1 \underset{d4}{\overset{a4}{\rightleftharpoons}} MEK^{P}\text{–}P'ase_1 \xrightarrow{k4} MEK + P'ase_1$
a5=0.0564; **d5**=10.0885; **k5**=3.5775;	$MEK^{P} + Raf^{P} \underset{d5}{\overset{a5}{\rightleftharpoons}} MEK^{P}\text{–}Raf^{P} \xrightarrow{k5} MEK^{PP} + Raf^{P}$
a6=0.0326; **d6**=0.8134; **k6**=1.1328;	$MEK^{PP} + P'ase_1 \underset{d6}{\overset{a6}{\rightleftharpoons}} MEK^{PP}\text{–}P'ase_1 \xrightarrow{k6} MEK^{P} + P'ase_1$
a7=0.0038; **d7**=11.5688; **k7**=0.7276;	$MEK^{PP} + ERK \underset{d7}{\overset{a7}{\rightleftharpoons}} MEK^{PP}\text{–}ERK \xrightarrow{k7} MEK^{PP} + ERK^{P}$
a8=0.0050; **d8**=5.0182; **k8**=0.5291	$ERK^{P} + P'ase_2 \underset{d8}{\overset{a8}{\rightleftharpoons}} ERK^{P}\text{–}P'ase_2 \xrightarrow{k8} ERK + P'ase_2$
a9=0.0056; **d9**=8.0892; **k9**=1.0955	$ERK^{P} + MEK^{PP} \underset{d9}{\overset{a9}{\rightleftharpoons}} ERK^{P}\text{–}MEK^{PP} \xrightarrow{k9} ERK^{PP} + MEK^{PP}$
a10=0.0162;**d10**=9.7908;**k10**=2.9318	$ERK^{PP} + P'ase_2 \underset{d10}{\overset{a10}{\rightleftharpoons}} ERK^{PP}\text{–}P'ase_2 \xrightarrow{k10} ERK^{P} + P'ase_2$
Conserved moieties (nM)	
Raf_{tot} = 9.2235e-1, MEK_{tot} = 5.1288e2, ERK_{tot} = 8.1552e2, $E1_{tot}$ = 5e-2, $E2_{tot}$ = 3.2830e-1, $P'ase1_{tot}$ = 2.1238e-1, $P'ase2_{tot}$ =5.0345e2	

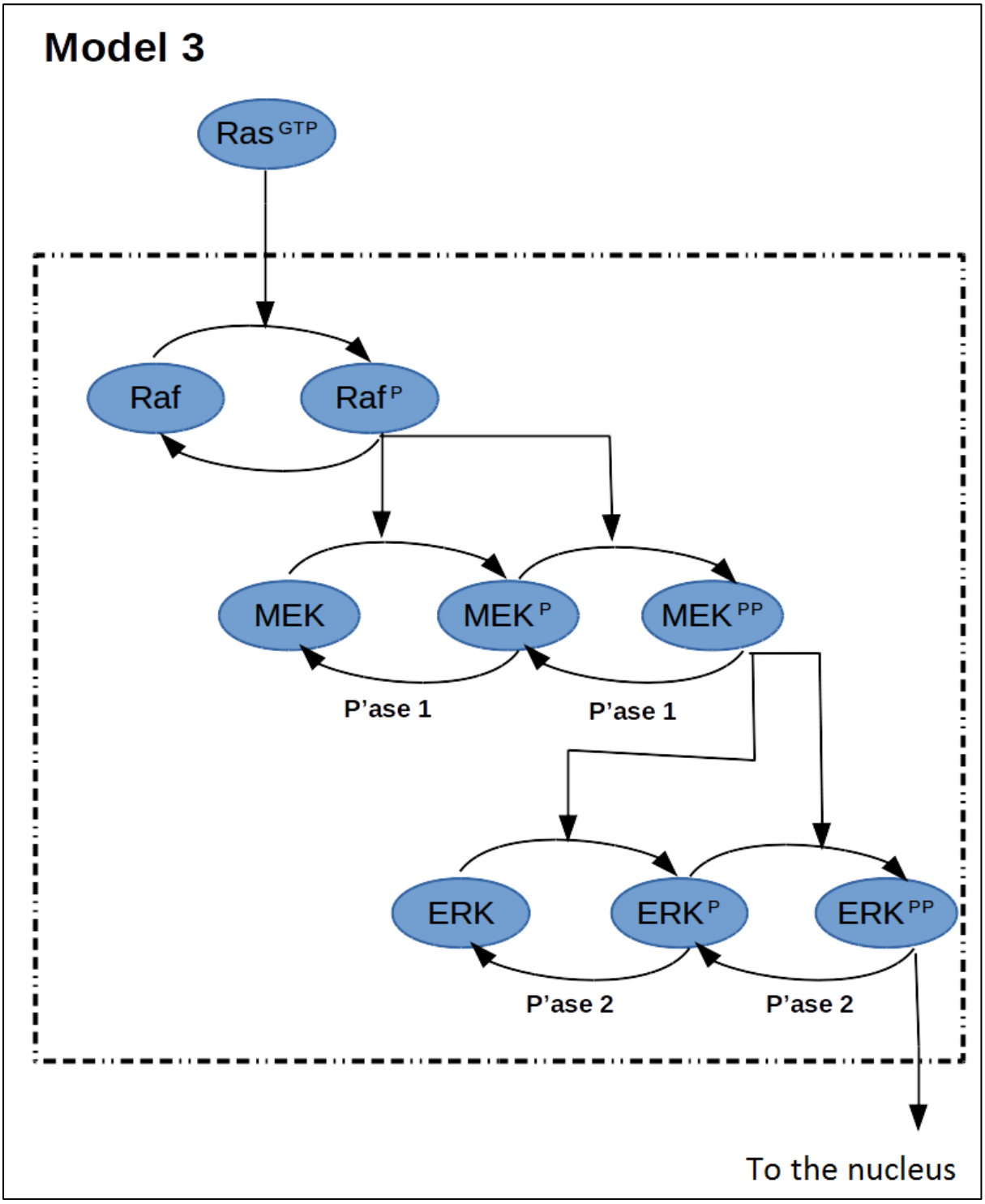

Figure 29 - The topological representation of Model 3. Adapted from [17]

3.2.4 Erk-mediated processes in the nucleus – Model 4

As discussed in the literature review, active ERK passes to the nucleus to phosphorylate many genes and eventually starts the cell cycle. Moreover, some of the transcribed genes produce specific proteins like ARGOS and TACE which effect the ligands triggering ERK signaling pathway, thus creating feedback loops. In this section, Model 4 describing the cell cycle (Figure 30) and formation of the stable Myc^{ser62} is discussed.

Table 5 – The parameters, reactions and kinetics for the Myc stability regulation model [65].

Parameter	Reaction	Kinetics
km=2.78e-4(s^{-1});	$* \xrightarrow{GF} Myc$	$k_M[GF]$
kAP=0.1(s^{-1}); KmAP=10(nM);	$Akt \xrightarrow{PI3K} Akt_p$	$\frac{k_{AP}[PI3K][Akt]}{K_{AP}+[Akt]}$
kAD=20.016($nM.s^{-1}$); KmAD=10(nM);	$Akt_p \longrightarrow Akt$	$\frac{k_{AD}[Akt_p]}{K_{AD}+[Akt_p]}$
kGP=0.1(s^{-1}); KmGP=10(nM);	$Gsk3\beta \xrightarrow{Akt_p} Gsk3\beta_p$	$\frac{k_{GP}[Akt_p][Gsk3\beta]}{K_{GP}+[Gsk3\beta]}$
kGD=20.016($nM.s^{-1}$); KmGD=10(nM);	$Gsk3\beta_p \longrightarrow Gsk3\beta$	$\frac{k_{GD}[Gsk3\beta_p]}{K_{GD}+[Gsk3\beta_p]}$
kMS=6.4e-4(s^{-1}); KmMS=2.8e-3($nM.s^{-1}$);	$Myc \xrightarrow{Erk} Myc^{Ser62}$	$\frac{k_{MS}[Erk][Myc]}{K_{MS}+[Myc]}$
kMT=1.12e-4(s^{-1}); KmMT=2.8e-3($nM.s^{-1}$)	$Myc^{Ser62} \xrightarrow{Gsk3\beta} Myc^{Thr58}$	$\frac{k_{MT}[Gsk3\beta][Myc^{Ser62}]}{K_{MT}+[Myc^{Ser62}]}$
dM=5.78e-4 (s^{-1});	$Myc \longrightarrow *$	$d_M[Myc]$
dMS=9.73e-5(s^{-1});	$Myc^{Ser62} \longrightarrow *$	$d_{MS}[Myc^{Ser62}]$
dMT=5.78e-4(s^{-1});	$Myc^{Thr58} \longrightarrow *$	$d_{MT}[Myc^{Thr58}]$

In the next table, we give the kinetics and the parameters for the cell cycle model.

Table 6 - The cell cycle Model 4 parameter values [12].

Parameters	
kE=0.1111 ($nM.s^{-1}$);	dM=1.9444e-4 (s^{-1});
kM=0.2778	dE=6.9444e-5 (s^{-1});
kCD=8.3333e-3	dCD=4.1667e-4
kCDS=0.1250	dCE=4.1667e-4 (s^{-1});
kR=0.05 ($nM.s^{-1}$);	dR=1.6667e-5 (s^{-1});
kRE=50.004	dRP=1.6667e-5 (s^{-1});
kb=0.06 ($nM.s^{-1}$);	dRE=8.3333e-6 (s^{-1});
KmS=500 (nM);	kP1=0.005 (s^{-1});
kCE=0.0972	kP2=0.005 (s^{-1});
	kDP=1.0001
	KmM=150 (nM);
	KmE=150 (nM);
	KmCD=920 (nM);
	KmCE=920 (nM);
	KmRP=10 (nM);

The reactions and their kinetics are given in Table 7.

Table 7 – The reactions and kinetics for the cell cycle Model 4 [12].

Index	Reactions	Kinetics
1	$* \xrightarrow[E2F]{Myc(ser62)} E2F$	$kE * \frac{[E2F]}{KmE + [E2F]} + kb * \frac{[Myc^{Ser62}]}{KmM + [Myc^{Ser62}]}$
2	$* \xrightarrow{growth\ signal(S)} CycD$	$kCDS * \frac{[S]}{KmS + [S]}$
3	$* \xrightarrow{Myc(ser62)} CycD$	$kCD * \frac{[Myc^{Ser62}]}{KmM + [Myc^{Ser62}]}$
4	$* \xrightarrow{E2F} CycE$	$kCE * \frac{[E2F]}{KmE + [E2F]}$
5	$* \longrightarrow Rb$	kR
6	$Rb\text{–}E2F \xrightarrow[CycD]{CycE} E2F + Rb^{P}$	$kP1 * [CycD] * \frac{[Rb - E2F]}{KmCD + [Rb - E2F]} + kP2 * CycE * \frac{[Rb - E2F]}{KmCE + [Rb - E2F]}$
7	$Rb + E2F \longrightarrow Rb\text{–}E2F$	$kRE * [Rb] * [E2F]$
8	$Rb \xrightarrow[CycE]{CycD} Rb^{P}$	$kP1 * [CycD] * \frac{[Rb]}{KmCD + [Rb]} + kP2 * [CycE] * \frac{[Rb]}{KmCE + [Rb]}$
9	$Rb^{P} \longrightarrow Rb$	$kDP * \frac{[Rb^{P}]}{KmRP + [Rb^{P}]}$
10	$Myc^{Ser62} \longrightarrow *$	$dM * [Myc^{Ser62}]$
11	$E2F \longrightarrow *$	$dE * [E2F]$

(continued on the next page)

12	$CycE \longrightarrow *$	$dCE * [CycE]$
13	$CycD \longrightarrow *$	$dCD * [CycD]$
14	$Rb \longrightarrow *$	$dR * [Rb]$
15	$Rb^{P} \longrightarrow *$	$dRP * [Rb^{P}]$
16	$Rb\text{–}E2F \longrightarrow *$	$dRE * [Rb - E2F]$

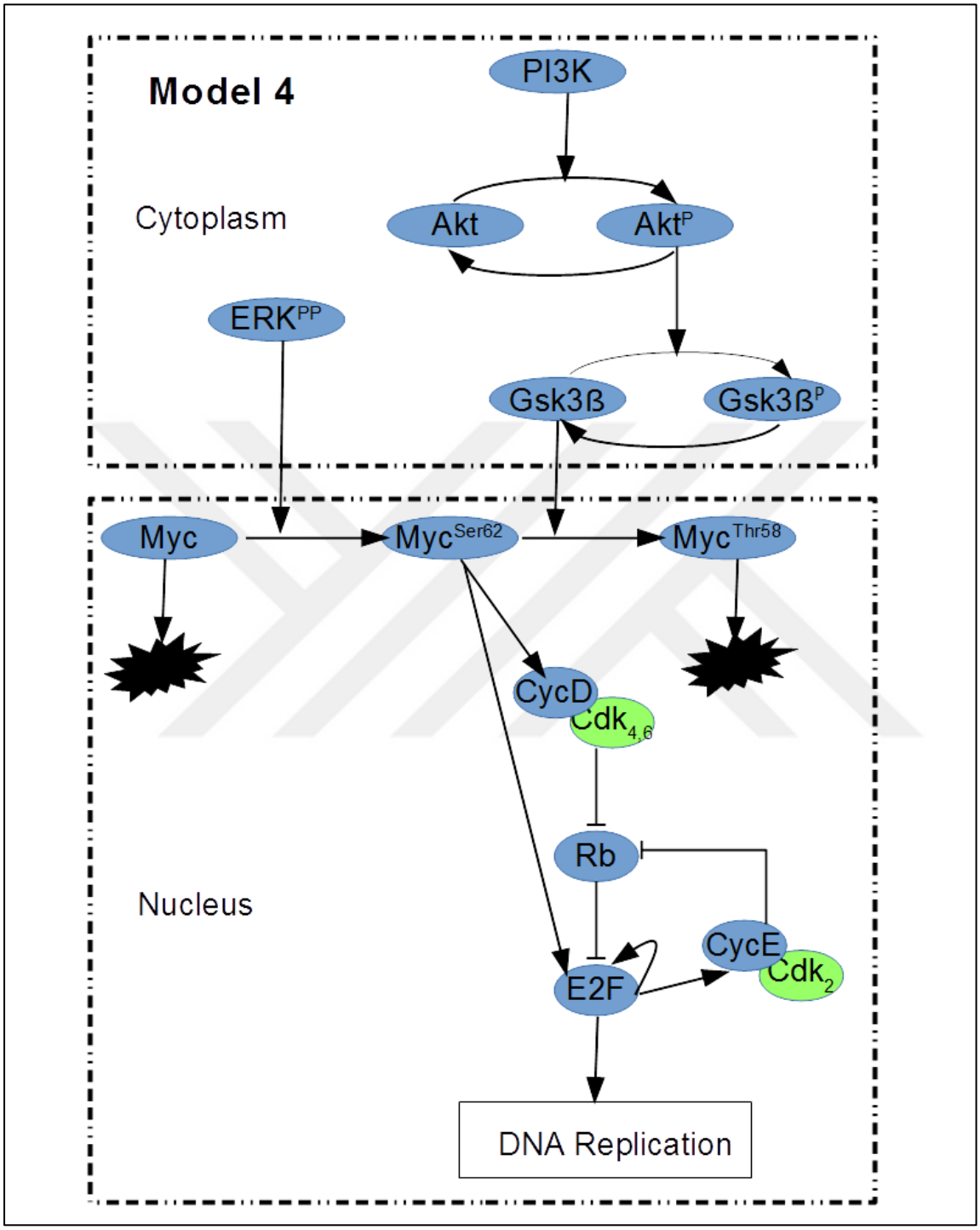

Figure 30 - The topological representation of Model 4.

The dynamics and steady-state response of *Rb* and *E2F* are given in Figure 31. where the cell cycle part Model 4 is simulated [12].

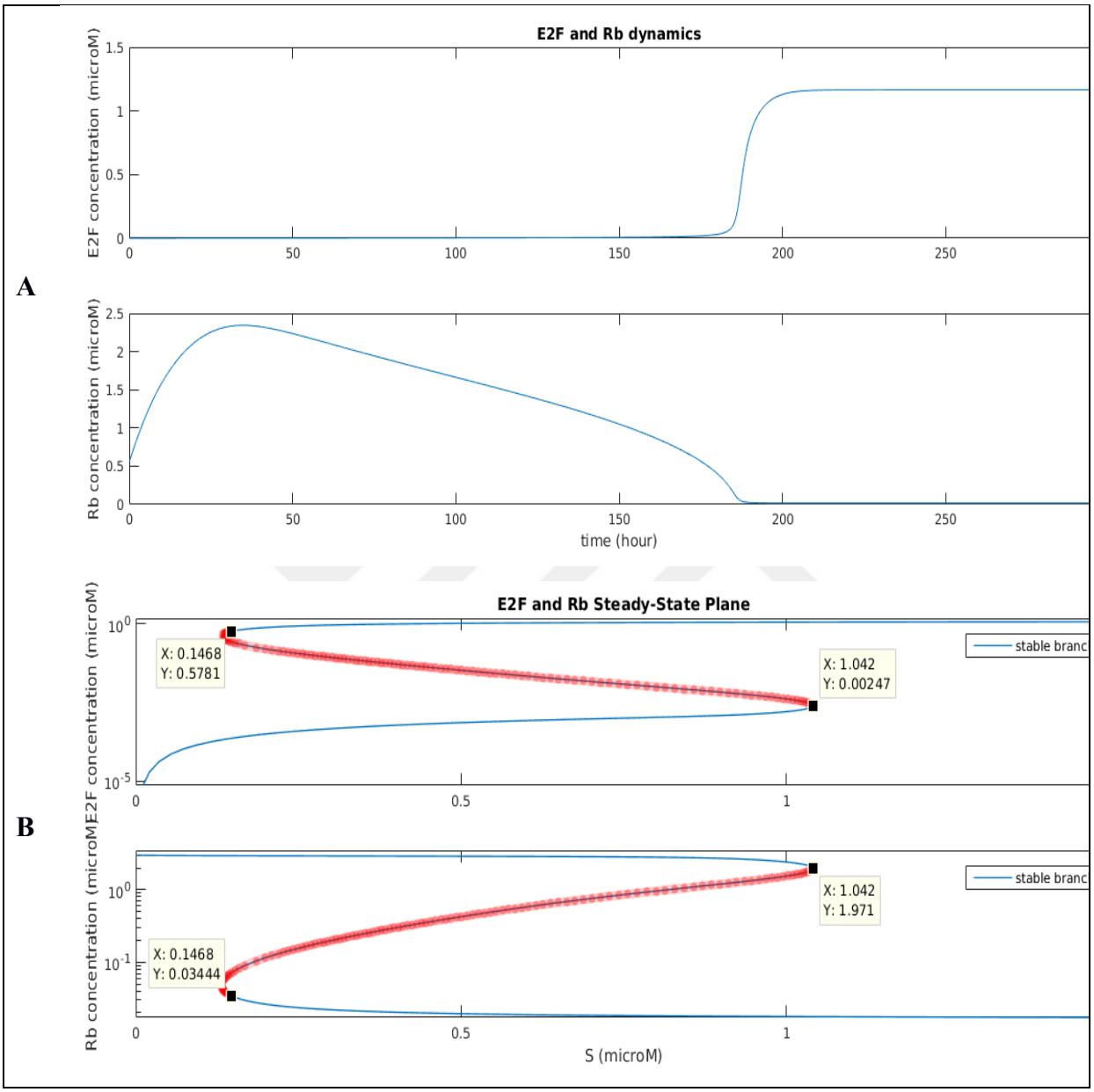

Figure 31 – The dynamics and steady-state response of Rb and E2F. ***(A)*** *The dynamics with S=1.5 (microM), represents E2F activation as Rb is deactivated.* ***(B)*** *The steady-state plane shows the reverse bistable region of the E2F and Rb. For example where E2F switches on at the bifurcation point S=1.042, Rb is switched off. Reproduced and modified from [*[12]*].*

3.2.5 Integration of models

As described in the preceding sections, for each subsystem of the signaling pathway there is an independent model borrowed from the literature. The total of four models must be combined in order to form a single model for the entire pathway. To this end, a systematic approach should be taken to make sure that no critical information is lost. At the same time, the resulting model should not be unduly complicated, allowing transparent analysis. Several steps were taken to tackle this issue:

First, the units of all the parameters involved in the individual models were converted to have a single unit set for the complete model. We chose to have the time in seconds and concentration in nano-molar. Despite that it may seem straightforward, this step is quite challenging since some parameters in the new unit set made the system to exhibit significantly different qualitative behavior. To address this problem, parameter sensitivity analysis was performed and the free parameters (Table 8) were carefully tuned to produce equivalent results to the original system before unit changes were made.

Table 8 - The tuned parameters for the sake of consistency

This study	**Reference** [44]	**Reference** [20]
a1=0.00049 ($nM^{-1}.s^{-1}$)	a1=0.0056	a1=0.00049
d1=0.049 (s^{-1})	d1=4.3517	d1=0.049
k1=0.049 (s^{-1})	k1=2.4345	k1=0.049
This study	**Reference** [70]	
kcati3=1 (s^{-1})	$k_3^{cat} = 0.038$	
ki5m=1.7869e1 (nM)	K_{5m}=1.7869e2	

Second, where the two models were connected, the output of one model had to be defined as the input for the other model. This was done by carefully tailoring and modifying the reactions

and the rate equations that were responsible for the particular connection between the two models. It is critically important that the output range of one model matches the input range of the other one.

Third, the transition from Model 3 to Model 4 demands crossing the nucleus membrane. It means that, activated ERK should translocate from cytoplasm to the nucleus. Reactions in these two different compartments of the cell take place with significantly different time-scales. ERK-mediated reactions inside the nucleus are slower than the ones in cytoplasm. Kinetic parameters accounted for this difference. Transportation delay from cytoplasm to nucleus was ignored in order not to complicate the analysis.

For the interface of Model 2 to Model 3, we replaced *E1* with *RasGTP* (see Figure 27). It changes the mass balance equation of *RasGTP* and *Raf-E1* complex as shown in Eq. (9) and (10).

$$\begin{aligned}\frac{d[RasGTP]}{dt} = {} & -kfi2 * \left[SOS_{complex}\right] * [RasGTP] + kbi2 * [SOS - RasGTP] \\ & + kcati3 * [RasGDP] * \frac{[SOS - RasGTP]}{Ki3m + [RasGDP]} + kcati4 \\ & * [RasGDP] * \frac{[SOS - RasGDP]}{Ki4m + [RasGDP]} - kcati5 * [GAPS] \\ & * \frac{[RasGTP]}{Ki5m + [RasGTP]} - a1 * [Raf] * [RasGTP] + (d1 + k1) \\ & * [Raf - RasGTP]\end{aligned} \tag{9}$$

$$\frac{d[Raf - RasGTP]}{dt} = a1 * [Raf] * [RasGTP] - (d1 + k1) * [Raf - RasGTP] \tag{10}$$

For building Model 4 it is assumed that there is no crosstalk between *PI3K* and *ERK* pathways. While in the original model in [65], both *PI3K* and *ERK* were considered as input, in our model only *PI3K* is manually entered and *ERK* comes as the output of Model 3. However, the crosstalk between ERK and PI3K was previously studied and modeled in [71]. Similarly, given

model for the cell cycle in literature [12] uses the growth signal, S, as its input which is replaced with ERK^{PP} in this work.

3.2.6 Feedback loops

This thesis studies effect of four FBLs (feedback loops) as shown in Figure 32.

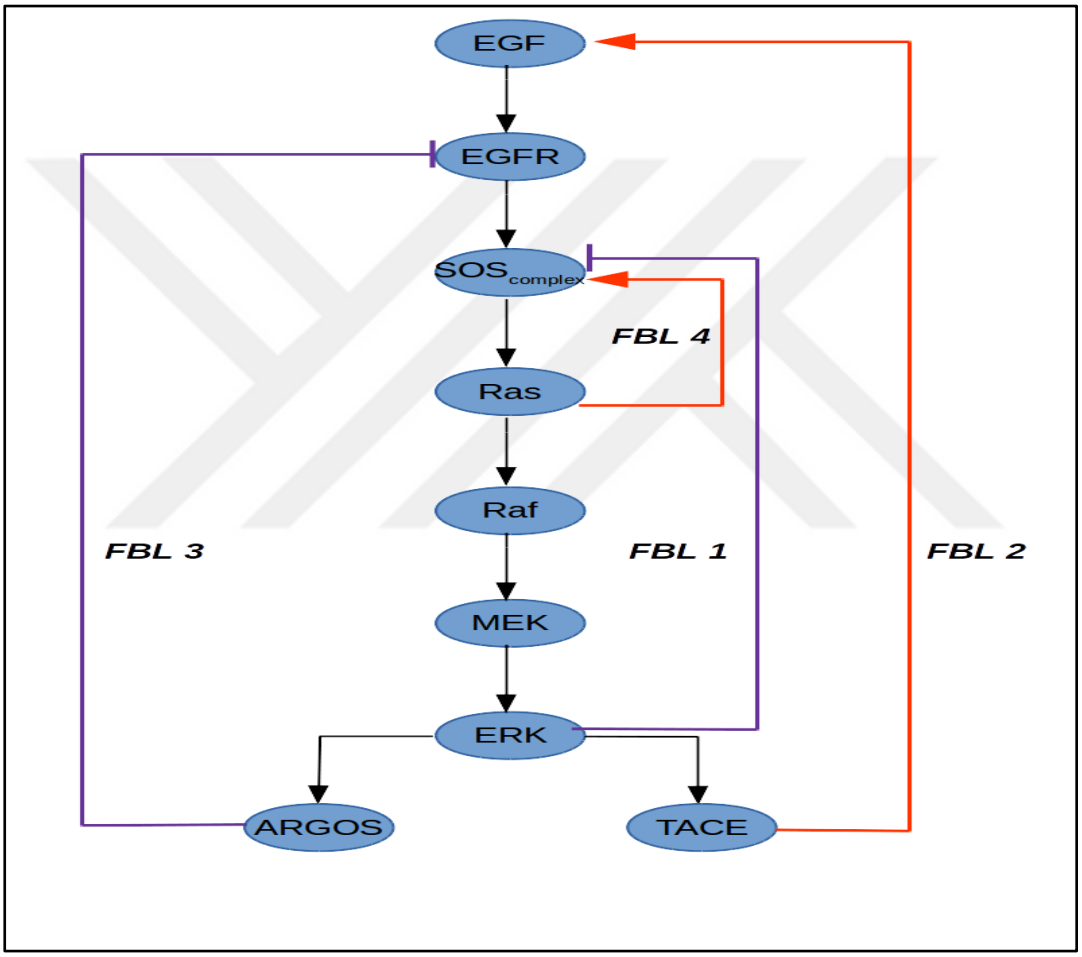

Figure 32 - The explicit feedback loops studied in this thesis.

(Negative) Feedback loop 1 (FBL 1):

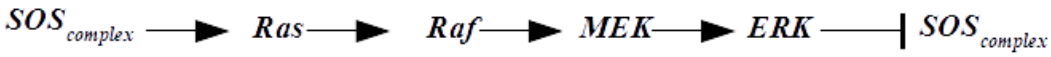

Total concentration of the *EGF* is the primary input to our model. The output of Model 1 is *Shc_Grb2_SOS (SOS$_{complex}$)* which passes as input for Model 2. Consequently, ODE for *SOS$_{complex}$* is derived as follows:

$$\frac{d[SOS_{complex}]}{dt} \tag{11}$$

$$= -kf23 * [SOS_{complex}] + kb23 * [Shc - P] * [Grb2 - SOS] + kf22 * [Shc - Grb2] * [SOS] - kb22 * [SOS_{complex}] + kf20 * [(EGF - EGFR)2 - Shc - Grb2 - SOS] - kb20 * [SOS_{complex}] * [(EGF - EGFR)2 - P] - kfi1 * [SOS_{complex}] * [RasGDP] + kbi1 * [SOS - RasGDP] - kfi2 * [SOS_{complex}] * RasGTP + kbi2 * [SOS - RasGTP] - k_{nfb} * [SOS_{complex}] * \frac{[ERK^{PP}]}{Km_{nfb} + [SOS_{complex}]}$$

The mechanism of the $SOS_{complex}$ downregulation by ERK^{PP} suggests that ERK^{PP} catalyzes SOS phosphorylation which in turn leads to dissociation of $SOS_{complex}$ [40][72]. Thus, we employed *Michaelis-Menten* equation to account for the negative feedback from ERK^{PP} to $SOS_{complex}$ which is the last term in Eq. (11). The parameters k_{nfb} and Km_{nfb} determine the feedback strength.

When $[SOS_{complex}] \gg Km_{nfb}$, the nonlinear feedback strength term reduces to $-k_{nfb} * [ERK^{PP}]$, which is linearly proportional to the activated *ERK* concentration.

(Positive) Feedback loop 2 (FBL 2):

The equations for modeling this autocrine loop was borrowed from [58] and [57].

$$\frac{d[TACE]}{dt} = gpT * \frac{[ERK^{PP}]}{KmT + [ERK^{PP}]} - dT * [TACE] \tag{12}$$

We assumed that *TACE* applies its positive effect on the *EGF* by increasing the released amount of active *EGF.* To model this, a new term is added to the algebraic equation for calculating total amount of *EGF:*

$$EGF_{released} = EGF_{tot} + grT * [TACE] - \sum EGF_{comlpex} \tag{13}$$

In Eq (13) *grT* acts like a switch for the feedback integration into the model and first term in the Eq (12) represents the *nonlinear feedback strength*.

(Negative) Feedback loop 3 (FBL 3):

Transcriptional programs induced by *ERK* lead to production of yet another inducible feedback inhibitor *ARGOS* [73]. Based on the assumption that ARGOS forms a complex with $EGFR_{available}$ [56], the negative feedback loop mediated by ARGOS is modeled here.

ARGOS production rate is given by:

$$\frac{d[ARGOS]}{dt} = gpA * \frac{[ERK^{PP}]}{KmA + [ERK^{PP}]} - dA * [ARGOS] \tag{14}$$

Produced *ARGOS* binds to the available *EGFR* and inhibits it by forming $ARGOS - EGFR$ complex*:*

$$\frac{d[ARGOS - EGFR]}{dt} = kAE * [EGFR_{available}] * [ARGOS] - dAE * [ARGOS - EGFR] \quad (15)$$

Then from the total amount of available EGFR is reduced accordingly:

$$EGFR_{available} = EGFR_{tot} - grAE * [ARGOS - EGFR] - \sum EGFR_{complex} \quad (16)$$

In this model *grAE* is the switch for the feedback loop integration and the first term in the Eq (14) shows nonlinear feedback strength. Table 8 gives the parameter values for this part.

Table 9 – The parameters for PFL 2 and PFL 3.

Parameter values
dT=1 (s^{-1})
gpT=10 ($nM.s^{-1}$)
grT=0 ($unitless$)
KmT=1000 (nM)
gpA=1e-6 (s^{-1})
KmA=10 (nM)
dA=1e6 (s^{-1})
kAE=5 ($nM^{-1}.s^{-1}$)
dAE=1 (s^{-1})
grAE=0 ($unitless$)

(Positive) Feedback loop 4 (FBL 4):

$SOS_{complex}$-$RasGTP$ ⟶ $RasGTP$ ⟶ $SOS_{complex}$-$RasGTP$

This feedback loop is embedded in Model 2:

$$\frac{d[RasGTP]}{dt} = -kfi2 * [SOS_{complex}] * [RasGTP] + kbi2 * [SOS - RasGTP] + kcati3 * [RasGDP] * \frac{[SOS - RasGTP]}{Ki3m + [RasGDP]} + kcati4 * [RasGDP] * \frac{[SOS - RasGDP]}{Ki4m + [RasGDP]} - kcati5 * [GAPS] * \frac{[RasGTP]}{Ki5m + [RasGTP]} - a1 * [Raf] * [RasGTP] + (d1 + k1) * [Raf - RasGTP] \quad (17)$$

$$\frac{d[SOS - RasGTP]}{dt} = kfi2 * [SOS_{complex}] * [RasGTP] - kbi2 * [SOS - RasGTP] \quad (18)$$

The parameters *kcati3* and *Ki3m* in the third term of Eq (15) regulate the feedback strength. The nominal parameters value can be found in Table 3.

Chapter 4: Results and discussions

4.1 Steady state analysis

Asymptotic behavior of biochemical networks can be categorized in two types, *convergence to a steady state* or *convergence to a sustained periodic oscillation*. The sustained periodic oscillation of the system is known as *limit cycle oscillation* [14].

Most of the time the system response changes to reflect the parameter perturbations. If a change in the stability or the number of steady-state solutions of the system, occurs at a point, it is referred to as *bifurcation point* and the corresponding diagram showing the change is called *bifurcation diagram*. The results in this section are derived by bifurcation analysis of the system.

The steady-state responses of the system are shown as a function of total amount of the ligand, EGF. $RasGTP$ and ERK^{PP} are of specific interest, since they are two of the decisive signaling molecules in ERK signaling pathway.

Table 10 categorizes the strengths of the feedback loops in different scenarios. Each scenario provides the assumed parameters of the model with the corresponding figure(s). Unless otherwise noted, the rest of the parameters are set to their nominal values.

Table 10 – Scenarios for the steady-state analysis of the system response. The FBLs strength are given for each scenario.

	k_nfb,Km_nfb	grT, gpT	grAE,gpAE	kcati3	Figure
Scenario1 (S.S1)	0,-	0,-	0,-	1	Figure 33
Scenario 2 (S.S2)	0,-	0, -	0,-	[0.6,0.69,0.7,1]	Figure 34
Scenario 3 (S.S3)	[0,0,0,0.03],1000	0,-	0,-	[1,1.5,1.75,1.75]	Figure 35
Scenario 4 (S.S4)	0.03,1000	0,-	0,-	1.75	Figure 36
Scenario 5 (S.S5)	[0.03,0.1,0.03,0.1], [1e4,1e4,1e3,1e3]	0,-	0,-	1	Figure 37
Scenario 6 (S.S6)	0.03,1000	1,[20,10,0]	0,-	1	Figure 40
Scenario 7 (S.S7)	0.03,1000	0,-	1,[1,3,5]*1e-8	1	Figure 40

Scenario 1 (S.S 1): The base case when only positive FBL4 is active.

A

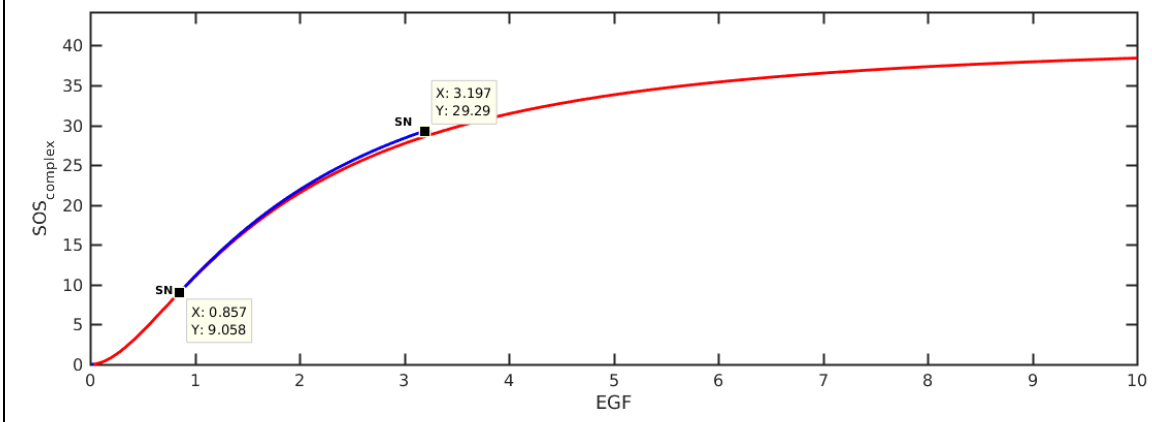

B

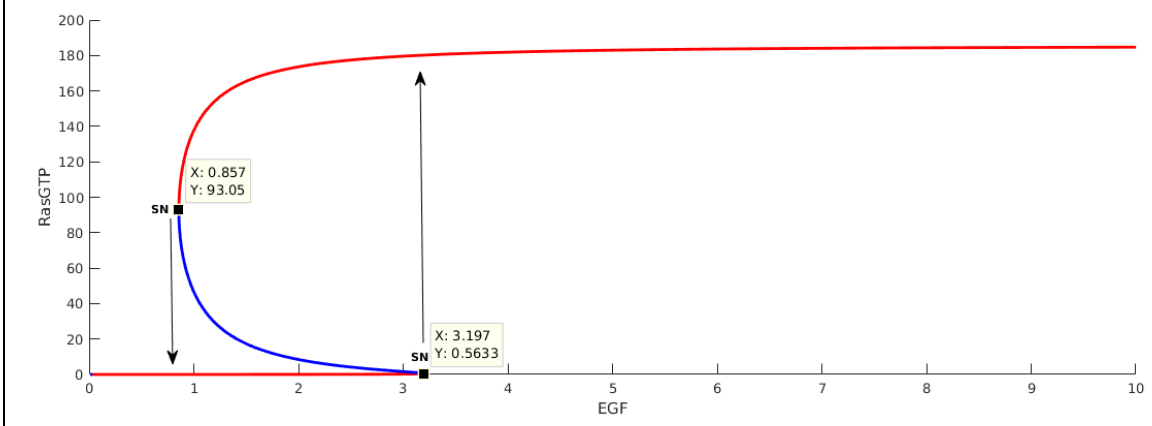
RasGTP
EGF
X: 0.857
Y: 93.05
SN
X: 3.197
Y: 0.5633
SN

C

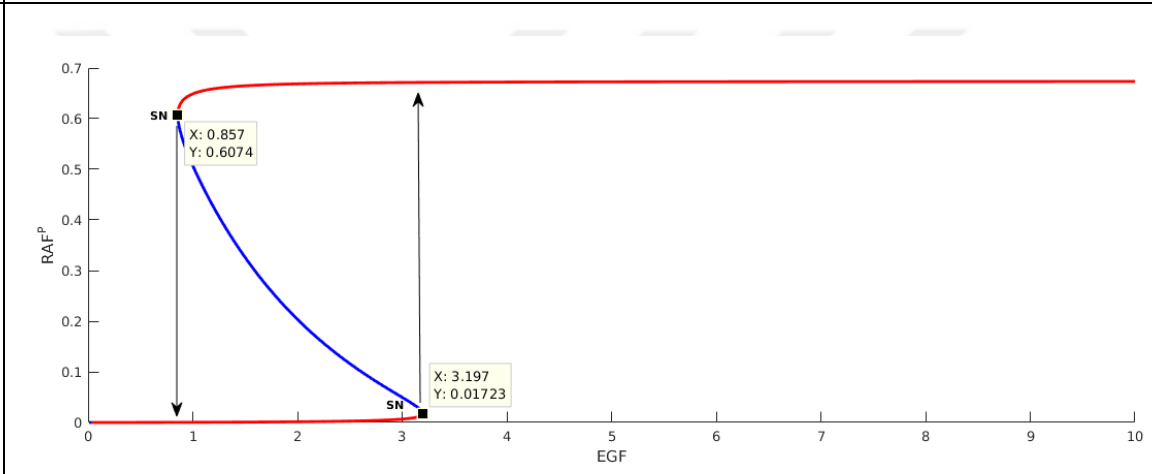
RAF^P
EGF
SN
X: 0.857
Y: 0.6074
X: 3.197
Y: 0.01723
SN

D

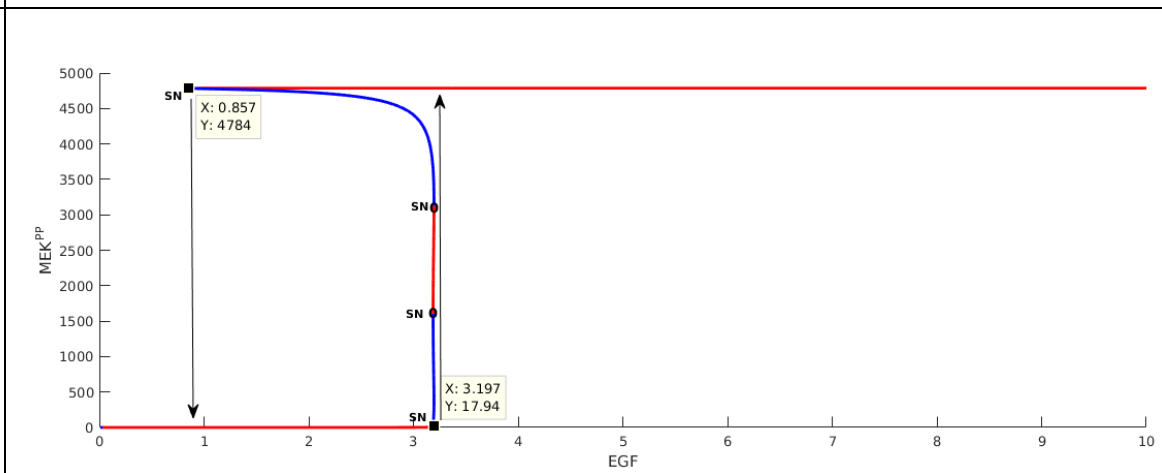
MEK^PP
EGF
SN
X: 0.857
Y: 4784
SN
SN
X: 3.197
Y: 17.94
SN

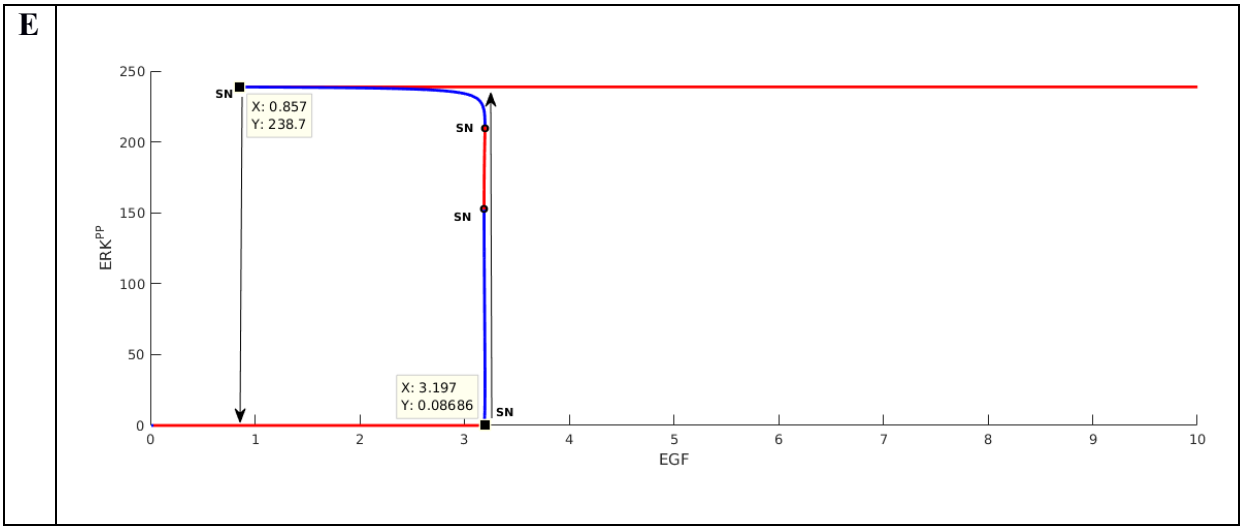

Figure 33- The sensitivity of ERK signaling pathway. (the stable steady-state solutions are shown in 'red' and the unstable steady-state branch is shown in 'blue').

In Figure 33, it is shown that the graded dose-response curve of $SOS_{complex}$ is changed to a *digital* switching response as the signal passes down the pathway. The presence of the positive FBL 4 creates bistability in *RasGTP*. Downstream of the *RasGTP*, ERK^{PP} exhibits switch-like behavior as a result. The sensitivity of the system to its input (*EGF*) increases, as signal propogates through the MAPK cascade as shown by the steep unstable branch (in blue) which is almost perpendicular to the low stable branch (in red) in Figure 33E.

Comparison of Figure 33B with Figure 33D and E shows the emergence of an intermediate stable branch. The second and third *SN's* mark two ends of the intermediate branch in ERK^{PP} bifurcation diagram. Saddle-node bifurcation point appears wherever two steady-state solutions collide. The system might settle on this branch , if EGF_{tot} is in the short range of 3.187 (*EGF* value of the second *SN*) and 3.197 (*EGF* value of the third *SN*) and for the initial conditions in its limited basin of attraction. If one of the states of the system is slightly perturbed it jumps to the upper stable branch or the lower branch.

$SN = [3.197, 0.08686]$ indicates where the stable steady-state branch collides with the unstable one. In order to activate *ERK,* concentration of *EGF* must exceed 3.197(nM). However,

when *ERK* becomes activated, it stays active even for *EGF* amounts lower than 3.197 (nM) but greater than 0.857(nM). Further decresing of *EGF* ligands switches off the system. Thus, activity of *ERK* when 0.857<*EGF*<*3.197 (nM)* depends on the previous state of the system. As mentioned in the literature review, this inherent property of the bistable responses is referred to as *hysteresis*.

Scenario 2 (S.S2): Effect of the strength of Positive FBL4

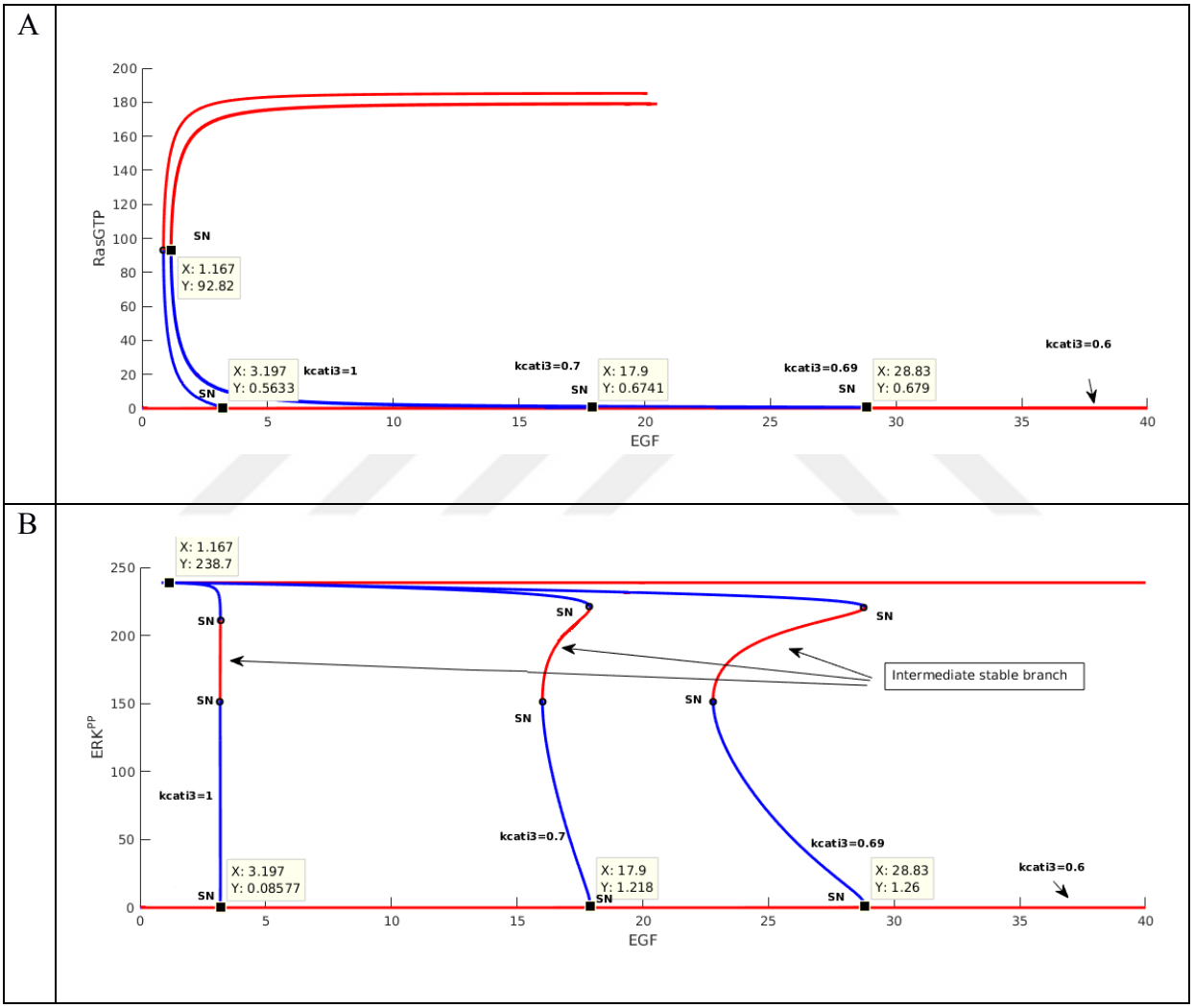

Figure 34 – The impact of decreasing strength of the positive FBL4.

Figure 34 shows that decreasing the strength, *kcati3, of* positive FBL 4 requires higher EGF for the bistable regime. In fact decreasing *kcati3* below 0.6 makes the system lose its bistability.

In addition, the intermediate stable branch spans over larger *EGF* concentrations as the feedback strenght decreases.

Scenario 3 (S.S3): Negative FBL 1.

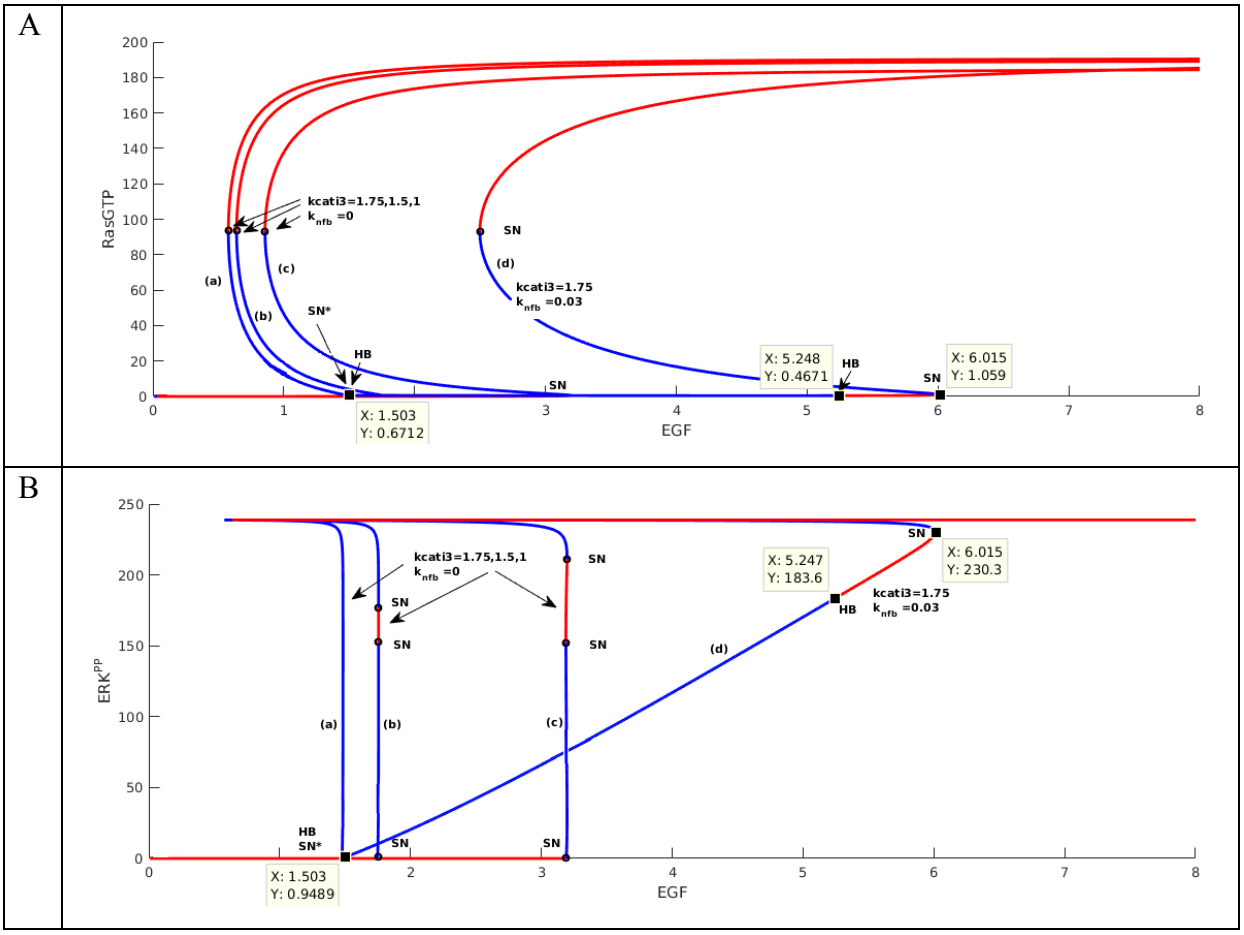

Figure 35 – The impact of the positive FBL 4 (increasing strength) and the impact of the negative FBL 1 imposed on it. ***(A)*** *Impact of FBL 4 on RasGTP steady-state response. Curve (d) shows the impact of the negative FBL 1, when kcati3=1.75.* ***(B)*** *Impact of FBL 4 on* ERK^{PP} *steady-state response. Curve (d) shows the impact of the negative FBL1, when kcati3=1.75.*

Figure 35 shows that the system's sensitivity decreases when negative feedback is added and switching between low and high stable states requires greater changes in EGF concentrations. Moreover, the intermediate stable branch shrinks and disappears as *kcati3* or strength of positive feedback increases. This behavior may be desirable for the cell, when it is deprived of the enough growth factor but needs to proliferate.

Adding negative FBL 1, creates a wider range over which it is possible for the system to occupy the intermediate stable branch.

Scenario 4 (S.S4): Hopf Bifurcation and Periodic Solutions

The other important change that appears in Figure35 is that the first two *SN's* at *EGF=3.197* turn into *HB (Hopf bifurcation)* points when negative feedback is added. Hopf

bifurcation and sustained periodic solution emerges whenever the unstable steady-state solutions meet with the stable ones. This is illustrated in Figure36 below.

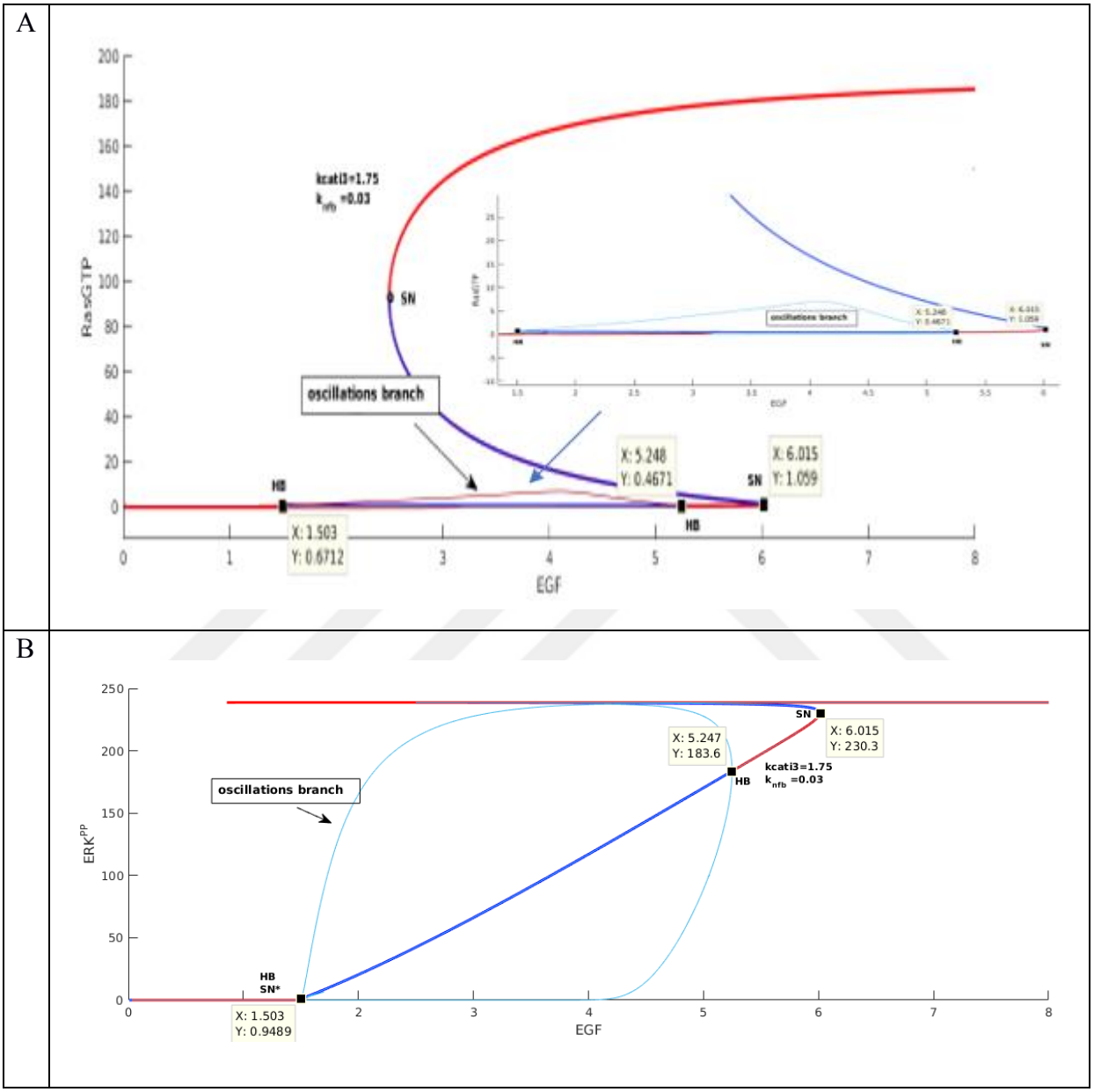

Figure 36 – Mapping of RasGTP and ERK^{PP} responses. ***(A)*** *RasGTP low activity stable branch is magnified.* ***(B)*** *ERK^{PP} response corresponding to RasGTP. The curve named "oscillations branch" represents minima and maxima of the periodic solutions waves of the corresponding state (ERK^{PP} and RasGTP) at the corresponding input values (EGF concentration).*

Figure 36A shows that both of the *HB* points emerge when *RasGTP* sits on its lower stable steady-state (not fully activated). This reveals that it is the upper stable branch of ERK^{PP} that corresponds to the *RasGTP* active state. Subplot in Figure 36A provides that *RasGTP* oscillates as well but with much smaller amplitude compared with ERK^{PP}. The hypothesis that the protein RAS may lead to ERK^{PP} oscillatory fashion while it is not fully activated (i.e *RasGTP* low concentration) is subject to be investigated experimentally.

Scenario 5 (S.S5): Effect of k_{nfb}, Km_{nfb}

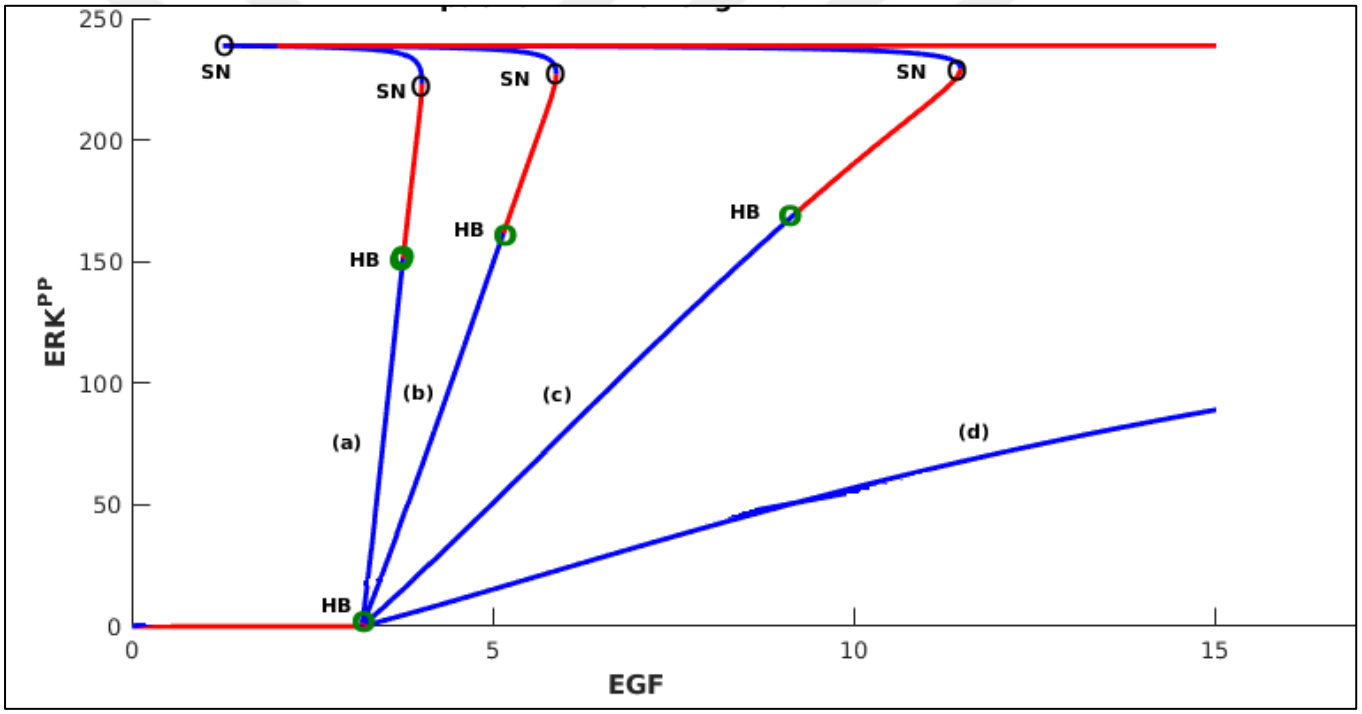

Figure 37 – The impact of the negative FBL 1 strength on ERK^{PP}. k_{nfb}, Km_{nfb} are assigned to the four sets of values in Eq.11. ***(a)*** $k_{nfb} = 0.03, Km_{nfb} = 1e4$ ***(b)*** $k_{nfb} = 0.1, Km_{nfb} = 1e4$ ***(c)*** $k_{nfb} = 0.03, Km_{nfb} = 1e3$ ***(d)*** $k_{nfb} = 0.1, Km_{nfb} = 1e3$. *HB shows the Hopf Bifurcation and SN indicates the Saddle-node Bifurcation point. (red) and (blue) curves are for the stable and unstable steady-state, respectively.*

Considering that the nominal strength of the FBL1 in our model is defined as $k_{nfb} = 0.03, Km_{nfb} = 1e3$, Figure 37 provides the impact of this negative feedback loop on ERK^{PP} response. While increasing k_{nfb} increases the nonlinear feedback gain presented in Eq 11, it is shown that Km_{nfb} is inversely proportional to the feedback strength.

For the feedback gains greater than $[k_{nfb} = 0.1, Km_{nfb} = 1e3]$, the system is not able to switch on in the normal input range, thus the bistability is lost. However, it is observed that *HB* points are robust to FBL 1 strength.

Scenario 6 (S.S6): Autocrine feedback loop FBL 2

A

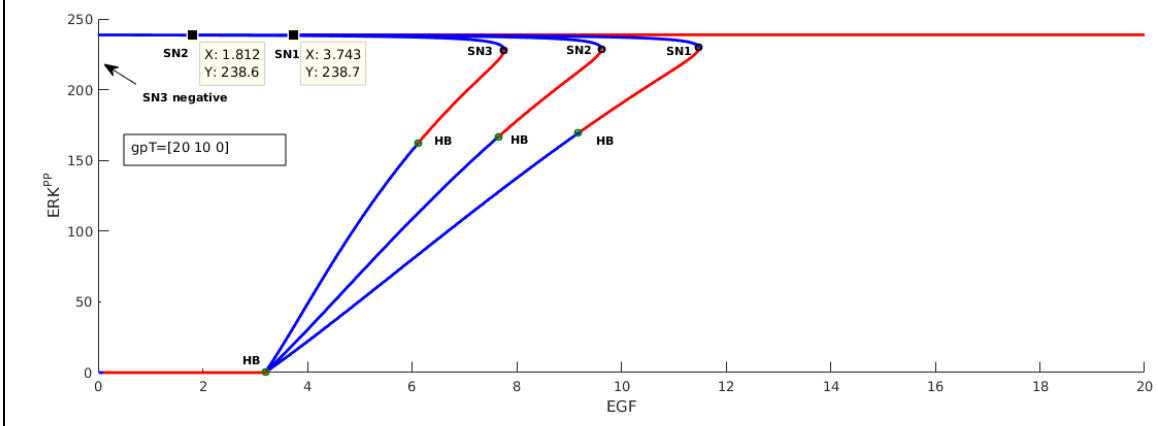

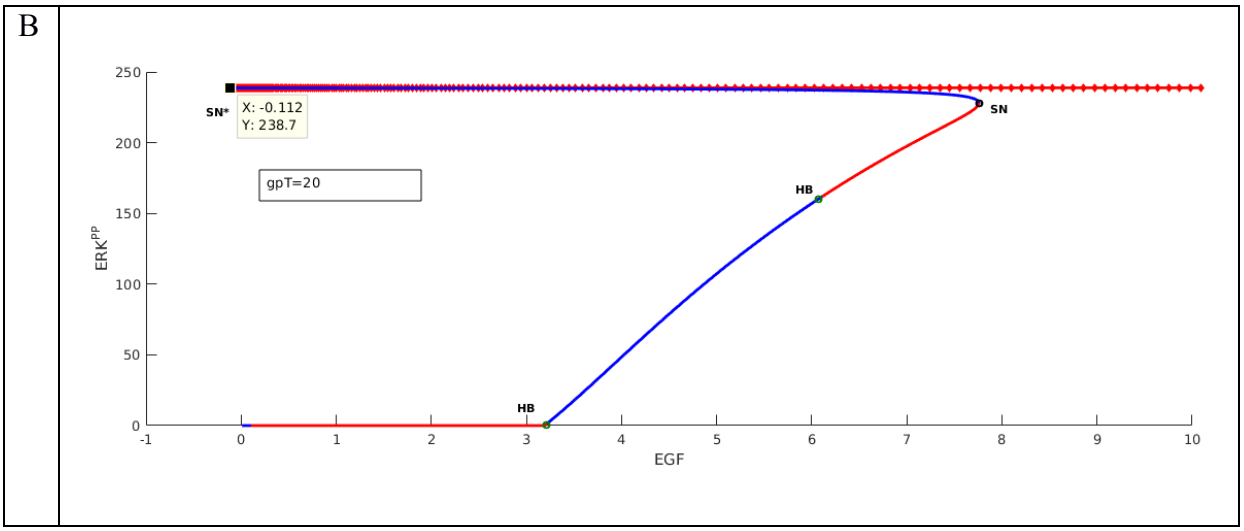

Figure 38 - The impact of the positive FBL 2 ***(A)*** *ERK^{PP} response to EGF. gpT increases from right to left.* ***(B)*** *shows that with gpT=20, SN* appears at negative EGF amount.*

Figure 38 compares the steady-state input-output relationship of ERK^{PP} to varying autocrine feedback loop strength (see Sec 2.4.1). Less *EGF* ligand is required to switch on ERK^{PP} when the positive FBL 2 strength increases.

In order to switch off ERK^{PP}, more ligands need to be removed as the positive FBL 2 strength increases. Figure 38B, suggests that for gpT>20, the system cannot switch off even after removing all of the *EGF* ligands.

Figure 39 reveals the same pattern for *RasGTP.*

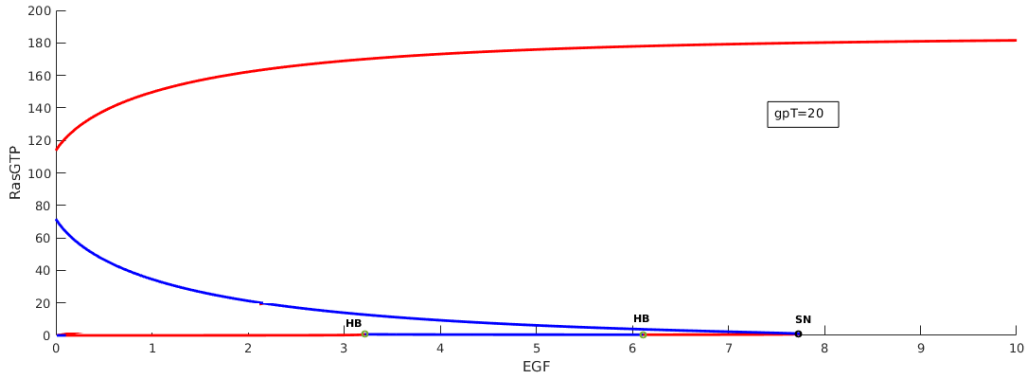

Figure 39 – RasGTP steady-state response with the strong positive FBL 2.

This type of response as a result of too much positive feedback loop strength must be tightly controlled in the cell. In principle, in this case, although the system is capable of settling on either of the two stable branches, it cannot toggle between *on* and off states anymore. In other words, when Ras is switched on it persistently stays active regardless of the stimulus presence, which is a hallmark of the cancerous signaling molecules [5].

Scenario 7 (S.S7): Negative FBL3

In Figure 40A it is shown that when negative FBL 3 is imposed on top of the negative FBL 1, the system loses its upper stable branch. One more *HB* point (*HB3*) appears, suggesting that another periodic solution exists for the system at *EGF=21.79(nM).* Strong inhibitory effect from FBL 1 and FBL 3 suppresses ERK^{PP} activation after it passes a certain threshold.

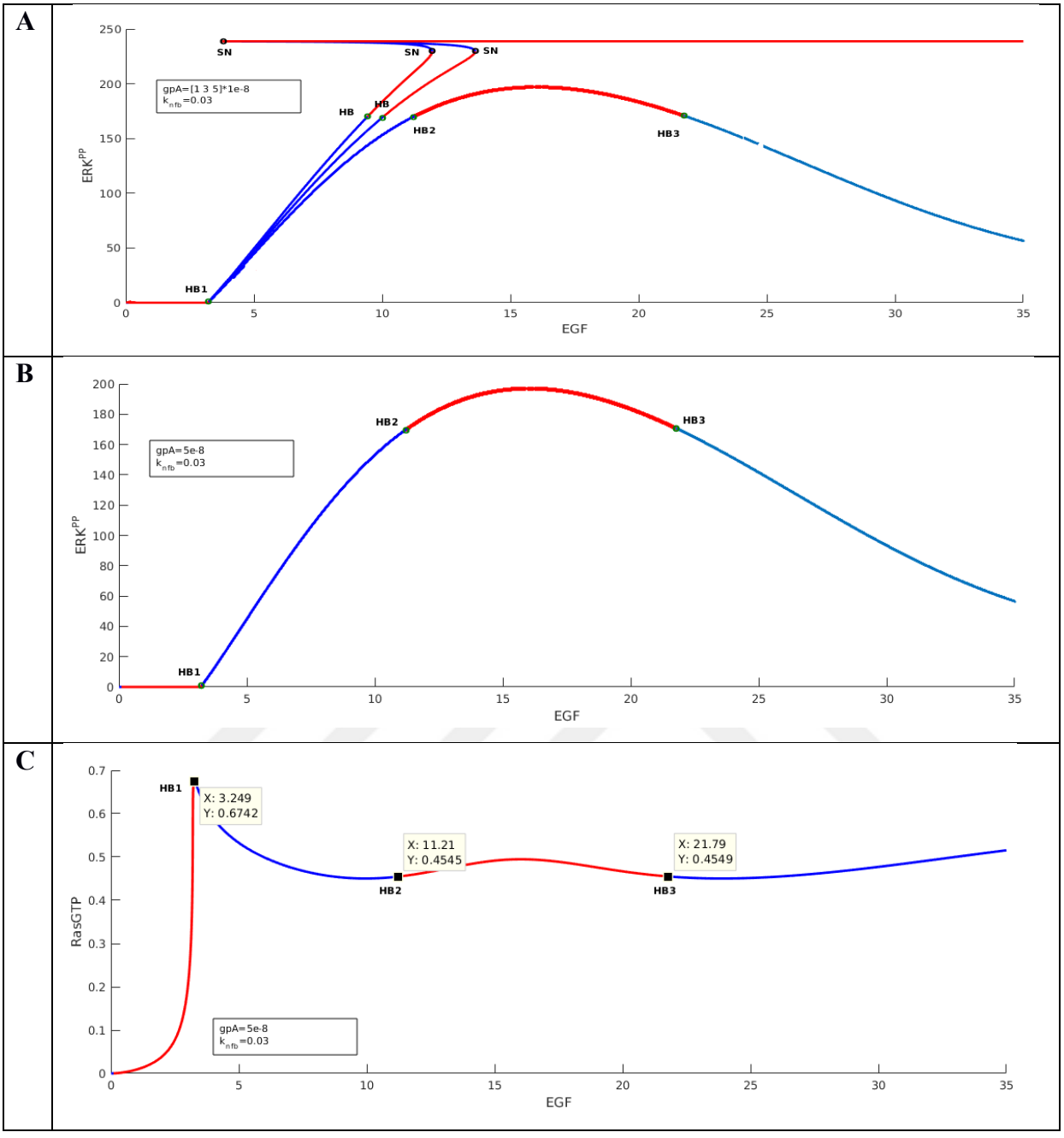

Figure 40 - The impact of the negative FBL 3 on the steady-state response of ERK^{PP} and RasGTP. ***(A)*** *Steady-state response of ERK^{PP} to varying FBL 3 strengths.* ***(B)*** *Steady-state response of ERK^{PP} to gpA=5e-8.* ***(C)*** *Steady-state response of RasGTP to gpA=5e-8 mapped on ERK^{PP} response.*

Comparison of Figure 40B and C, explains the corresponding behavior of *RasGTP* and ERK^{PP}. It is observed that *RasGTP* sits only on its low branch in this scenario, supporting the idea that without *RasGTP* switch, ERK^{PP} is unable to become stably activated.

Myc ^{Ser62} Steady-State input-output relationship

In the following figures activity of Myc^{Ser62}, the stable form of the protein Myc, is presented in response to *EGF*. The responses closely follow ERK^{PP} behavior.

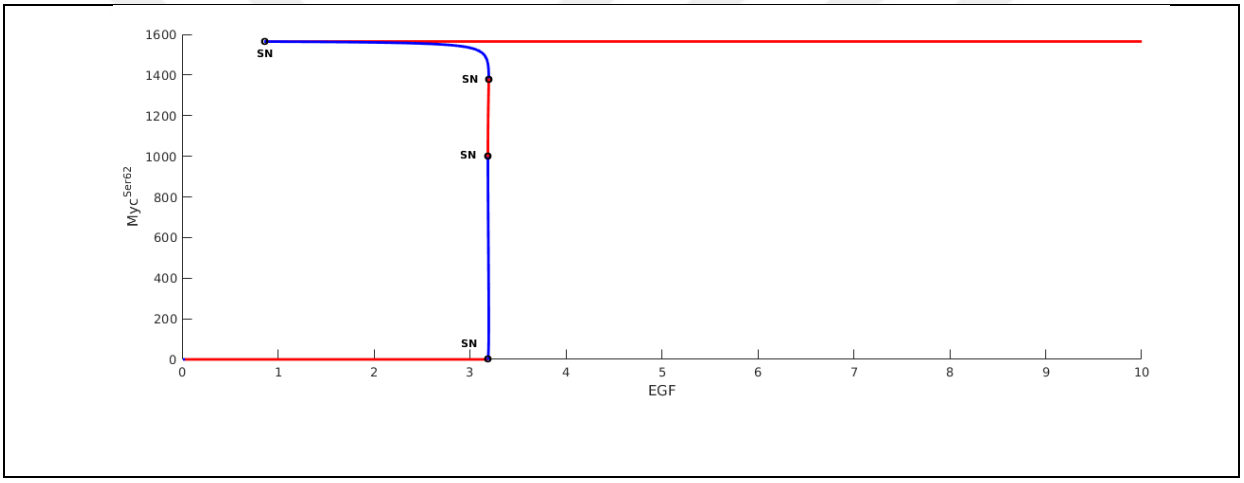

Figure 41 - Myc^{Ser62} response curve in (S.S1).

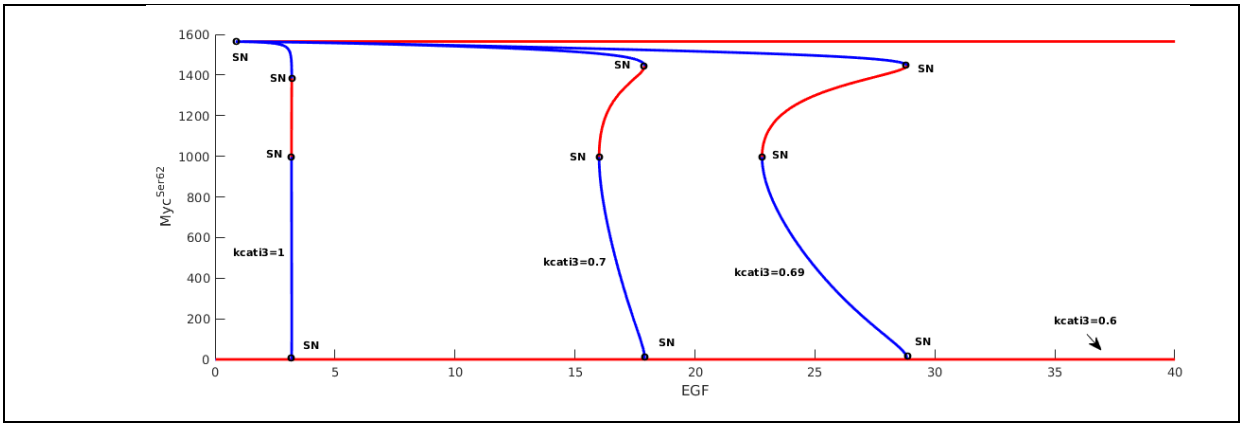

Figure 42 - Myc^{Ser62} response curve in (S.S2).

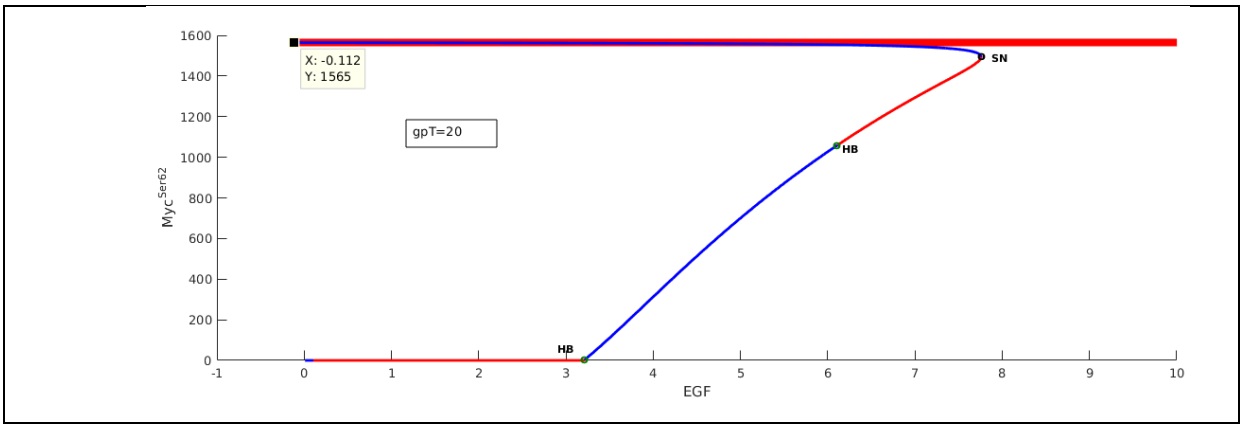

Figure 43 - Myc^{Ser62} response curve in (S.S6).

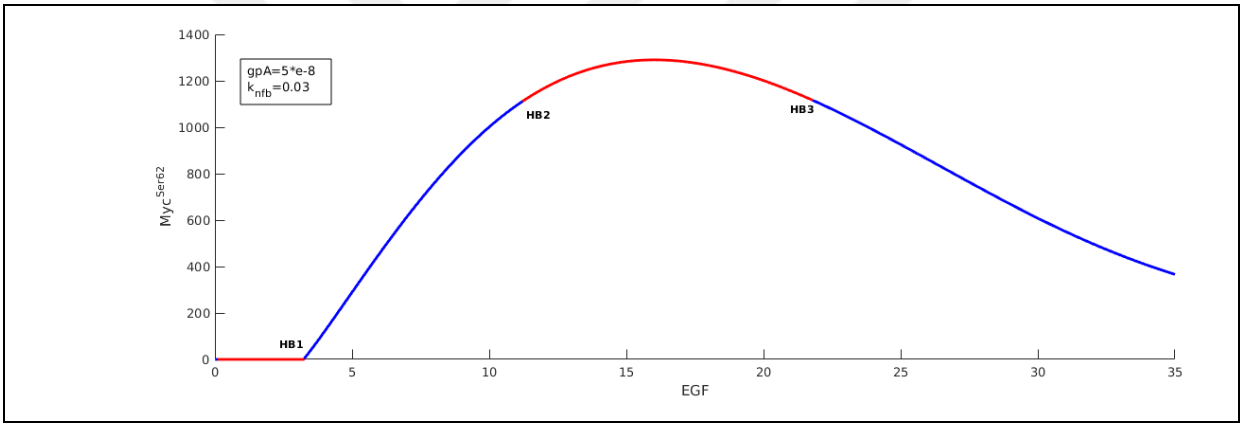

Figure 44 - Myc^{Ser62} response curve in (S.S7)

5.2 Dynamics analysis

The dynamic behavior of the species is illustrated next by plotting their concentration evolution against time. The dynamics analysis reveals the duration, amplitude, frequency and stability of the signal. The effect of these characteristics of the signaling molecules is significant on the cell fate.

Several scenarios were generated to investigate the dynamics behavior of the system in

hand. Time simulations and *phase planes* represent the outcome of the applied scenarios. *Phase planes* are such plots that show change of one variable as function of the other. In this work, the phase planes are plotted for the change of ERK^{PP} against *RasGTP* variation.

Table 11 provides the scenarios outline.

Table 11 - The dynamics analysis scenarios.

	k_nfb,Km_nfb	grT, gpT	grAE,gpAE	kcati3
Scenario1 (D.S1)	0,-	0,-	0,-	1
Scenario 2 (D.S2)	varying	0, -	0,-	1
Scenario 3 (D.S3)	0.03,1000	0,-	0,-	1.75
Scenario 4 (D.S4)	0.03,1000	0,-	1,3e-8	1
Scenario 5 (D.S5)	0.03, 1000	1,[10 20]	0,-	1

Scenario 1 (D.S1): Dynamics of Bistability in Response To Positive FBL 4

For *EGF* values between 0.857 and 3.197, the system can settle on either of the two stable branches (see Figure 33). It is shown in Figure 45 that the initial conditions of the system determine which state is occupied.

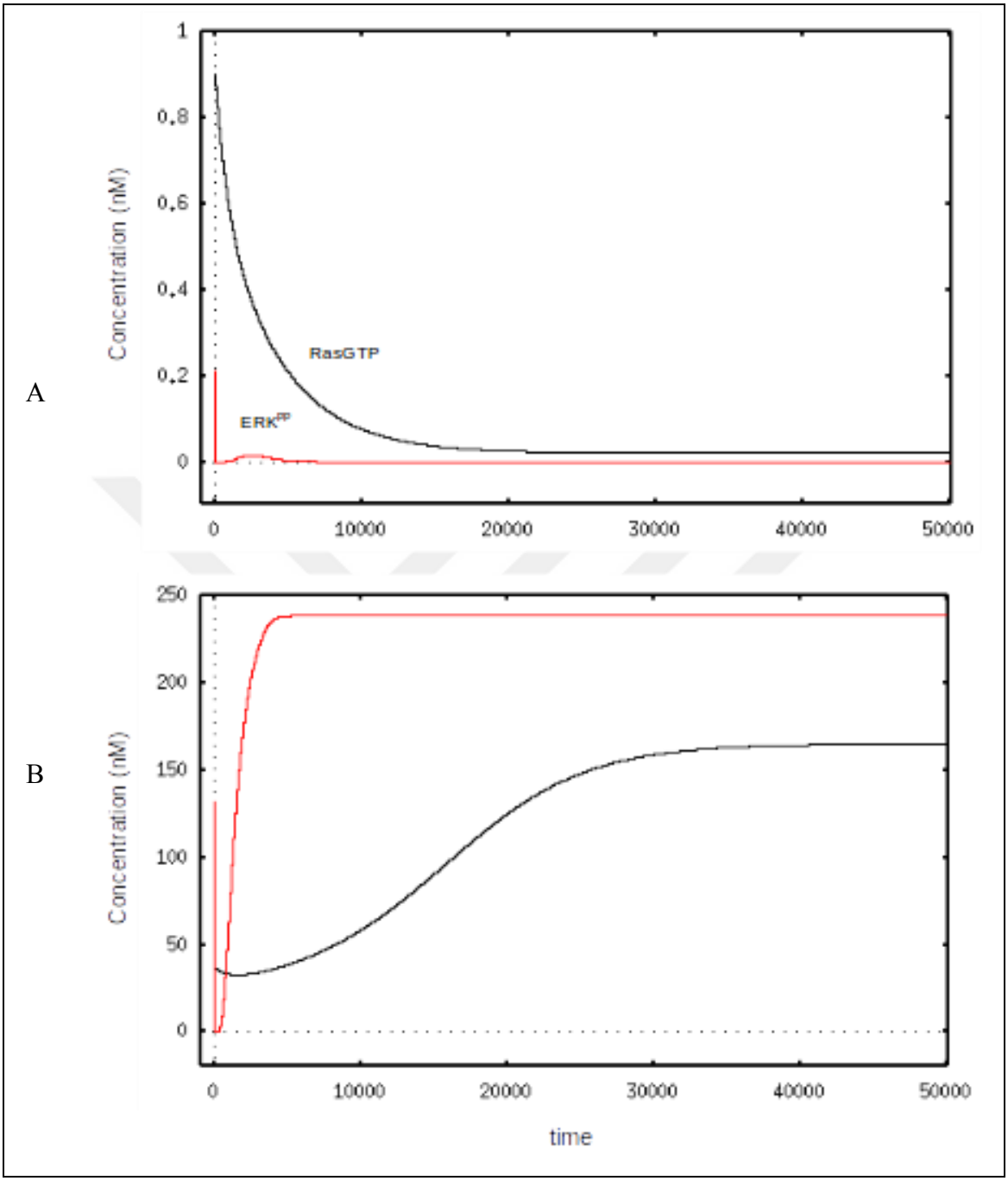

Figure 45 – Bistability dynamics as result of the positive FBL 4 effect. ***(A)*** *ERK^{PP} and RasGTP dynamics, with high ICs (initial conditions).* ***(B)*** *ERK^{PP} and RasGTP dynamics, with low ICs. EGF_{tot} is set to 1.5 (nM).*

The initial conditions of the states of the system (signaling molecules) are set to their steady-state solutions on lower branch, except for *RasGTP* and ERK^{PP}. In Figure 45A, their ICs

are set to the values that are close to the upper branch, and in Figure 45B their ICs are small, close to the inactive state. The exact values which are assigned to them are given below:

For the inactive branch:

$$RasGTP\ (t = 0) = \ 0.9\ (nM)$$

$$ERK^{PP}\ (t = 0) = 0.21\ (nM)$$

For the active branch:

$$RasGTP\ (t = 0) = 37\ (nM)$$

$$ERK^{PP}\ (t = 0) = 132\ (nM)$$

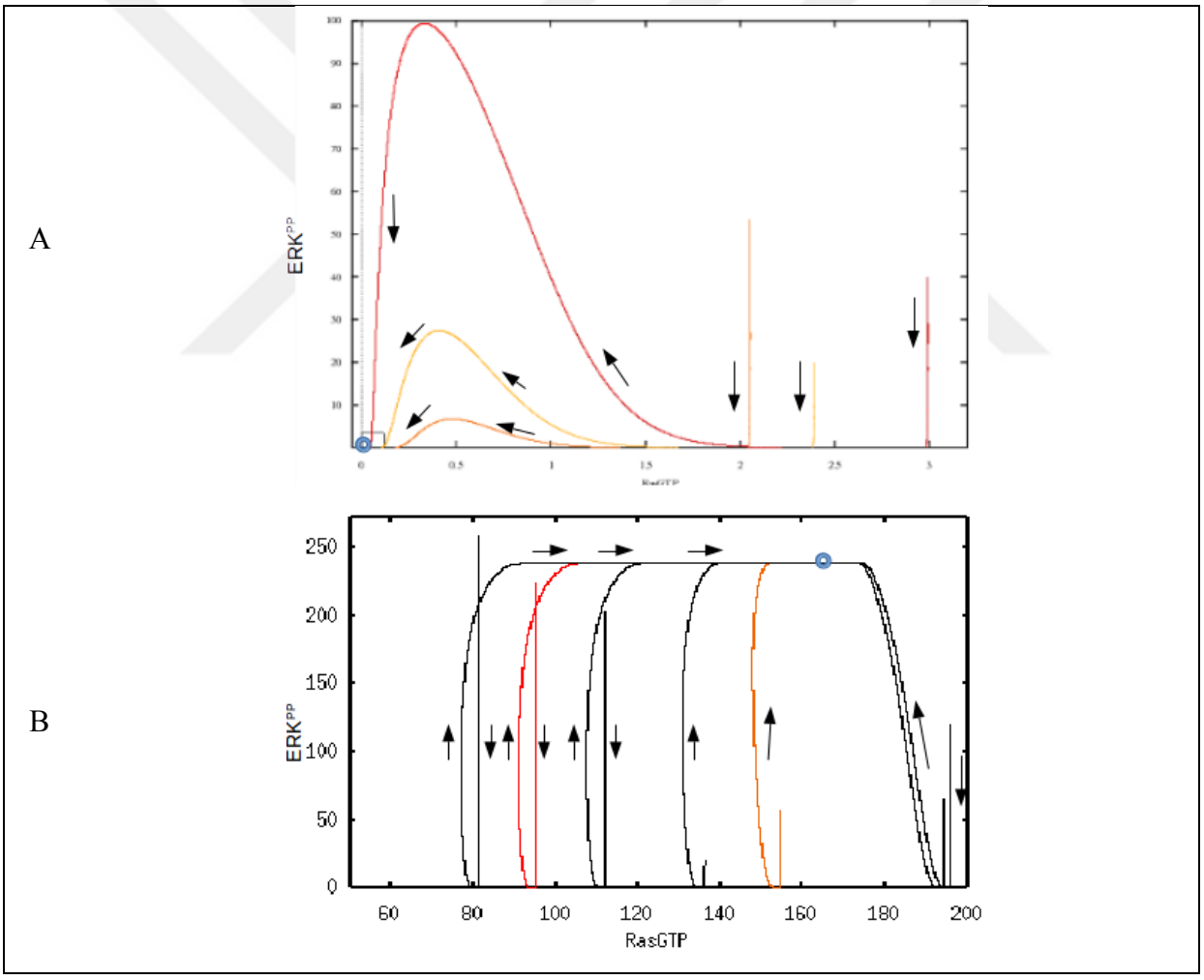

Figure 46 – The phase plane for ERK^{PP} vs. RasGTP. ***(A)*** *Inactive stable steady-state.* ***(B)*** *Active stable steady-state. The 'blue' empty circles indicate the stable steady-states.*

In Figure 46, the time simulations are represented as the trajectories on the phase plane. The small arrows show the directions of trajectories.

Comparison of Figures A and B illustrates the hysteresis of the system in this scenario. The previous history of the system, i.e. initial conditions, determines which steady-state must be approached.

Figure 46 provides that, when ERK signaling pathway is operating in the bistable regime, in addition to the ligand concentration that the cell is induced by, the current state of the cell contributes to the determination of the cell fate too.

Scenario 2 (S.D2): Effect of k_{nfb} and Km_{nfb}

First, EGF_{tot} is set to 10 (nM) as the constant input in Figure 47:

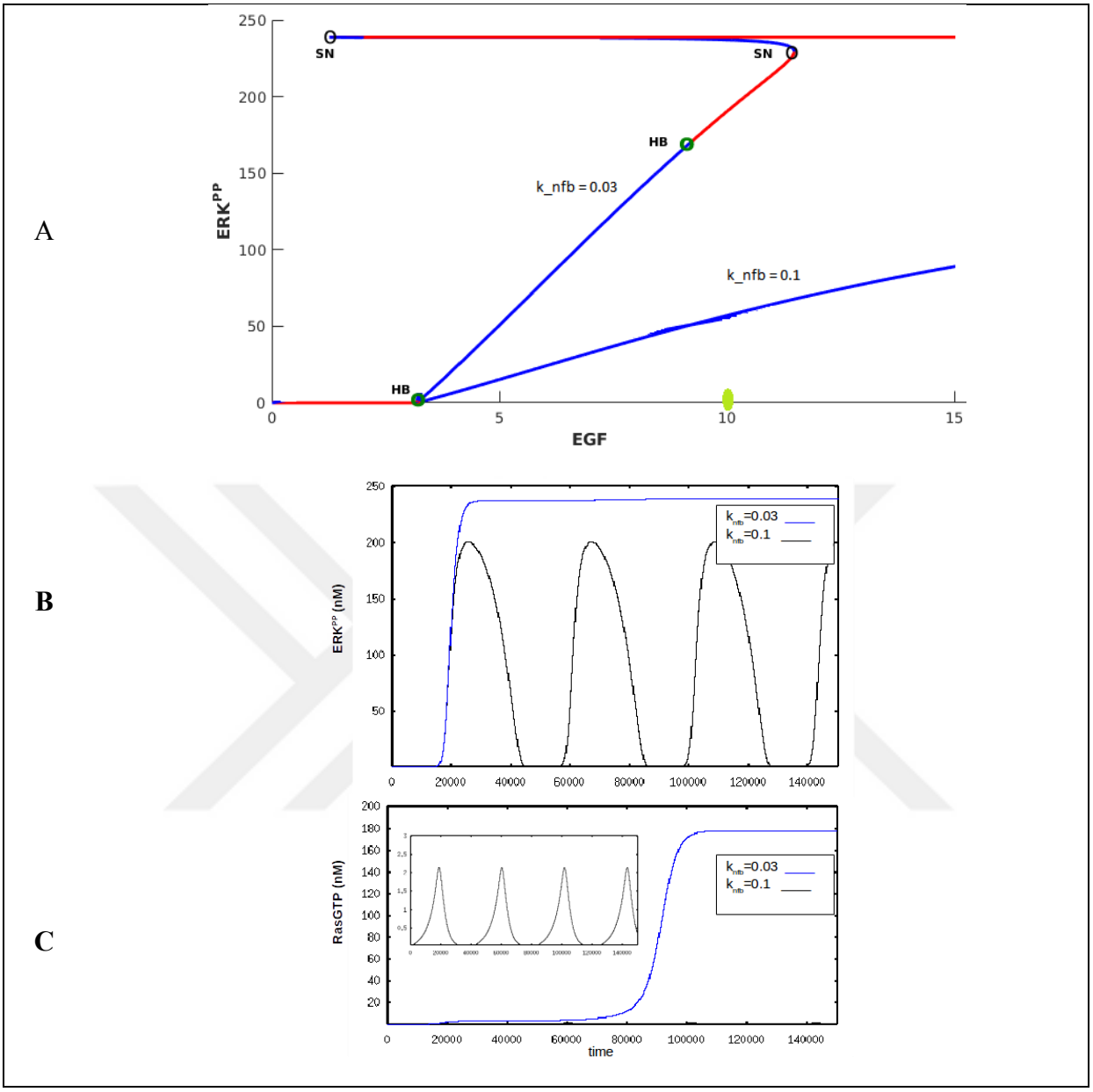

*Figure 47 - The dynamics of ERK^{PP} and RasGTP ($Km_{nfb} = 1e3$). **(A)** Represents where the steady-state for $EGF_{tot} = 10$ lies (see Figure 37). **(B)** ERK^{PP} dynamics. **(C)** RasGTP dynamics.*

Figure 47A demonstrates the steady-state solutions for $k_{nfb} = 0.1$ and $k_{nfb} = 0.03$. The greater nonlinear negative feedback action, $k_{nfb} = 0.1$ brings about the oscillatory fashion. When $k_{nfb} = 0.03$, since the constant input is bigger than *EGF* value for the top *HB* point, the system approaches its active stable state.

In the following two figures, ERK^{PP} is simulated in response to the step decrease in EGF concentration from 10 to 2 (nM).

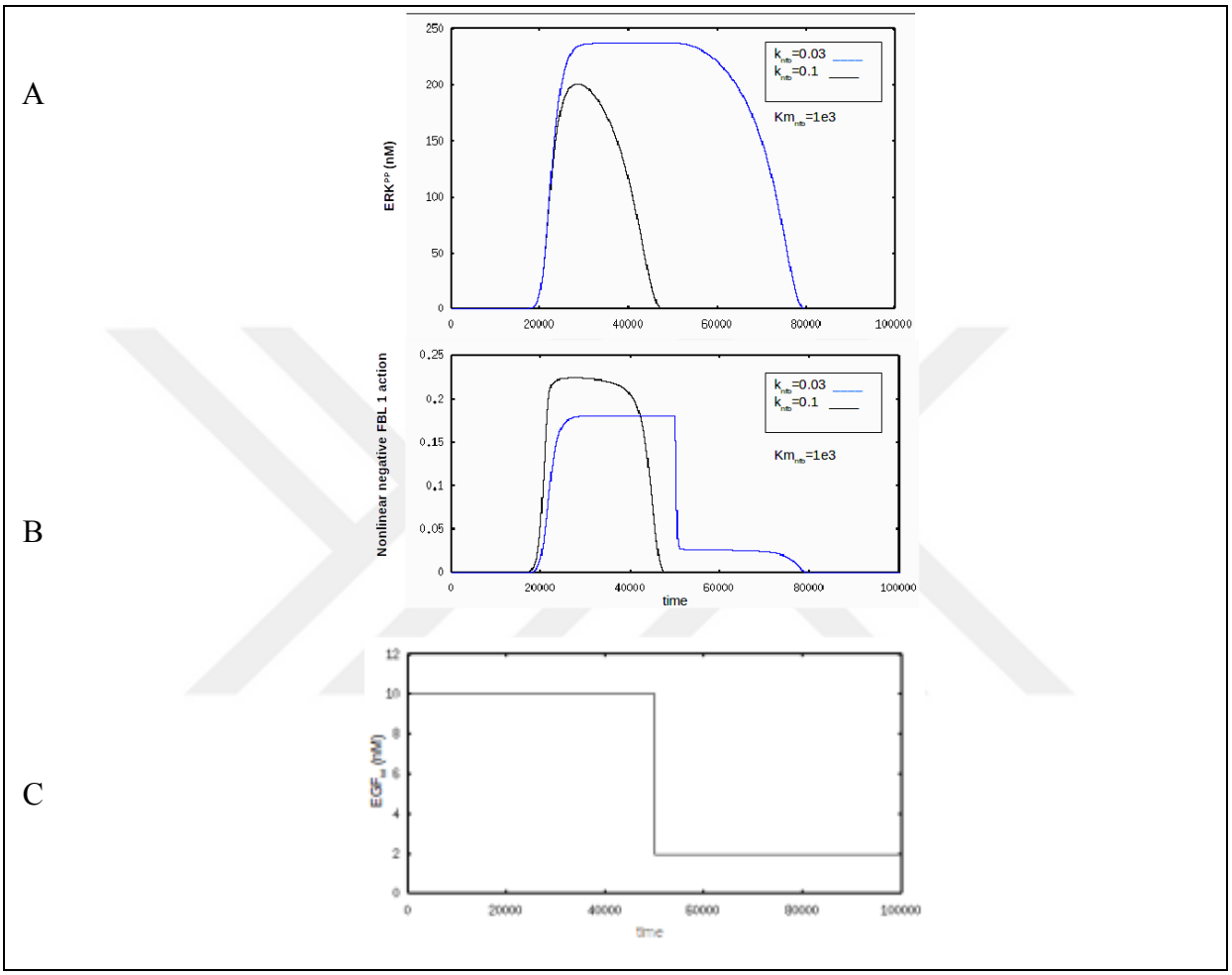

*Figure 48 - The impact of the negative FBL 1 on ERK^{PP} dynamics ($Km_{nfb} = 1e3$). **(A)** ERK^{PP} simulation for the two different negative FBL 1 actions. **(B)** The negative FBL 1 action as $k_{nfb} * [SOS_{complex}] * \frac{[ERK^{PP}]}{Km_{nfb}+[SOS_{complex}]}$ in Eq. (11).*

A

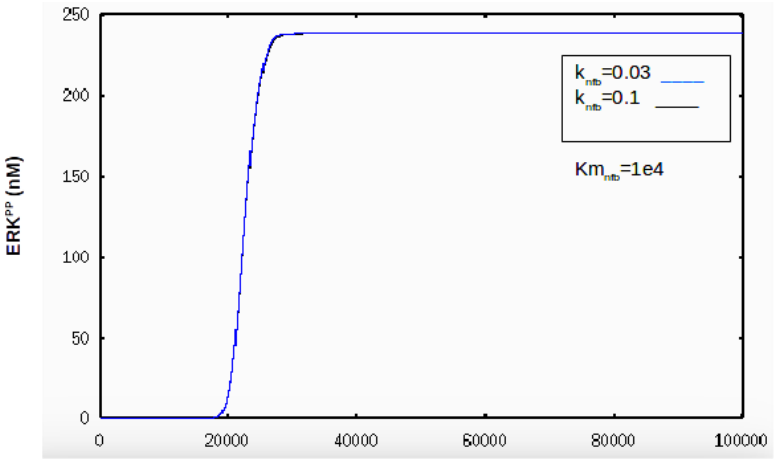

B

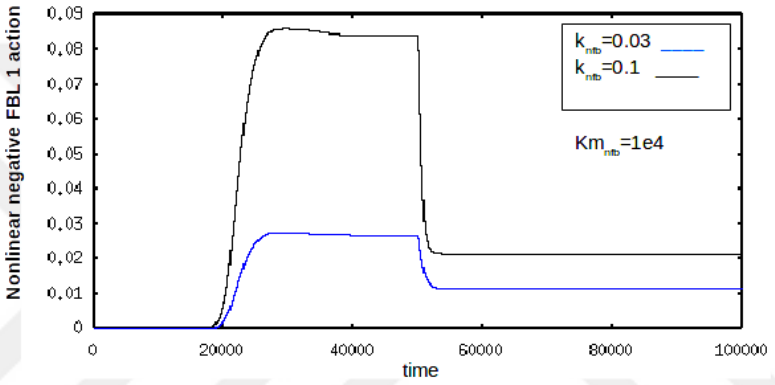

C

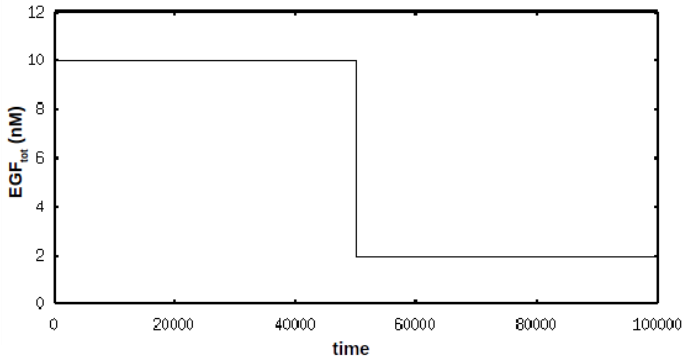

*Figure 49 - The impact of the negative FBL 1 on ERK^{PP} dynamics ($Km_{nfb} = 1e4$). **(A)** ERK^{PP} simulation for the two different negative FBL 1 actions (the curves overlapped). **(B)** The negative FBL 1 action as $k_{nfb} * [SOS_{complex}] * \frac{[ERK^{PP}]}{Km_{nfb}+[SOS_{complex}]}$ in Eq. (11).*

The nonlinearity and dependence of the negative feedback loop action on the $SOS_{complex}$ concentration, creates the difference between ERK^{PP} dynamics pattern and the nonlinear negative FBL 1 action.

Scenario 3 (D.S3): Oscillations and Periodic Solutions

In the steady-state analysis, it was observed that periodic oscillations emanate from the *HB* points. In Figure 50, the input was assigned to *EGF* values for the three different periodic solutions.

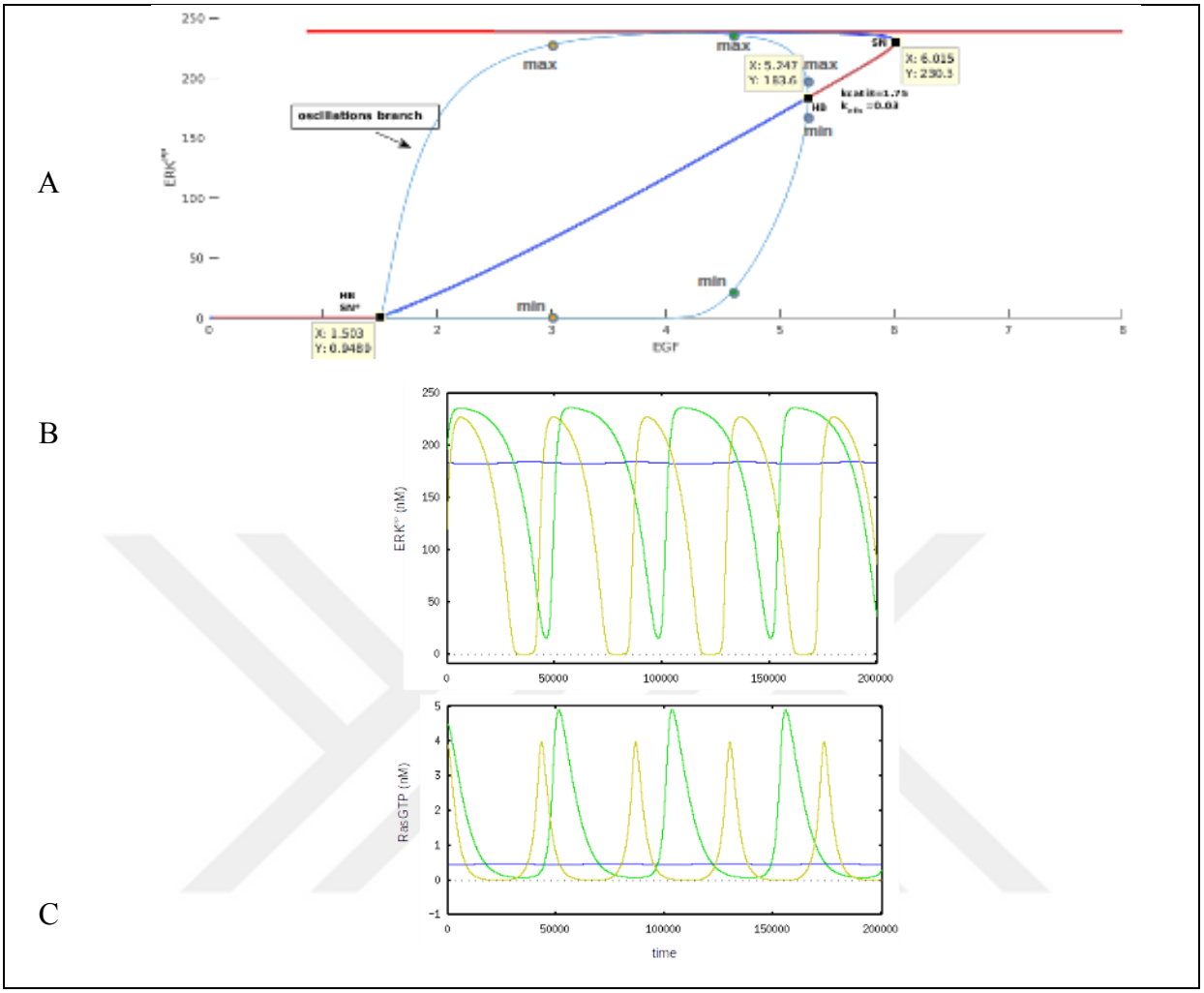

Figure 50 – Oscillations in response to the three different EGF values.

***(A)** The filled circles on the plot represent the minimum and maximum of the oscillations waves at the corresponding input. Blue: $EGF_{tot} = 5.248$, green: $EGF_{tot} = 4.501$, brown:$EGF_{tot} = 3$. **(B)** The oscillatory behavior of ERK^{PP}. **(C)** The oscillatory behavior of RasGTP.*

The initial conditions were set to the steady-state solutions of the variables. Perturbing one of the states leads to the oscillatory fashion. Unstable sustained oscillations emerge with the maximum and minimum amplitude dictated by the input value. Thus, the oscillations at $EGF_{tot} = 5.248$ (close to *HB* point), exhibit very small amplitude which is magnified in the following figure.

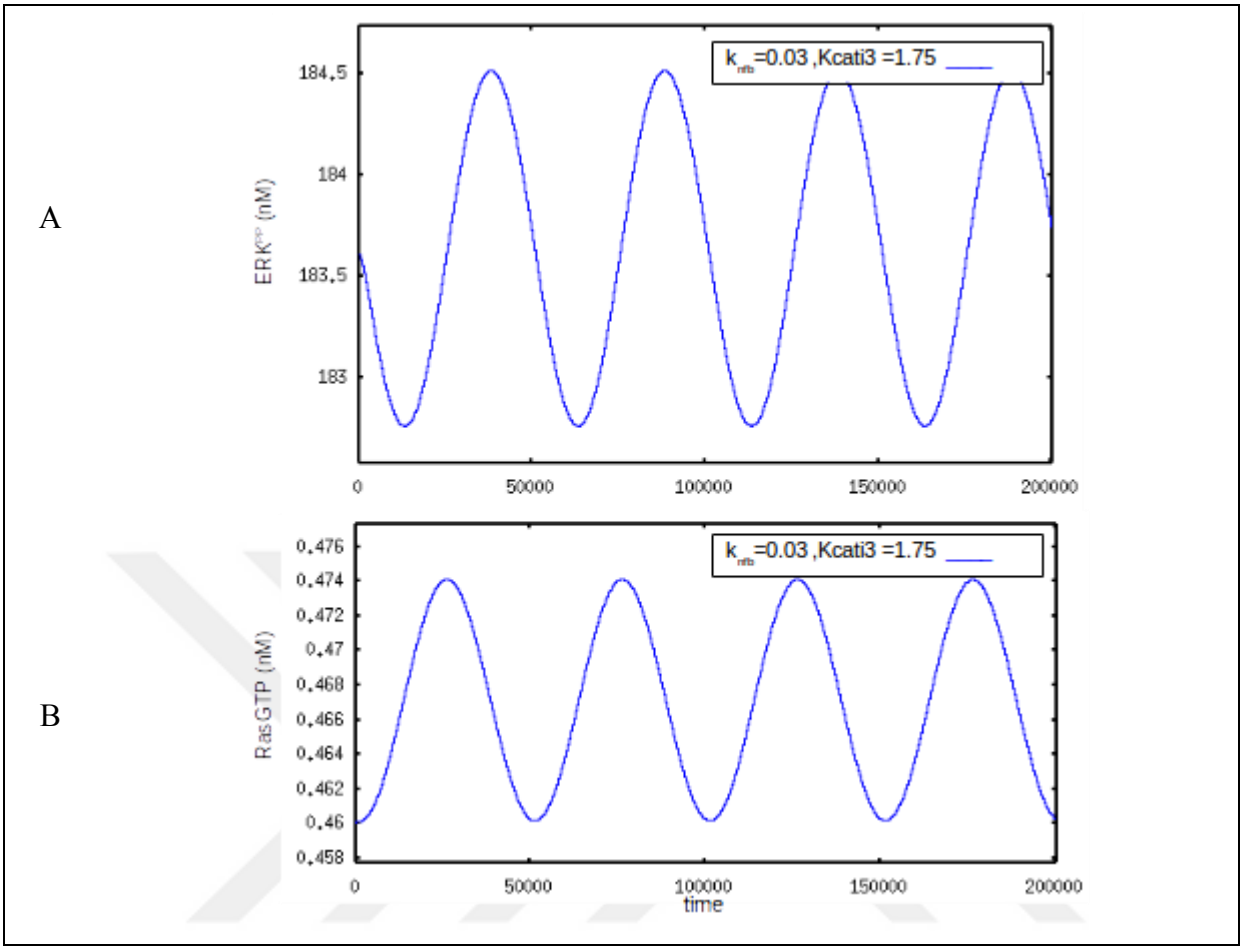

Figure 51 - The oscillatory behavior of ERK^{PP} and RasGTP, where $EGF_{tot} = 5.248\ (nM)$. ***(A)*** *The oscillatory behavior of ERK^{PP}.* ***(B)*** *The oscillatory behavior of RasGTP.*

The phase planes for the illustrating ERK^{PP} time evolution as a function of *RasGTP* for the three input values are shown in Figure 52.

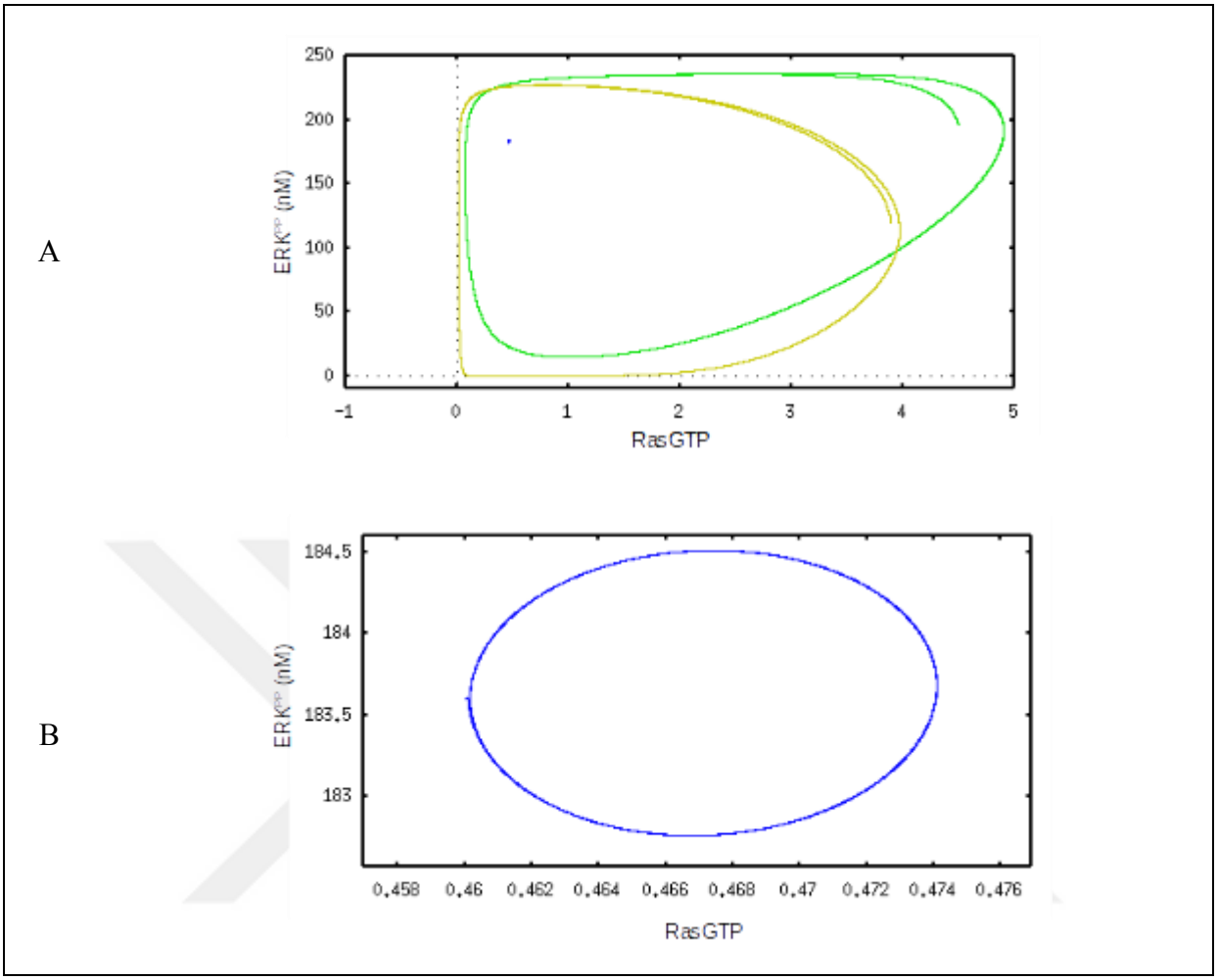

Figure 52 - The phase plane of ERK^{PP} and RasGTP oscillatory behavior. ***(A)*** *The phase plane for the Figure 50.* ***(B)*** *The phase plane for the case where $EGF_{tot} = 5.248\ (nM)$.*

Figure 52 shows that when the oscillatory dynamics exist, the phase plane resembles *limit cycle.* Two necessary conditions for the sustained limit cycles to exist are: negative feedback and nonlinearity [14]. Both of which coexist in our model for the negative FBL 1.

The green and brown oscillations waves resemble so-called *relaxation oscillators*. This type of sustained oscillations is generated as the result of the positive and negative feedback loops combination, while the positive feedback loop establishes *near* bistable behavior, the negative feedback loop causes the system to cycle between the two quasi-stable conditions (see Figure 36). The hallmark of the relaxation oscillators is their "pulse-like" oscillations, usually followed by a

longer time interval of settling on deactivated state [14].

As discussed in Sec 4.1, an intermediate stable branch emerges as the result of the cascade sensitivity. In Figure 53 and Figure 54, the input and the initial conditions for occupying this stable branch are studied.

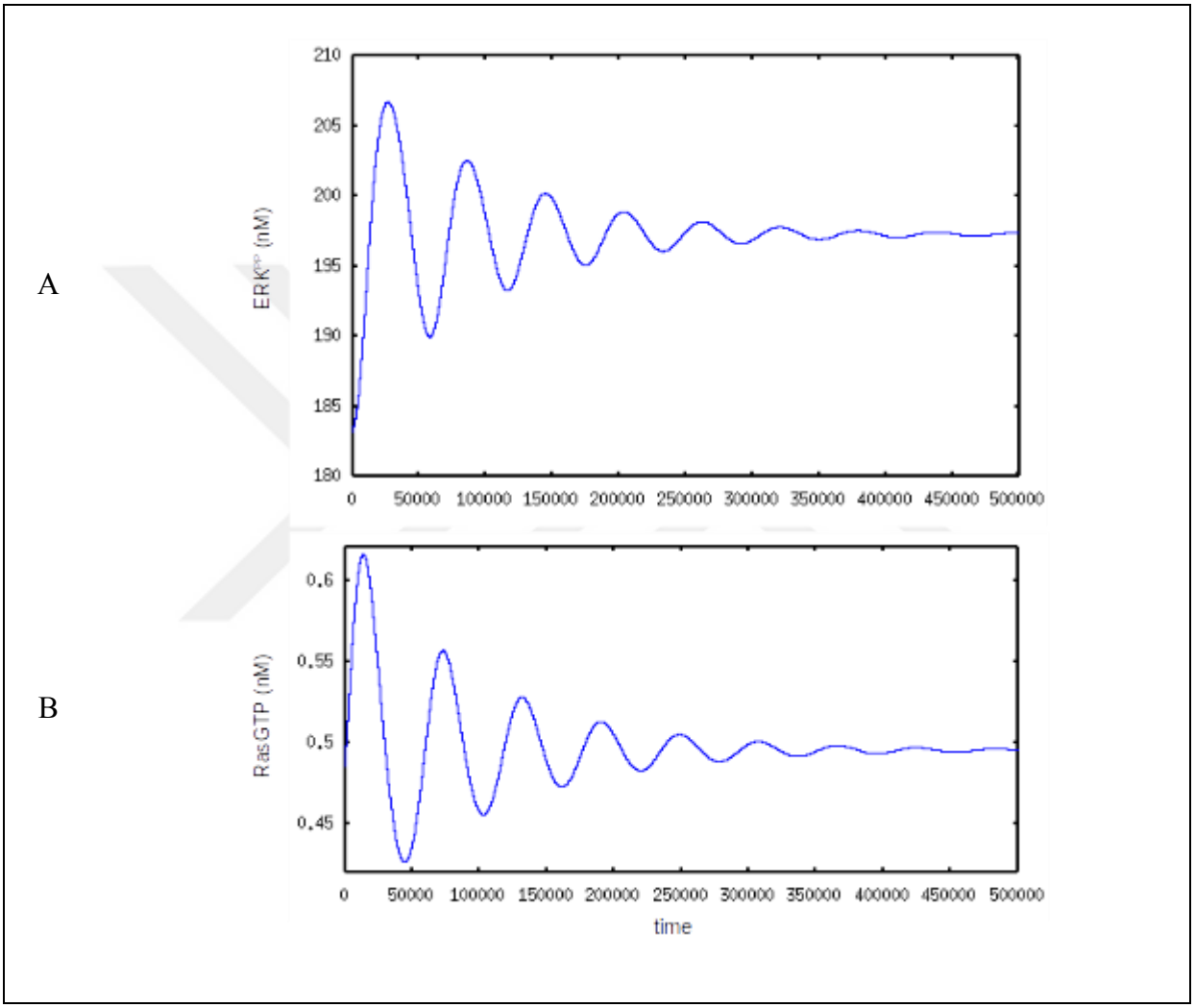

*Figure 53 - The dynamics of RasGTP and ERK^{PP} in response to the constant input $EGF_{tot} = 5.5\ (nM)$. **(A)** ERK^{PP} response. **(B)** RasGTP response.*

When $EGF = 5.5\ (nM)$, the system might settle on the intermediate branch. In Figure 53, the initial conditions for all the variables except for *RasGTP* and ERK^{PP} are set to their steady-state solutions. Perturbing ERK^{PP} and *RasGTP* slightly off their steady-state solutions leads to

decaying oscillations.

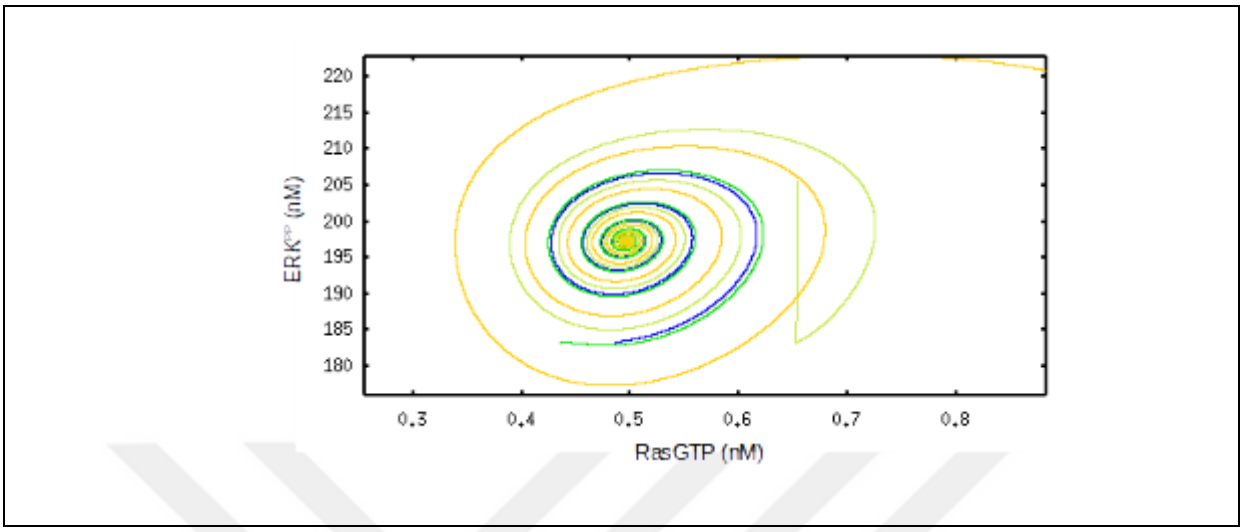

Figure 54 - ERK^{PP} vs. RasGTP phase plane for the varying initial conditions at $EGF_{tot} = 5.5\ (nM)$.

Figure 54 illustrates that for a range of initial conditions close to the steady-state solutions of *RasGTP* and ERK^{PP}, the system is attracted to the intermediate branch.

Decaying oscillations create *spirals* when they are plotted on the phase plane.

A

B

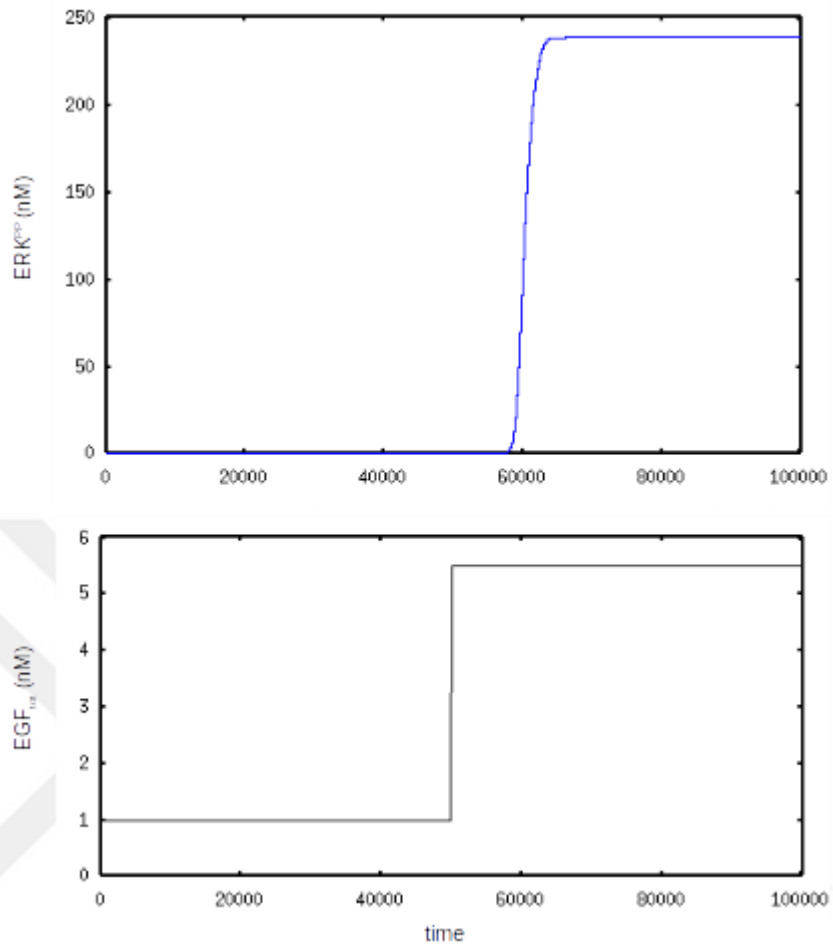

Figure 55 - ERK^{PP} dynamics in response to the step change in EGF_{tot} from 1 to 5.5 (nM).

Predictably, in Figure 55 it is shown that for step increase in EGF_{tot} concentration the system jumps to the upper stable steady-state.

Scenario 4 (D.S4): Effect of ARGOS Negative Feedback Loop on ERK^{PP} and RasGTP Dynamics

The constant input $EGF_{tot} = 6\ (nM)$ can lead to both the stable active steady-state solutions or to the sustained oscillatory dynamic behavior, dependent on the initial conditions of the system as shown in Figure 56 and Figure 57.

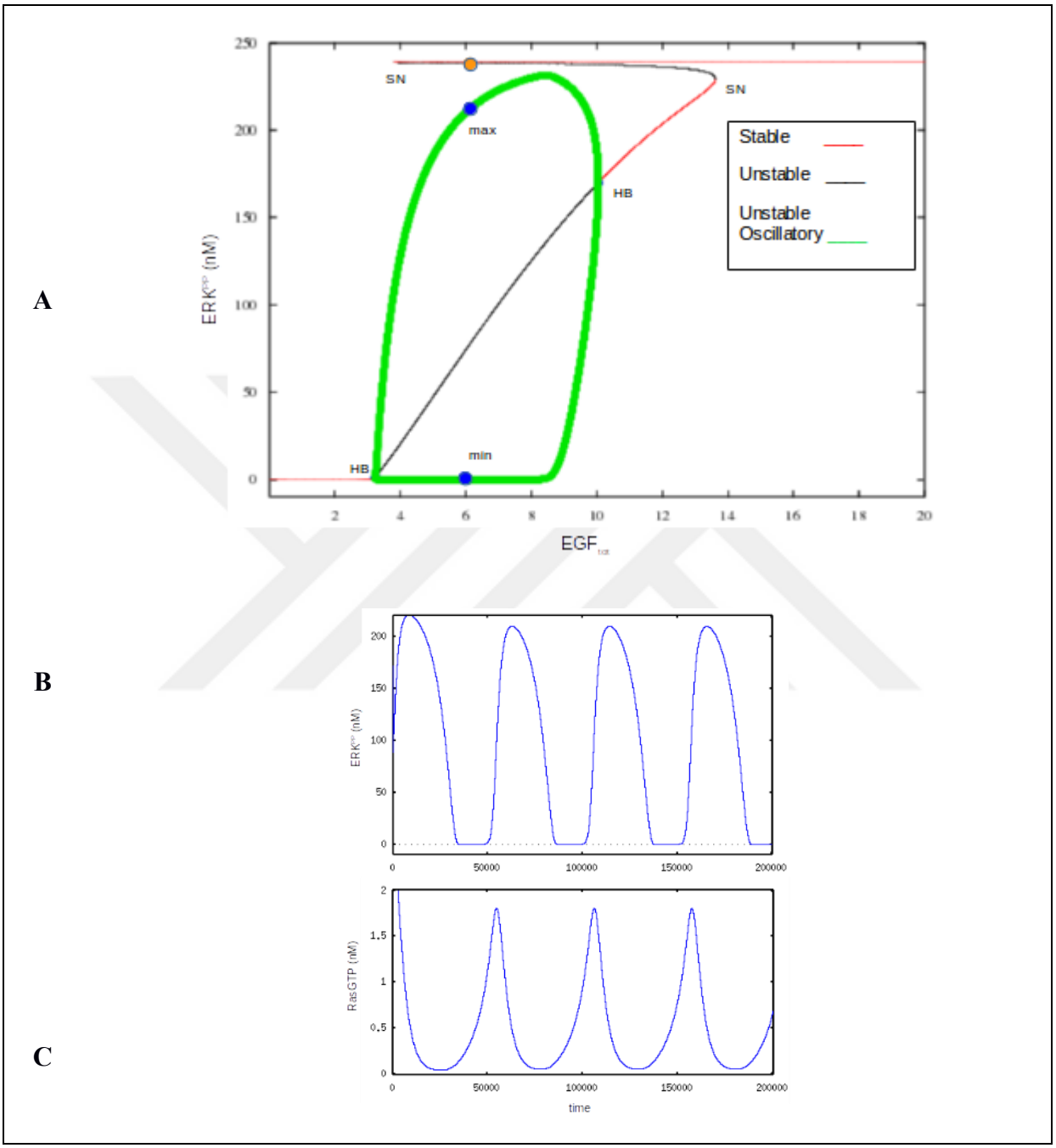

Figure 56 – The impact of the negative FBL 3 on ERK^{PP} and RasGTP oscillatory dynamics in response to the constant $EGF_{tot} = 6\ (nM)$ $(gpA = 3e^{-8})$.

The relaxation oscillators appear in the dynamics of the system affected by ARGOS negative feedback loop (FBL 3).

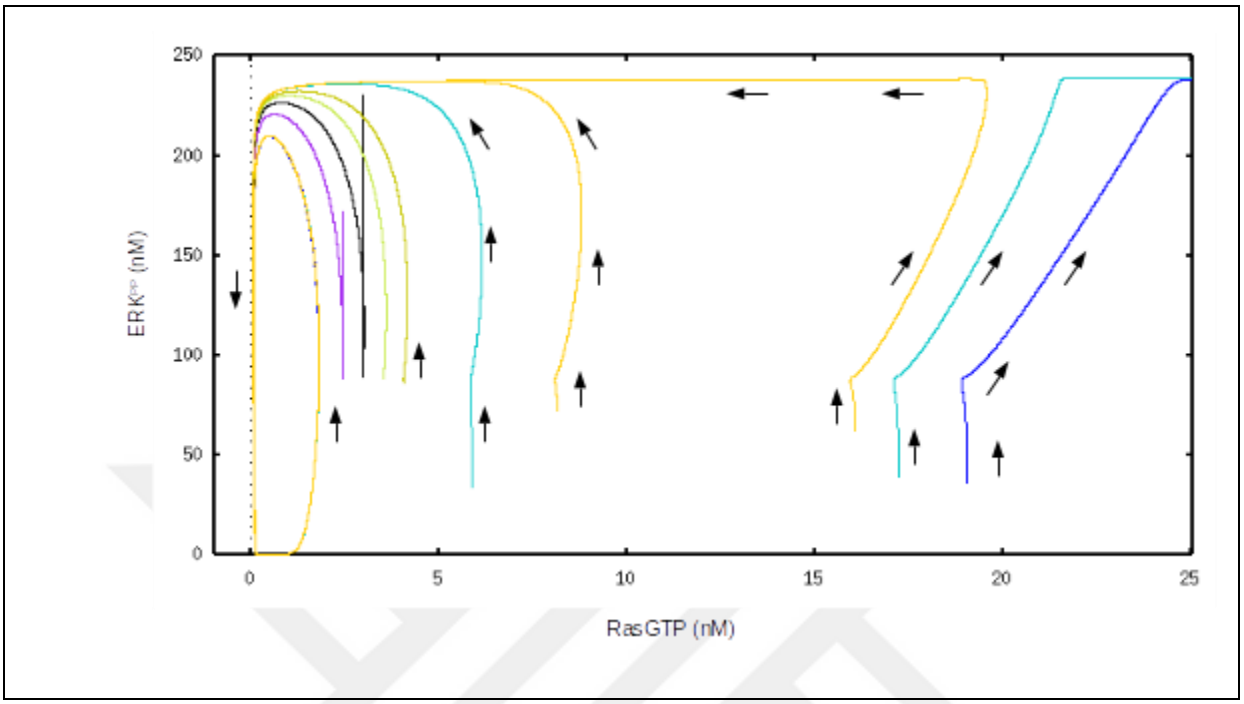

Figure 57 - The phase plane of ERK^{PP} vs. RasGTP for the varying initial conditions.

Figure 57 illustrates that when the initial condition of *RasGTP* is large enough to switch the system on, trajectories approach the upper stable steady-state.

Scenario 5 (D.S2): Effect of Autocrine on ERK^{PP} Dynamics

To study effect of the autocrine loop (FBL 2), the input was given to the system as a pulse with the duration of $8e^4$ (seconds) and the amplitude of 10 units change in EGF_{tot} concentration.

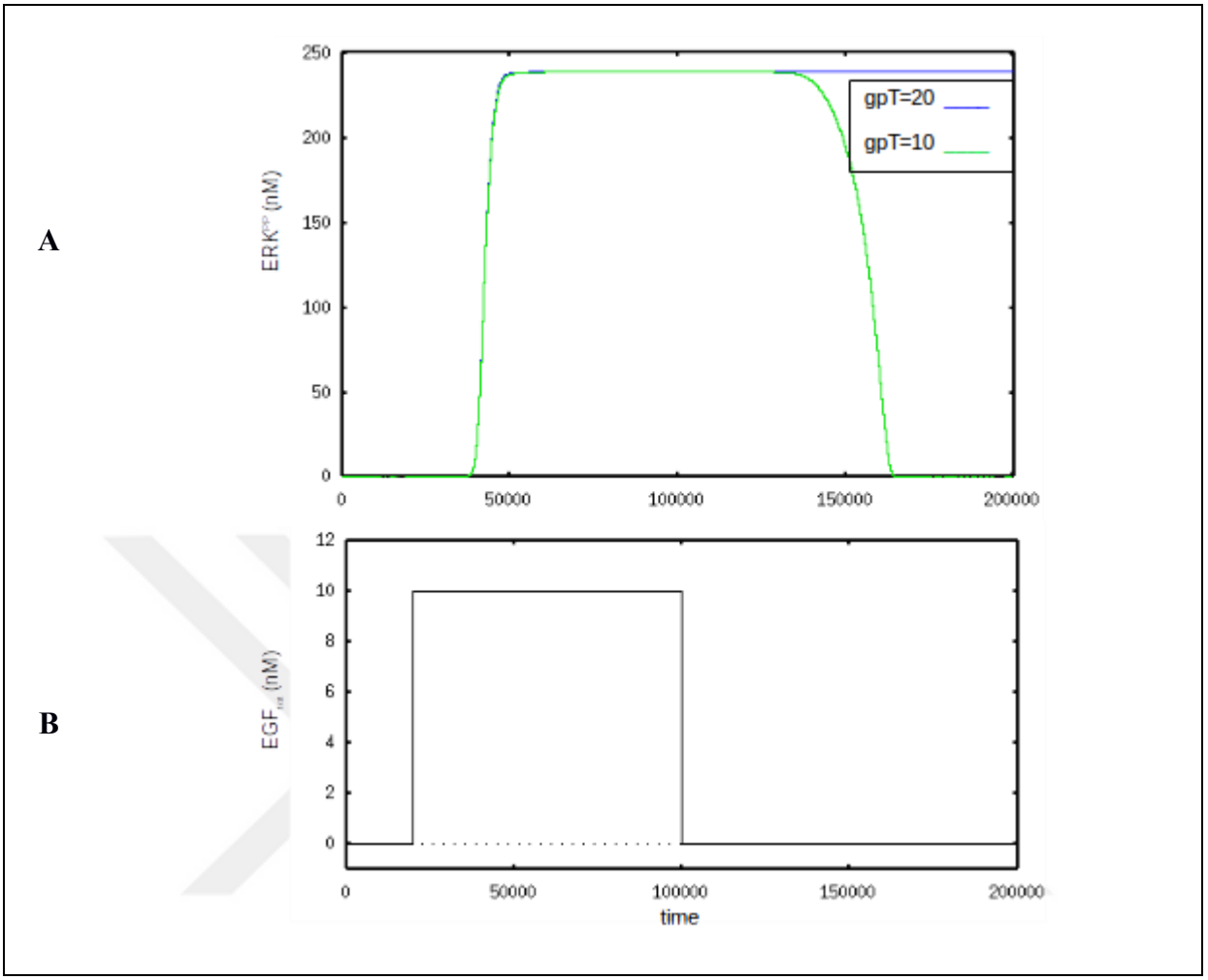

Figure 58 - ERK^{PP} dynamics in response to the pulse EGF_{tot} input.

Figure 58 shows that the autocrine loop with $gpT = 20$, is strong enough to make the system incapable of the switching from on state to the off state.

Chapter 5: Conclusions

In this thesis, we proposed a new mathematical model to study the steady-state and dynamic characteristics of ERK signaling pathway. We studied the impact of four key negative and positive feedback loops on the system behavior. Notable amount of biological knowledge was exploited to grasp the biological purpose of this critically important pathway for the cell fate determination.

Earlier models for the separate sections of the pathway were integrated and interconnected to construct the complete model. When deemed necessary the model parameters were tuned and validated against reliable experimental or theoritical data.

It is a fundamental question that how the cell is able to determine and extract information from an external stimulus. It has been discovered that each receptor can activate no more than a handful of pathways. Thus, the role of the regulatory control loops with distinct characteristics is undisputable. Several regulatory feedback loops contribute to shape the activated *ERK* response.

Based on a careful investigation of literature data, four feedback loops, two negative and two positive loops, were chosen to be analyzed.

We showed that any mutations or alterations in the feedback loops strength can lead to the

irreversible adverse effects ultimately resulting in disease states. The abnormally strong positive feedback action from *RasGTP* or autocrine can lead to the deactivation of the toggle switch between the active and inactive states of ERK^{PP} and *RasGTP*. The persistent activity of *RasGTP* was proved to be involved in one-third of the cases diagnosed with cancer [2].

We proposed that the negative feedback loop action combined with the positive feedback loop effect can give rise to the relaxation oscillators for the various range of the ligand concentrations.

We were able to relate *RasGTP* bistability to *ERK* bistable regime. It was shown that the positive feedback loop from *RasGTP to* $SOS_{complex}$ creates the bistable switch-like behavior of *RasGTP* which is the upstream activator of MAPK cascade. Consequently, the bistable regime transmits and amplifies through MAPK cascade which ultimately determines bistability in the activated *ERK* response.

We observed an intermediate stable branch in the activated *ERK* and *MEK* steady-state response to the *EGF* that was not reported before. Our results suggest that while *RasGTP* operates in its low activity state, *ERK* is capable of occupying the intermediate stable steady-state branch.

Although in the literature the negative feedback loop from activated *ERK* to $SOS_{complex}$ was discussed, its harmony with the autocrine and ARGOS negative feedback loop received less attention. However, in this thesis we investigated the interactions among these loops.

The structure of the model is developed such that it can easily incorporate new interactions and cross-talks as a future step to enrich the model in order to make it more encompassing and predicting.

Using our model, we generated new hypotheses that hopefully can give a clue for future experimental design and verification.

APPENDIX I

A.1 Equilibrium approximation: Michaelis-Menten equation

Michaelis and Menten (1913) suggested the mechanism in the following Figure for enzymatic biochemical reactions:

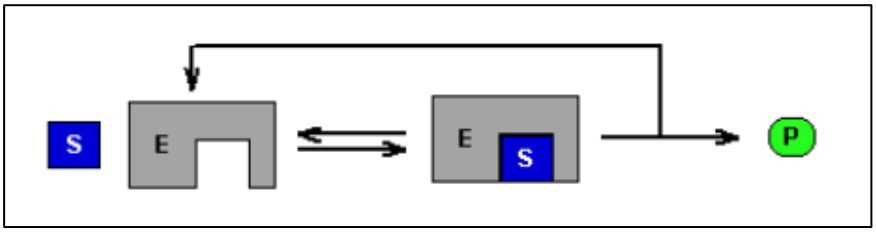

Figure 59 - Michaelis-Menten mechanism for enzymatic reactions

The reaction and its species velocities are given below:

$$E + S \underset{k-1}{\overset{k1}{\rightleftharpoons}} C \xrightarrow{k2} E + P \tag{19}$$

$$v_{forward} = k_1.E.S \tag{20}$$

$$v_{backward} = k_{-1}.C \tag{21}$$

$$v_{catalytic} = k_2.C \tag{22}$$

$$\frac{dS}{dt} = -k_1.E.S + k_{-1}.C \tag{23}$$

$$\frac{dE}{dt} = -k_1.E.S + k_{-1}.C + k\_2.C \tag{24}$$

$$\frac{dC}{dt} = k_1.E.S - k_{-1}.C - k_2.C \tag{25}$$

$$\frac{dP}{dt} = k_2.C \tag{26}$$

It was assumed by Michaelies and Menten that the substrate S instantly reaches equilibrium with the enzyme-substrate complex, C.

This assumption needs the rate constants for the forward and backward reactions (k_1, k_{-1}) to be greater than the rate constant for the catalytic reaction (k_2):

$$k_1, k_{-1} \gg k_2 \tag{27}$$

This leads to:

$$v_{forward} = v_{backward} \tag{28}$$

$$k_1.E.S = k_{-1}.C$$

Total concentration of enzyme is conserved, thus:

$$E_T = E + C \tag{29}$$

$$and\ C = \frac{E_T.S}{\frac{k_{-1}}{k_1} + S}$$

Consequently, the rate of production of the product P is given as:

$$v_{catalytic} = \frac{dP}{dt} = k_2.C = \frac{k2.E_T.S}{\frac{k_{-1}}{k_1} + S} \quad (30)$$

Defining $V_{max} = k_2.E_T\ and\ K_s = \frac{k_{-1}}{k_1}$, Michaelis-Menten equation is derived as follows:

$$v = \frac{V_{max}.S}{K_s + S} \quad (31)$$

A.2 Quasi-steady state assumption: Briggs-Haldane equation

Briggs and Haldane (1925) suggested another hypothesis for the same mechanism of enzymatic reaction (see Figure 59).

Based on this hypothesis, in *enzymatic* reactions where the enzyme is available in *catalytic* amount (i.e. $E \ll S$), quickly after mixing *E* and *S*, *ES* reaches a steady-state in which it is essentialy constant with respect to time. This is called *quasi-steady state assumption (QSSA)*.

This assumption suggests that:

$$\frac{dC}{dt} = 0 \quad (32)$$

Since $E_{tot} = E + C = constant$:

$$E_{tot} = E + C = constant \quad (33)$$

$$\frac{dE}{dt} = 0 \quad (34)$$

When substituted in Equations (24) and (25), it is implied that:

$$k_1.E.S - k_{-1}.C - k_2.C = 0 \quad (35)$$

This equation along with Eq. (33) provides the eqution for complex (*C*) concentration:

$$C = \frac{k_1.E_{tot}.S}{k_1.S + (k_{-1} + k_2)} = \frac{E_{tot}.S}{S + \frac{k_{-1} + k_2}{k_1}} \quad (36)$$

Thus, rate of P production can be written as:

$$v = \frac{dP}{dt} = k_2.C = \frac{k_2.E_{tot}.S}{S + \frac{k_{-1} + k_2}{k_1}} \quad (37)$$

Considering $V_{max} = k_2.Etot\ and\ K_M = \frac{k_{-1}+k_2}{k_1}$, we have the well-known format:

$$v = V_{max}.\frac{S}{S + K_M} \quad (38)$$

This is similar to Eq (31) which was derived with *equilibrium assumption*. However, K_M is usually referred to as *Michaelis-Menten* constant.

Where $k_1, k_{-1} \gg k_2$ (assumed in Michaelis-Menten equation), $K_M \rightarrow K_S$.

APPENDIX II

Table 12 - Variables Vs. Molecules name

Variable name	Molecule Name	Variable name	Molecule name
z1	EGF_EGFR	z2	(EGF_EGFR)2
z3	(EGF_EGFR)2-P	z4	(EGF_EGFR)2_PLCg
z5	(EGF_EGFR)2_PLCg-P	z6	(EGF_EGFR)2_Grb2
z7	(EGF_EGFR)2_Grb2_SOS	z8	(EGF_EGFR)2_Shc
z9	(EGF_EGFR)2_Shc-P	z10	(EGF_EGFR)2_Shc_Grb2
z11	(EGF_EGFR)2_Shc_Grb2_Sos	z12	Grb2_SOS

(continued on the next page)

z13	Shc-P	z14	Shc_Grb2
z15	PLCg-P	z16	PLCg-P-I
z17	Shc_Grb2_SOS or $SOS_{complex}$	z18	EGFR
z19	EGF	z20	PLCg
z21	Grb2	z22	Shc

z23	SOS		
Rd	RasGDP	Rt	RasGTP
SRd	$SOS_{complex}$-RasGDP	SRt	$SOS_{complex}$-RasGTP
x1	Raf_RasGTP		
x2	Raf*	x3	Raf*_E2
x4	MEK_Raf*	x5	MEK-P
x6	MEK-P_P'ase 1	x7	MEK-P_Raf*
x8	MEK-PP	x9	MEK-PP_P'ase 1
x10	ERK_MEK-PP	x11	ERK-P
x12	ERK-P_P'ase 2	x13	ERK-P_MEK-PP]
x14	ERK-PP	x15	ERK-PP_P'ase 2
x16	Raf	x17	MEK
x18	ERK	x19	-
x20	E2	x21	P'ase 1
x22	P'ase 2		

Next Table gives total amount of the conserved moieties

Table 13 - Total amount of conserved moieties

EGFR	tot1=10;
EGF	tot2=0.1;
PLCg	tot3=105;
Grb2	tot4=85;

Shc	tot5=150;
SOS	tot6=50
Ras	tot7=200
GAPS	Rgap=0.1
Raf	tot8=9.2235e-001
MEK	tot9=5.1288e+003
ERK	tot10=8.1552e+002
RasGTP (merged to tot7)	tot11=5e-002
E2	tot12=3.2830e-001
P'ase 1	tot13=2.1238e-001
P'ase 2	tot14=5.0345e+002
Akt	Akttot=600
Gsk3β	Gsk3βtot=600
Rb	R=550

The model parameters are given as follows:

Table 14 - Model 1 parameters.

kf1=0.003	kb1=0.06	kf2=0.01	kb2=0.1
kf3=1	kb3=0.01	Vu4=450	Ku4=50
kf5=0.06	kb5=0.2	kf6=1	kb6=0.05
kf7=0.3	kb7=0.006	Vu8=1	Ku8=100
kf9=0.003	kb9=0.05	kf10=0.01	kb10=0.06

kf11=0.03	kb11=4.5e-3	kf12=1.5e-3	kb12=1e-4
kf13=0.09	kb13=0.6	kf14=6	kb14=0.06
kf15=0.3	kb15=9e-4	Vu16=1.7	Ku16=340
kf17=0.003	kb17=0.1	kf18=0.3	kb18=9e-4
kf19=0.01	kb19=2.14e-2	kf20=0.12	kb20=2.4e-4
kf21=0.003	kb21=0.1	kf22=0.03;	kb22=0.064;
kf23=0.1;	kb23=0.021;	kf24=0.009;	kb24=4.29e-2;
kf25=1;	kb25=0.03;		

Table 15 - Model 2 parameters.

kfi1=1.125e-4	kbi1=3	kfi2=1.0625e-4	kbi2=0.4
kcati3=1	kcati4=0.003	kcati5=0.1	ki3m=2.7388e3
ki4m=1.52304e4	ki5m=1.7869e1		

Table 16 - Model 3 parameters.

a1=0.00049;	a2=0.0307;	a3=0.0204;	a4=0.0493;
a5=0.0564;	a6=0.0326;	a7=0.0038;	a8=0.0050;
a9=0.0056;	a10=0.0162;	d1=0.049;	d2=3.3078;
d3=10.3862;	d4=2.7167;	d5=10.0885;	d6=0.8134;
d7=11.5688;	d8=5.0182;	d9=8.0892;	d10=9.7908;
k1=0.049;	k2=5.6407;	k3=7.0000;	k4=11.1367;

k5=3.5775;	k6=1.1328;	k7=0.7276;	k8=0.5291;
k9=1.0955;	k10=2.9318;		

Table 17 - Model 4 parameters

km=2.78e-4;	kAP=0.1;	KmAP=10;	kAD=20.016;
KmAD=10;	kGP=0.1;	KmGP=10;	kGD=20.016;
KmGD=10;	kMS=6.4e-4;	KmMS=2.8e-3;	kMT=1.12e-4;
KmMT=2.8e-3;	dM=5.78e-4;	dMS=9.73e-5;	dMT=5.78e-4;
GF=1000;	Constant input: PI3K=1000	kkE=0.1111;	kkM=0.2778;
kkCD=8.3333e-3;	kkCDS=0.1250;	kkR=0.05;	kkRE=50.004;
kkb=0.06;	KKmS=500;	kkCE=0.0972;	ddM=1.9444e-4;
ddE=6.9444e-5;	ddCD=4.1667e-4;	ddCE=4.1667e-4;	ddR=1.6667e-5;
ddRP=1.6667e-5;	ddRE=8.3333e-6;	kkP1=0.005;	kkP2=0.005;
kkDP=1.0001;	KKmM=150;	KKmE=150;	KKmCD=920;
KKmCE=920;	KKmRP=10;	dT=1;	gpT=10;
grT=0;	KmTACE=1000;	kAE=5;	dAE=1;
dA=1e-6;	gpA=1e-6;	KmA=10;	grAE=1;

Algebraic equations representing conserved moieties:

$$z18 = tot1 - (z1 + 2 * (z2 + z3 + z4 + z5 + z6 + z7 + z8 + z9 + z10 + z11)) - grAE * AE$$

$$z19 = tot2 + grT * TACE - (z1 + 2 * (z2 + z3 + z5 + z4 + z8 + z9 + z6 + z7 + z10 + z11))$$

$$z20 = tot3 - (z4 + z5 + z15 + z16)$$

$$z21 = tot4 - (z12 + z14 + z17 + z6 + z7 + z10 + z11 + SRd + SRt)$$

$$z22 = tot5 - (z13 + z14 + z17 + z8 + z9 + z10 + z11 + SRd + SRt)$$

$$z23 = tot6 - (z12 + z17 + z7 + z11 + SRd + SRt)$$

$$Rd = tot7 - (Rt + SRd + SRt + x1)$$
$$x16 = tot8 - (x2 + x1 + x3 + x4 + x7)$$
$$x17 = tot9 - (x5 + x8 + x4 + x7 + x6 + x9 + x10 + x13)$$
$$x18 = tot10 - (x11 + x14 + x10 + x13 + x12 + x15)$$
$$x20 = tot12 - (x3)$$
$$x21 = tot13 - (x6 + x9)$$
$$x22 = tot14 - (x12 + x15)$$
$$Akt = Akttot - pAkt$$
$$Gsk3b = Gsk3btot - pGsk3b$$

Model 1 reactions:

$$r1 = kf1 * z18 * z19 - kb1 * z1$$
$$r2 = kf2 * z1 * z1 - kb2 * z2$$
$$r3 = kf3 * z2 - kb3 * z3$$
$$r4 = Vu4 * z3/(Ku4 + z3)$$
$$r5 = kf5 * z3 * z20 - kb5 * z4$$

$$r6 = kf6 * z4 - kb6 * z5$$
$$r7 = kf7 * z5 - kb7 * z3 * z15$$
$$r8 = Vu8 * z15/(Ku8 + z15)$$
$$r9 = kf9 * z3 * z21 - kb9 * z6$$
$$r10 = kf10 * z6 * z23 - kb10 * z7$$
$$r11 = kf11 * z7 - kb11 * z3 * z12$$
$$r12 = kf12 * z12 - kb12 * z21 * z23$$
$$r13 = kf13 * z3 * z22 - kb13 * z8$$
$$r14 = kf14 * z8 - kb14 * z9$$
$$r15 = kf15 * z9 - kb15 * z13 * z3$$
$$r16 = Vu16 * z13/(Ku16 + z13)$$
$$r17 = kf17 * z9 * z21 - kb17 * z10$$
$$r18 = kf18 * z10 - kb18 * z3 * z14$$
$$r19 = kf19 * z10 * z23 - kb19 * z11$$
$$r20 = kf20 * z11 - kb20 * z17 * z3$$
$$r21 = kf21 * z13 * z21 - kb21 * z14$$
$$r22 = kf22 * z14 * z23 - kb22 * z17$$
$$r23 = kf23 * z17 - kb23 * z13 * z12$$
$$r24 = kf24 * z9 * z12 - kb24 * z11$$
$$r25 = kf25 * z15 - kb25 * z16$$

The rate of the species changes (ODEs) for Model 1:

$$\frac{dz1}{dt} = r1 - 2 * r2$$
$$\frac{dz2}{dt} = r2 + r4 - r3$$
$$\frac{dz3}{dt} = r3 + r7 + r11 + r15 + r18 + r20 - r4 - r5 - r9 - r13$$

$$\frac{dz4}{dt} = r5 - r6$$

$$\frac{dz5}{dt} = r6 - r7$$

$$\frac{dz6}{dt} = r9 - r10$$

$$\frac{dz7}{dt} = r10 - r11$$

$$\frac{dz8}{dt} = r13 - r14$$

$$\frac{dz9}{dt} = r14 - r24 - r15 - r17$$

$$\frac{dz10}{dt} = r17 - r18 - r19$$

$$\frac{dz11}{dt} = r19 - r20 + r24$$

$$\frac{dz12}{dt} = r11 + r23 - r12 - r24$$

$$\frac{dz13}{dt} = r15 + r23 - r21 - r16$$

$$\frac{dz14}{dt} = r18 + r21 - r22$$

$$\frac{dz15}{dt} = r7 - r8 - r25$$

$$\frac{dz16}{dt} = r25$$

$$\frac{dz17}{dt} = -r23 + r22 + r20 - kfi1 * z17 * Rd + kbi1 * SRd - kfi2 * z17 * Rt + kbi2 * SRt - k\_nfb * z17 * x14/(km\_nfb + z17)$$

The rate of the species changes (ODEs) for Model 2:

$$\frac{dSRd}{dt} = kfi1 * z17 * Rd - kbi1 * SRd + kfi2 * z17 * Rt - kbi2 * SRt - (kfi2 * z17 * Rt - kbi2 * SRt)$$

$$\frac{dSRt}{dt} = kfi2 * z17 * Rt - kbi2 * SRt$$

$$\frac{dRt}{dt} = -kfi2 * z17 * Rt + kbi2 * SRt + (kcati3 * Rd * SRt)/(ki3m + Rd) + (kcati4 * Rd * SRd)/(ki4m + Rd) - (kcati5 * Rgap * Rt)/(ki5m + Rt) - a1 * x16 * Rt + (d1 + k1) * x1$$

The rate of the species changes (ODEs) for Model 3:

$$\frac{dx1}{dt} = a1 * x16 * Rt - (d1 + k1) * x1$$

$$\frac{dx2}{dt} = k1 * x1 - a2 * x2 * x20 + d2 * x3 - a3 * x2 * x17 + (k3 + d3) * x4 - a5 * x5 * x2 + (k5 + d5) * x7$$

$$\frac{dx3}{dt} = a2 * x2 * x20 - (d2 + k2) * x3$$

$$\frac{dx4}{dt} = a3 * x17 * x2 - (d3 + k3) * x4$$

$$\frac{dx5}{dt} = k3 * x4 - a4 * x5 * x21 + d4 * x6 - a5 * x5 * x2 + d5 * x7 + k6 * x9$$

$$\frac{dx6}{dt} = a4 * x5 * x21 - (d4 + k4) * x6$$

$$\frac{dx7}{dt} = a5 * x5 * x2 - (d5 + k5) * x7$$

$$\frac{dx8}{dt} = k5 * x7 - a6 * x8 * x21 + d6 * x9 - a7 * x8 * x18 + (d7 + k7) * x10 - a9 * x11 * x8 + (d9 + k9) * x13$$

$$\frac{dx9}{dt} = a6 * x8 * x21 - (d6 + k6) * x9$$

$$\frac{dx10}{dt} = a7 * x18 * x8 - (d7 + k7) * x10$$

$$\frac{dx11}{dt} = k7 * x10 - a8 * x11 * x22 + d8 * x12 - a9 * x11 * x8 + d9 * x13 + k10 * x15$$

$$\frac{dx12}{dt} = a8 * x11 * x22 - (d8 + k8) * x12$$

$$\frac{dx13}{dt} = a9 * x11 * x8 - (d9 + k9) * x13$$

$$\frac{dx14}{dt} = k9 * x13 - a10 * x14 * x22 + d10 * x15$$

$$\frac{dx15}{dt} = a10 * x14 * x22 - (d10 + k10) * x15$$

The rate of the species changes (ODEs) for Model 4:

$$\frac{d\ pAkt}{dt} = kAP * PI3K * Akt/(KmAP + Akt) - kAD * pAKT/(KmAD + pAKT)$$

$$d\frac{pGsk3b}{dt} = kGP * pAKT * Gsk3b/(KmGP + Gsk3b) - kGD * pGsk3b/(KmGD + pGsk3b)$$

$$\mathrm{d}\frac{Myc}{dt} = km * GF - kMS * x14 * Myc/(KmMS + Myc) - dm * Myc$$

$$\frac{dMyc_{ser62}}{dt} = kMS * x14 * Myc/(KmMS + Myc) - kMT * Gsk3b * Myc\_ser62/(KmMT + Myc\_ser62) - dms * Myc\_ser62$$

$$\frac{dMyc_{thr58}}{dt} = kMT * Gsk3b * Myc\_ser62/(KmMT + Myc\_ser62) - dmt * Myc\_thr58$$

$$\frac{dE}{dt} = kkE * (E/(KKmE + E)) + kkb * Myc\_ser62/(KKmM + Myc\_ser62) + kkP1 * CD * RE/(KKmCD + RE) + kkP2 * CE * RE/(KKmCE + RE) - ddE * E - kkRE * R * E$$

$$\frac{dCD}{dt} = kkCD * Myc\_ser62/(KKmM + Myc\_ser62) + kkCDS * x14/(KKmS + x14) - ddCD * CD$$

$$\frac{dCE}{dt} = kkCE * E/(KKmE + E) - ddCE * CE$$

$$\frac{dR}{dt} = kkR + kkDP * RP/(KKmRP + RP) - kkRE * R * E - kkP1 * CD * R/(KKmCD + R) - kkP2 * CE * R/(KKmCE + R) - ddR * R$$

$$\frac{dRP}{dt} = kkP1 * CD * R/(KKmCD + R) + kkP2 * CE * R/(KKmCE + R) + kkP1 * CD * RE/(KKmCD + RE) + kkP2 * CE * RE/(KKmCE + RE) - kkDP * RP/(KKmRP + RP) - ddRP * RP$$

$$\frac{dRE}{dt} = kkRE * R * E - kkP1 * CD * RE/(KKmCD + RE) - kkP2 * CE * RE/(KKmCE + RE) - ddRE * RE$$

$$\frac{dTACE}{dt} = gpT * x14/(KmTACE + x14) - dT * TACE$$

$$\frac{dARGOS}{dt} = gpA * x14/(KmA + x14) - dA * ARGOS$$

$$\frac{dAE}{dt} = kAE * z19 * ARGOS - dAE * AE$$

Bibliography

[1] S. D. M. Santos, P. J. Verveer, and P. I. H. Bastiaens, “Growth factor-induced MAPK network topology shapes Erk response determining PC-12 cell fate,” vol. 9, no. 3, 2007.

[2] A. Dhillon, S. Hagan, O. Rath, and W. Kolch, “MAP kinase signalling pathways in cancer,” *Oncogene*, vol. 26, pp. 3279–3290, 2007.

[3] L. Santarpia, S. L. Lippman, and A. K. El-Naggar, “Targeting the Mitogen-Activated Protein Kinase RAS-RAF Signaling Pathway in Cancer Therapy.”

[4] H. Ryu *et al.*, “Frequency modulation of ERK activation dynamics rewires cell fate.,” *Mol. Syst. Biol.*, vol. 11, no. 11, p. 838, 2015.

[5] D. Fey, D. Matallanas, J. Rauch, O. S. Rukhlenko, and B. N. Kholodenko, “The complexities and versatility of the RAS-to-ERK signalling system in normal and cancer cells,” *Semin. Cell Dev. Biol.*, vol. 58, pp. 96–107, 2016.

[6] N. Kawashima, K. Nakayama, K. Itoh, T. Itoh, M. Ishikawa, and V. Biju, “Reversible Dimerization of EGFR Revealed by Single-Molecule Fluorescence Imaging Using Quantum Dots,” *Chem. - A Eur. J.*, vol. 16, no. 4, pp. 1186–1192, Jan. 2010.

[7] B. N. B. N. Kholodenko, O. O. V Demin, G. Moehren, and J. B. Hoek, “Quantification of Short Term Signaling by the Epidermal Growth Factor Receptor *,” *J. Biol. Chem.*, vol. 274, no. 42, pp. 30169–30181, 1999.

[8] J. J. Hornberg, B. Binder, F. J. Bruggeman, B. Schoeberl, R. Heinrich, and H. V Westerhoff, “Control of MAPK signalling: from complexity to what really matters.,” *Oncogene*, vol. 24, no. 36, pp. 5533–5542, 2005.

[9] K. Wennerberg, L. Kent, C. J. Der, K. Wennerberg, K. L. Rossman, and C. J. Der, “The Ras superfamily at a glance The Ra s Superfamily at a Glance,” vol. 2005, pp. 843–846, 2005.

[10] J. Das *et al.*, “Digital Signaling and Hysteresis Characterize Ras Activation in Lymphoid Cells,” *Cell*, vol. 136, no. 2, pp. 337–351, 2009.

[11] T. Nakakuki *et al.*, “Ligand-specific c-fos expression emerges from the spatiotemporal control of ErbB network dynamics,” *Cell*, vol. 141, no. 5, pp. 884–896, 2010.

[12] G. Yao, T. J. Lee, S. Mori, J. R. Nevins, and L. You, “A bistable rb–e2F switch underlies the restriction point.”

[13] N. T. Ingolia and A. W. Murray, “The Ups and Downs of Modeling the Cell Cycle.”

[14] B. P. Ingalls, “Mathematical Modelling in Systems Biology : An Introduction,” *J. Chem. Inf. Model.*, vol. 53, no. 9, pp. 1–396, 2014.

[15] J. E. Ferrell, “Feedback loops and reciprocal regulation: recurring motifs in the systems biology of the cell cycle,” *Curr. Opin. Cell Biol.*, vol. 25, pp. 676–686, 2013.

[16] H. S. Wiley, S. Y. Shvartsman, and D. A. Lauffenburger, “Computational modeling of the EGF-receptor system: A paradigm for systems biology,” *Trends Cell Biol.*, vol. 13, no. 1, pp. 43–50, 2003.

[17] C. F. Huang, J. E. Ferrell, and C. E. by Daniel Koshland, “Ultrasensitivity in the mitogen-activated protein kinase cascade,” *Biochemistry*, vol. 93, pp. 10078–10083, 1996.

[18] M. Hatakeyama *et al.*, “A computational model on the modulation of mitogen-activated protein kinase (MAPK) and Akt pathways in heregulin-induced ErbB signalling.,” *Biochem. J.*, vol. 373, no. Pt 2, pp. 451–63, 2003.

[19] R. J. Orton, O. E. Sturm, V. Vyshemirsky, M. Calder, D. R. Gilbert, and W. Kolch, “Computational modelling of the receptor-tyrosine-kinase-activated MAPK pathway,” vol. 261, pp. 249–261, 2005.

[20] A. Fujioka *et al.*, “Dynamics of the Ras/ERK MAPK cascade as monitored by fluorescent probes,” *J. Biol. Chem.*, vol. 281, no. 13, pp. 8917–8926, 2006.

[21] F. A. Brightman and D. A. Fell, “Differential feedback regulation of the MAPK cascade underlies the quantitative differences in EGF and NGF signalling in PC12 cells.,” vol. 482, pp. 169–174, 2000.

[22] J. Downward, “Control of ras activation.,” *Cancer Surv.*, vol. 27, pp. 87–100, 1996.

[23] B. Schoeberl, C. Eichler-Jonsson, E. D. Gilles, and G. Müller, “Computational modeling of the dynamics of the MAP kinase cascade activated by surface and internalized EGF receptors.,” *Nat. Biotechnol.*, vol. 20, no. 4, pp. 370–375, 2002.

[24] M. H. Meinke, J. S. Bishop, and R. D. Edstrom, “Zero-order ultrasensitivity in the regulation of glycogen phosphorylase.,” *Proc. Natl. Acad. Sci. U. S. A.*, vol. 83, no. 9, pp. 2865–2868, 1986.

[25] S. Y. Kim and J. E. Ferrell, “Substrate Competition as a Source of Ultrasensitivity in the Inactivation of Wee1,” *Cell*, vol. 128, no. 6, pp. 1133–1145, 2007.

[26] T. Y. Tsai, J. A. Theriot, and J. E. Ferrell Jr., “Changes in oscillatory dynamics in the cell cycle of early Xenopus laevis embryos,” *PLoS Biol*, vol. 12, no. 2, p. e1001788, 2014.

[27] J. E. Ferrell Jr and S. Hoon Ha, “Ultrasensitivity part I: Michaelian responses and zero-order ultrasensitivity,” *Trends Biochem. Sci.*, vol. 39, pp. 496–503, 2014.

[28] B. N. Kholodenko, “Negative feedback and ultrasensitivity can bring about oscillations in the mitogen-activated protein kinase cascades,” *Eur. J. Biochem.*, vol. 267, no. 6, pp. 1583–1588, 2000.

[29] “An amplified sensitivity arising from covalent modification in biological systems.”

[30] A. V. Hill, “The possible effects of the aggregation of the molecules of hæmoglobin on its dissociation curves,” *J. Physiol.*, vol. 40, no. Supplement-Proceedings of the physiological society, pp. iv–vii, 1910.

[31] J. E. Ferrell and S. H. Ha, “Ultrasensitivity part II: Multisite phosphorylation, stoichiometric inhibitors, and positive feedback,” *Trends in Biochemical Sciences*. 2014.

[32] J. N. Weiss, “The Hill equation revisited: uses and misuses.,” *FASEB J.*, vol. 11, no. 11, pp. 835–41, Sep. 1997.

[33] “Operating Regimes of Signaling Cycles: Statics, Dynamics, and Noise Filtering.”

[34] J. E. Ferrell Jr and S. Hoon Ha, “Ultrasensitivity part III: cascades, bistable switches, and oscillators,” *Trends Biochem. Sci.*, vol. 39, pp. 612–618, 2014.

[35] J. E. Ferrell and S. H. Ha, “Ultrasensitivity part II: Multisite phosphorylation, stoichiometric inhibitors, and positive feedback,” *Trends Biochem. Sci.*, vol. 39, no. 11, pp. 556–569, 2014.

[36] F. Ortega, J. L. Garcés, F. Mas, B. N. Kholodenko, and M. Cascante, "Bistability from double phosphorylation in signal transduction: Kinetic and structural requirements," *FEBS J.*, vol. 273, no. 17, pp. 3915–3926, 2006.

[37] N. I. Markevich, J. B. Hoek, and B. N. Kholodenko, "Signaling switches and bistability arising from multisite phosphorylation in protein kinase cascades," *J. Cell Biol.*, vol. 164, no. 3, pp. 353–359, 2004.

[38] A. Goldbeter and D. E. Koshland, "Sensitivity amplification in biochemical systems," *Q. Rev. Biophys.*, vol. 15, no. 3, p. 555, Aug. 1982.

[39] S. Hooshangi, S. Thiberge, and R. Weiss, "Ultrasensitivity and noise propagation in a synthetic transcriptional cascade.," *Proc. Natl. Acad. Sci. U. S. A.*, vol. 102, no. 10, pp. 3581–6, 2005.

[40] S.-Y. Shin *et al.*, "Positive- and negative-feedback regulations coordinate the dynamic behavior of the Ras-Raf-MEK-ERK signal transduction pathway.," *J. Cell Sci.*, vol. 122, no. Pt 3, pp. 425–435, 2009.

[41] F. Badalà, K. Nouri-mahdavi, and D. A. Raoof, "Functional motifs in Biochemical Reaction Networks," *Computer (Long. Beach. Calif).*, vol. 144, no. 5, pp. 724–732, 2008.

[42] U. S. Bhalla, "Understanding complex signaling networks through models and metaphors," *Prog. Biophys. Mol. Biol.*, vol. 81, no. 1, pp. 45–65, 2003.

[43] J. W. Evenson, M. Karplus, S. Priyadarshy, S. M. Risser, D. N. Beratan, and J. J. J. Regan, "Emergent properties of networks of biological signaling pathways," *Sci. Bioinorg. Chem. Chem. Biol. Nat. Beechem Biophys. J. Proc. Natl. Acad. Sci. U.S.A. J. Phys. Chem*, vol. 262, no. 102, pp. 1247–12759, 1993.

[44] L. Qiao, R. B. Nachbar, I. G. Kevrekidis, and S. Y. Shvartsman, "Bistability and oscillations in the Huang-Ferrell model of MAPK signaling," *PLoS Comput. Biol.*, vol. 3, no. 9, pp. 1819–1826, 2007.

[45] J.-A. Sepulchre and A. C. Ventura, "Intrinsic Feedbacks in MAPK Signaling Cascades Lead to Bistability and Oscillations."

[46] U. S. Bhalla and Ravi Iyengar and R. Iyengar, "Emergent Properties of Networks of Biological Signaling Pathways," *Science (80-.).*, vol. 283, no. 5400, pp. 381–387, Jan. 1999.

[47] O. S. Soyer, M. Salathé, and S. Bonhoeffer, “Signal transduction networks: Topology, response and biochemical processes,” *J. Theor. Biol.*, vol. 238, no. 2, pp. 416–425, 2006.

[48] X.-J. Tian, X.-P. Zhang, F. Liu, and W. Wang, “Interlinking positive and negative feedback loops creates a tunable motif in gene regulatory networks.”

[49] B. Novák and J. J. Tyson, “Design principles of biochemical oscillators.,” *Nat. Rev. Mol. Cell Biol.*, vol. 9, no. 12, pp. 981–991, 2008.

[50] J. J. T. Ãy, K. C. C. Ãz, and B. Novak, “Sniffers , buzzers , toggles and blinkers : dynamics of regulatory and signaling pathways in the cell,” pp. 221–231, 2003.

[51] M. Kochańczyk *et al.*, “Relaxation oscillations and hierarchy of feedbacks in MAPK signaling,” *Sci. Rep.*, vol. 7, p. 38244, Jan. 2017.

[52] W. J. Langlois, T. Sasaoka, A. R. Saltiel, and J. M. Olefsky, “Negative feedback regulation and desensitization of insulin- and epidermal growth factor-stimulated p21ras activation,” *J. Biol. Chem.*, vol. 270, no. 43, pp. 25320–25323, 1995.

[53] B. N. Kholodenko, J. F. Hancock, and W. Kolch, “Signalling ballet in space and time.,” *Nat. Rev. Mol. Cell Biol.*, vol. 11, no. 6, pp. 414–426, 2010.

[54] M. Kochańczyk *et al.*, “Relaxation oscillations and hierarchy of feedbacks in MAPK signaling,” *Nat. Publ. Gr.*, 2016.

[55] M. A. Lemmon, D. M. Freed, J. Schlessinger, and A. Kiyatkin, “The Dark Side of Cell Signaling: Positive Roles for Negative Regulators,” *Cell*, vol. 164, no. 6, pp. 1172–1184, 2016.

[56] R. Avraham and Y. Yarden, “Feedback regulation of EGFR signalling: decision making by early and delayed loops,” *Nat. Rev. Mol. Cell Biol.*, vol. 12, no. 2, pp. 104–117, Feb. 2011.

[57] S. Y. Shvartsman, C. B. Muratov, and D. A. Lauffenburger, “Modeling and computational analysis of EGF receptor- mediated cell communication in Drosophila oogenesis.”

[58] M. Přibyl, C. B. Muratov, and S. Y. Shvartsman, “Discrete Models of Autocrine Cell Communication in Epithelial Layers,” *Biophys. J.*, vol. 84, pp. 3624–3635, 2003.

[59] M. Golembo, R. Schweitzer, M. Freeman, and B. Z. Shilo, “Argos transcription is induced by the Drosophila EGF receptor pathway to form an inhibitory feedback loop,” *Development*, vol. 122, no. 1, pp. 223–230, 1996.

[60] “Argos inhibits epidermal growth factor receptor signalling by ligand sequestration.”

[61] G. T. Reeves, R. Kalifa, D. E. Klein, M. A. Lemmon, and S. Y. Shvartsman, "Computational analysis of EGFR inhibition by Argos," 2005.

[62] S. Y. Shvartsman, M. P. Hagan, a Yacoub, P. Dent, H. S. Wiley, and D. a Lauffenburger, "Autocrine loops with positive feedback enable context-dependent cell signaling.," *Am. J. Physiol. Cell Physiol.*, vol. 282, no. 3, pp. C545–C559, 2002.

[63] Katherine Hyland, "Cell Proliferation and Its Regulation."

[64] J. J. Tyson *et al.*, "Dynamic modelling of oestrogen signalling and cell fate in breast cancer cells," *Nat. Publ. Gr.*, vol. 11, 2011.

[65] T. Lee, G. Yao, J. Nevins, and L. You, "Sensing and Integration of Erk and PI3K Signals by Myc," *PLoS Comput Biol*, vol. 4, no. 2, 2008.

[66] A. S. Dhillon, S. Hagan, O. Rath, and W. Kolch, "MAP kinase signalling pathways in cancer," pp. 3279–3290, 2007.

[67] G. Leone, J. DeGregori, R. Sears, L. Jakoi, and J. R. Nevins, "Myc and Ras collaborate in inducing accumulation of active cyclin E/Cdk2 and E2F.," *Nature*, vol. 387. pp. 422–426, 1997.

[68] S. Choi, *Introduction to Systems Biology*. 2007.

[69] H. Kitano, "Systems Biology: A Brief Overview."

[70] J. Das *et al.*, "Digital Signaling and Hysteresis Characterize Ras Activation in Lymphoid Cells," *Cell*, vol. 136, pp. 337–351.

[71] Y. Arkun, "Dynamic Modeling and Analysis of the Cross-Talk between Insulin/AKT and MAPK/ERK Signaling Pathways.," *PLoS One*, vol. 11, no. 3, p. e0149684, 2016.

[72] D. Dong Chen, S. B. Waters, K. H. Holt, and J. E. Pessin, "SOS phosphorylation and disassociation of the Grb2-SOS complex by the ERK and JNK signaling pathways.," *J. Biol. Chem.*, vol. 271, no. 11, pp. 6328–32, Mar. 1996.

[73] "Regulation of epidermal growth factor receptor signalling by inducible feedback inhibitors."

Vita

Mohammadreza was born in 1990, in Kashan, Iran. He graduated from Sharif University with a major in Chemical Engineering. In September of 2015, he enrolled in Koc University as research and teaching assistant.